Solutions to Decomposed Branching Trajectories with Powered Flyback Using Multidisciplinary Design Optimization

A Thesis

Presented to

The Academic Faculty

by

Laura Anne Ledsinger

In Partial Fulfillment
of the Requirements for the Degree of
Doctor of Philosophy in Aerospace Engineering

Georgia Institute of Technology

July 2000

Solutions to Decomposed Branching Trajectories with Powered Flyback Using Multidisciplinary Design Optimization

Approved:

_____
John R. Olds, Chairman

_____
R. Braun

_____
D. Mavris

Date Approved by Chairman _____

To all the teachers throughout my life, my family foremost among them

ACKNOWLEDGEMENTS

There are many people whom I would like to thank. All those who have touched my life in any positive way deserve some recognition. All those who have helped me with my education and especially with my doctoral pursuits deserve recognition and my deepest appreciation. A good number of those people are listed below.

My advisor, Dr. John R. Olds, is one of the most intelligent people I have ever had the privilege to know and work with. Thank you, Dr. Olds, for imparting a small amount of your knowledge to me. Thank you for your comments, suggestions, edits, and advice concerning this thesis and all my other work. I have truly appreciated your giving me the opportunity to be the 'guinea pig.'

Thank you to Dr. Bobby Braun and Dr. Dimitri Mavris, the other members of my thesis advisory committee. I realize that both of you are extremely busy men and I have appreciated your time. I have also appreciated your comments and suggestions, which have been invaluable.

Dr. Lakshmi Sankar and Dr. Daniel Schrage, of my thesis reading committee, thank you both for your time and ideas.

There are more people that I am indebted to for helping me complete my work at Georgia Tech. Dr. Jeff Jagoda, you have my sincerest gratitude for your continued support – for aiding me in becoming Dr. Olds' student, for helping Hitoshi, Lee, and I through a difficult time, and for finding me some needed funding. While I'm on the subject of funding, I would like to express my appreciation to the Georgia Space Grant Consortium and the NASA Marshall Space Flight Center for their sponsoring my research. I thank Mr. D. R. Komar of NASA Marshall and Mr. Dick Kohrs of Kistler Aerospace whose help with the applications of this research, *Stargazer* and the Kistler *K-1*, respectively, enabled me to complete this thesis. I would also like to thank Mr. John Riehl of the NASA Glenn Research Center for his elucidation on OTIS options.

I owe a great amount of thanks to the people whom I've worked with every day in the Space Systems Design Lab. Irene Budianto, thank you for keeping me sane and for

helping to give me hope and perseverance. You are the best cubemate and a generous and true friend. Thanks also to John Bradford, Dave McCormick, Dave Way, Jeff Scott, Jeff Whitfield, Ashraf Charania, Kris Cowart, Kirk Sorensen, Brad St. Germain, and Jeff Tooley; your help in class, in the lab, and at other times has been appreciated. To all my friends and lab mates, thank you for your assistance with my research and for being my friends, and good luck to you in your future endeavors.

Some other friends and coworkers from Aerospace Engineering that I would like to thank are: Anurag Gupta, Taih-Shyun Lee, Hitoshi Morimoto, Alex Leonessa, Pete Thomas, Kelsey Watts, Catherine Matos, and Sammy Holland. I appreciate everything you all have done for me on both professional and personal levels.

To my friend, Tisha Meeker, thanks for having faith in me. To my friends and former college roommates: Kelly Collins and Milly Kali, your support has been immeasurable and your friendship priceless. Thank you to all three of you for being there when I've needed you.

With great gratitude, I would like to recognize my family and the Krothapalli family. Your words of encouragement and acts of kindness have been of immense help through the years.

A special thank you to my sister, Barbara Ledsinger. You are my dearest friend and an inspiration. Thank you for your help, love, and encouraging presence over the years.

Words like thanks, appreciation, and gratitude are certainly not enough to express what I owe my parents, Bob and Martha Ledsinger, for their years of sacrifice, patience, and love. I will always be grateful, Mom and Dad, for the love of learning that you have instilled in me, without which I would not have come this far. My thanks and love to you both always.

With this last paragraph, I would like to thank the man who is first in my heart, Krish Krothapalli. It has been a long and difficult journey to reach this point in my career and you have made it much easier. When I wanted to quit and give up, you were always there to give me your support, encouragement, strength, and love. I could not have completed the journey without the generosity that you have shown, but most importantly, not without you. Thank you, so very much.

TABLE OF CONTENTS

LIST OF TABLES

LIST OF FIGURES

NOMENCLATURE

ABBREVIATIONS

deg	degree
Dry	*Stargazer* booster dry weight
ft	feet
ft/s	feet per second
lbs	pounds
log	logarithm
min	minutes
Mix	*Stargazer* booster mixture ratio
MRb	*Stargazer* booster mass ratio
MRfb	*Stargazer* flyback mass ratio
MRus	*Stargazer* upper stage mass ratio
nmi	nautical mile
psf	pounds per square foot
psi	pounds per square inch
RSquare	residual squared
sec	seconds
Sref	*Stargazer* booster wing planform area
USSref	*Stargazer* upper stage wing planform area
USwg	*Stargazer* upper stage gross weight
Wg	*Stargazer* booster gross weight

ACRONYMS

CO	Collaborative Optimization
DOE	Design of Experiments

DOT	Design Optimization Tool
DSM	Design Structure Matrix
DDT&E	Design, Development, Testing, and Evaluation
FOBD	Full Optimization-Based Decomposition
FPI	Fixed-Point Iteration
GA	Genetic Algorithm
HSCT	High Speed Civil Transport
IUS	Inertial Upper Stage
KSC	NASA Kennedy Space Center
LFBB	Liquid Flyback Booster
LOX	Liquid OXygen
LRU	Line Replacement Units
MDO	Multidisciplinary Design Optimization
MMFD	Modified Method of Feasible Directions
NAND	Nested ANalysis and Design
NASA	National Aeronautics and Space Administration
OBD	Optimization-Based Decomposition
OTIS	Optimal Trajectories by Implicit Simulation
PERL	Practical Extraction and Report Language
POBD	Partial Optimization-Based Decomposition
POST	Program to Optimize Simulated Trajectories
RBCC	Rocket-Based Combined Cycle
RLV	Reusable Launch Vehicle
RSM	Response Surface Methods
RTLS	Return to Launch Site
SAND	Simultaneous ANalysis and Design
SCCREAM	Simulated Combined-Cycle Rocket Engine Analysis Module
SLP	Sequential Linear Programming
SQP	Sequential Quadratic Programming
SSTO	Single-Stage-to-Orbit
TABI	Tailorable Advance Blanket Insulation
TPS	Thermal Protection System
TSTO	Two-Stage-to-Orbit
TUFI	Toughened Uni-Piece Fibrous Insulation

UHTC	Ultra-High Temperature Ceramic

SYMBOLS

\$M	million dollars
A, B, and C	design analyses/contributing analyses/disciplines
A, **B**, and **C**	output vectors (OBD & CO)
A', **B'**, and **C'**	intermediate values for compatibility constraint formulation
$\bar{\mathbf{A}}$, $\bar{\mathbf{B}}$, and $\bar{\mathbf{C}}$	targets for error formulation
$\mathbf{A_C}$ and $\mathbf{B_C}$	C's local version of target coupling variables
$\mathbf{B_A}$ and $\mathbf{C_A}$	A's local version of target coupling variables
$\mathbf{C_B}$ and $\mathbf{A_B}$	B's local version of target coupling variables
$\mathbf{c}_l$	subsystem local variables
D	drag
$F(\mathbf{x})$	generic objective function
g	gravity
$g_j(\mathbf{x})$	single inequality constraint
$h_k(\mathbf{x})$	single equality constraint
J_A, J_B, and J_C	error between A, B, and C's, local variables & target variables
J_A	error between Ascent's local variables & target variables
J_O	error between Orbit's local variables & target variables
J_F	error between Flyback's local variables & target variables
I_{sp}	specific impulse
l	number of equality constraints
m	number of inequality constraints
mg	weight, mass times gravity
n	number of design variables
$\mathbf{P_s}$	staging vector
$\mathbf{P_s'}$	prescribed staging vector
$\bar{\mathbf{P}}_s$	staging vector target
T	thrust
V	velocity
w_{fb}	flyback fuel weight

w_{fb}'	flyback fuel weight guess
$\bar{w}_{fb}$	flyback fuel weight target
w_{us}	upper stage weight
w_{us}'	prescribed upper stage weight
$\bar{w}_{us}$	upper stage weight target
$\mathbf{x}$	design variable vector
x_i^l	lower bound of x_I
x_i^u	upper bound of x_I
$\mathbf{x}_{ss}$	subsystem design variable vector
ε	angle between velocity and thrust in the vertical plane/small tolerance
γ	flight path angle

SUMMARY

In the advanced launch vehicle design community, there exists considerable interest in fully reusable, two-stage-to-orbit vehicle designs that use ‘branching trajectories’ during their missions. For these reusable systems, the booster must fly to a predetermined landing site after staging occurs.

The solution to this problem using an industry-standard trajectory optimization code typically requires at least two separate computer jobs — one for the orbital branch from the ground to orbit (in some cases, this can be broken into two computer jobs) and one for the flyback branch from the staging point to the landing site. These jobs are tightly coupled and their data requirements are interdependent. In addition, the objective functions for each computer job differ and conflict.

This research produces a method to solve these distributed branching trajectory problems with respect to an overall system-level objective while maintaining data consistency within the problem. This method is used to solve the trajectories of two relevant two-stage-to-orbit vehicles: the Kistler *K-1* and the *Stargazer* launch vehicles. Both of these vehicles require a powered flyback. Thus, optimization contingent on the feedback of the flyback fuel is a relevant part of this study.

The solutions of the branching trajectory problems via traditional methods, termed ‘One-and-Done’ and manual iteration, are compared with those involving the multidisciplinary design optimization techniques of fixed-point iteration, optimization-based decomposition, and collaborative optimization. Optimization-based decomposition was used to solve each problem; the *K-1* trajectory includes a fixed-point iteration solution. The use of collaborative optimization as an solution technique for branching trajectories is introduced in the solution to each problem.

Results show that proposed method involving collaborative optimization and optimization-based decomposition performed well for both the *K-1* and *Stargazer* branching trajectories. The use of these methods for the Kistler *K-1* problem shows that an increase in payload weight of 1.0%, on average, could be obtained. Similarly, a reduction in *Stargazer*'s dry weight of approximately 0.8% was achieved through the MDO methods. Conclusions concerning the method outline, comparisons of the method with differing solution techniques, staging flight path angle trends, and the automation of the optimization process are included.

CHAPTER I

INTRODUCTION

Fully reusable two-stage-to-orbit vehicle designs that incorporate 'branching' trajectories during their ascent are of current interest in the advanced launch vehicle design community. Unlike expendable vehicle designs, the booster of a reusable system must fly to a designated landing site after staging. Therefore, in addition to the ascent trajectory, both the flyback, or booster return, branch and the orbital upper stage branch are of interest and must be simultaneously optimized in order to achieve an overall system objective. Current and notable designs in this class include the U. S. Air Force Space Operations Vehicle designs with their 'pop-up' trajectories, the Kelly Astroliner, the Kistler K-1, one of the preliminary designs for NASA's Bantam-X and Bimese studies, and NASA's proposed liquid flyback booster designs (Space Shuttle solid booster upgrade).

1.1 The Definition of Branching Trajectories

In an effort to lower costs, designers of advanced two-stage-to-orbit (TSTO) launch vehicles are beginning to consider launch systems in which the booster stage can be recovered, serviced, and reflown. Often the reusable booster is required to land at a predesignated recovery site either near the original launch site (RTLS-style trajectory, Figure 1) or downrange of the staging point (Figure 2). In these cases, the entire trajectory is composed of three parts. The ascent trajectory follows the vehicle from launch to staging. At this point, the trajectory is assumed to split into two 'branches.' One is the *orbital branch* beginning at staging and following the orbital upper stage all the way to orbit. The

second branch, or *flyback branch*, starts at the staging point and follows the reusable booster to its landing site. Due to recovery distance or out-of-plane maneuvers required, the booster is often powered for its flight to the landing site. In simulations where the booster is jettisoned from an orbital vehicle, it may be convenient to combine the ascent trajectory and the orbital branch to create one computer job. The same may be said about a launch vehicle with an upper stage that is jettisoned; the ascent trajectory and the flyback branch may be combined.

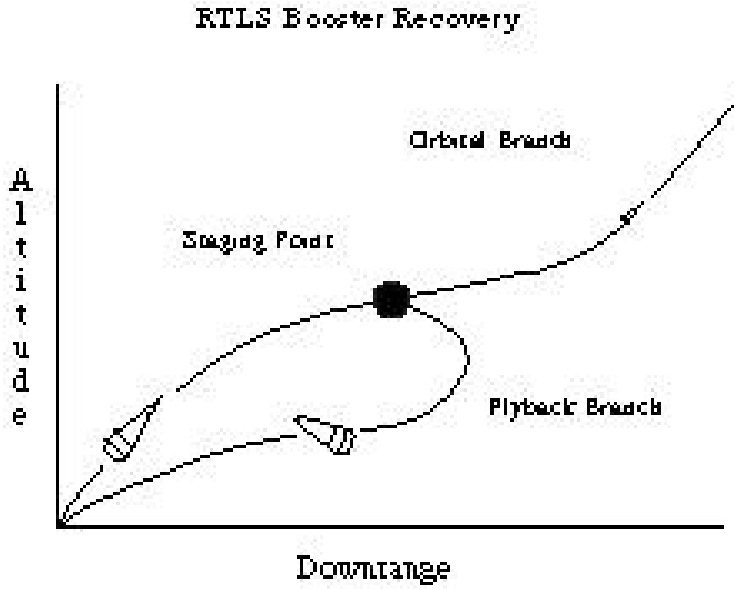

Figure 1: RTLS Branching Trajectory

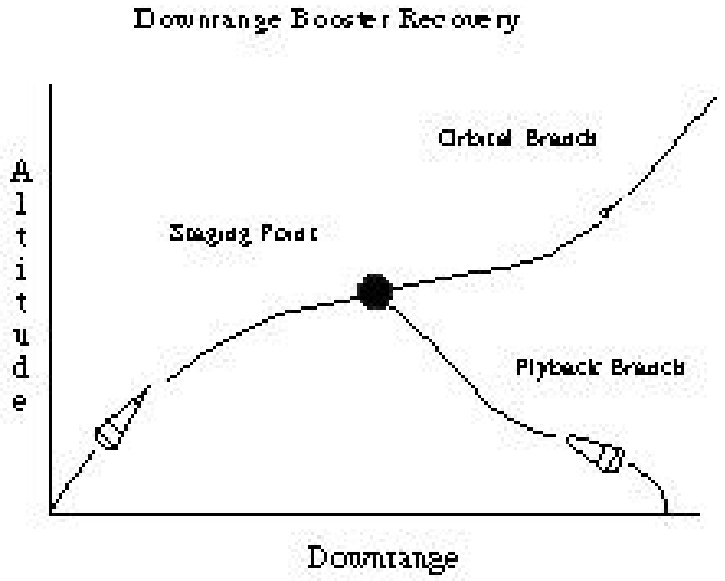

Figure 2: Downrange Branching Trajectory

In general, both the orbital branch and the flyback branch rely upon the ascent trajectory for their respective initial conditions. These initial conditions are vectors composed of geographical position, altitude, velocity, flight path angle, velocity azimuth, and staging weight. The ascent trajectory also depends on both branches. Assuming that the booster is powered, the amount of flyback fuel required by the booster influences the gross lift-off weight of the vehicle and thus the ascent path. The weight of the upper stage (which is dependent upon initial staging conditions) also affects the gross lift-off weight of the vehicle and thus the ascent path. Consequently, all the parts of the entire trajectory are coupled or interdependent.

1.2 Motivation for Research

In the public domain or otherwise open literature, no computationally efficient method exists for solving branching trajectories, as defined above, that include the feedback of data. This pertains specifically to those trajectories in which separate branches are simulated and the data from the trajectory branches that occur after staging is required by the ascent path.

Faced with the lack of a suitable solution method, today's trajectory analysts are forced to either 1) compromise the optimality of their solutions, or 2) create large, complex optimization problems that are difficult to solve numerically. In the former case, later referred to as the manual iteration method, the analyst may choose to decompose the branching trajectory into several subproblems (one for each branch) that are individually and sequentially optimized. In most situations, this approach will undermine any natural compromise between the branches and lead to a suboptimal overall objective. The latter case, later referred to as the fixed-point iteration approach, generally requires the analyst to create a large, slow computer simulation in which all independent variables and all constraints for each branch are treated by a single optimizer. This problem is made more difficult by the presence of the natural coupling between the ascent and the branches of the trajectory and the resulting iteration that must occur between them. A branching trajectory solved in this way often exhibits numerical convergence problems and does not scale well to very large problems.

The shortcomings in the two current state-of-practice approaches above can be significant. At current payload delivery prices of more than $3,000/lb of payload to orbit, a suboptimal solution that loses just 0.1% of payload for a typical medium-sized booster would result in a loss of potential revenue of more than $500,000 per flight. Alternately, with engineering time costing as much as $100/hour, a new solution method, that might save 25% of the time it would take an engineer fill out a payload performance map with 100's of branching trajectory cases, might save almost $20,000. These effects are significant and provide some of the motivation for the present research.

As was mentioned previously, the manual iteration method results will not exploit the compromises of the branches. These compromises are revealed through the staging vector components. Thus, another motivating factor for this research involves identifying potential staging vector compromises for branching trajectories in general.

1.3 Research Goals

It is the goal of this research, and ultimately its contribution to the field of trajectory optimization, to develop and demonstrate a new open-literature method for solving branching trajectories in which feedback data is accurately and efficiently modeled.

It is further a goal of this research that the new method be computationally efficient by allowing the problem to be decomposed into smaller, more numerically manageable subproblems (one for each branch) that can be solved in a distributed fashion. The new method must be as simple and straightforward as possible without introducing extensive set-up complexities or set-up times. It cannot produce a series of suboptimal solutions for each branch nor can it produce solutions that are internally inconsistent between branches. (Internal consistency meaning that the coupling variables produced by the branches are numerically identical to those same variables passed into the ascent and vice versa). Lastly, the new method should be scalable and adaptable to a wide variety of large and small branching problems having this particular coupling characteristic.

1.4 Research Objectives

In support of the aforementioned research goals, specific research objectives (or targets) were established to measure the success of the methodology development effort. Some of the objectives are qualitative in nature, while others represent specific quantitative targets. These research objectives for the new method are outlined as follows:

- Demonstrate an efficient computation approach that can be distributed on several computing processors to reduce overall solution time enough such that the solution process would be applicable in a vehicle design framework.

- Demonstrate an improvement of 1% or greater in the objective function relative to the suboptimal solution of the manual iteration method.

- Decrease the computing time relative to a fixed-point iteration approach by 10% or more for a single trajectory solution.

· Maintain a reasonable level of method complexity and a set-up time that is no more than 50% greater than the set-up time of a suboptimal method like the manual iteration method.

· Guarantee internal data consistency between the individual branches at the solution.

· Demonstrate the scalability and robustness of the new method for small and large branching trajectory problems.

· Formulate generalities of staging vector compromises for the branching trajectory problem.

1.5 Approach

After the current solution techniques for branching trajectories and their deficiencies was researched, a rough framework for the new solution method was established (the full details of the new method will be disclosed in subsequent chapters). Since an objective of this research was that the new method be computationally efficient in terms of computation time and distribution of computing resources, the proposed method advocates the decomposition of the individual branches of the trajectory into separate subproblems. Subsequently, these distributed subproblems had to be coordinated into a consistent and optimal solution.

The field of multidisciplinary design optimization (MDO) provided several techniques that have been successfully applied to the decomposition and subsequent coordination of the individual subproblems. Therefore, a key element of the present research was to examine several pertinent MDO techniques to determine their applicability to this class of branching trajectory. Based on the results of this investigation, one MDO solution technique was recommended for use in the overall method.

Two ‘test case’ applications were formed to help guide the development of the method and to demonstrate its utility toward reaching the research goals and objectives. The

first testcase, the Kistler *K-1* launch vehicle, was a relatively small, coupled branching trajectory problem. The second testcase, the *Stargazer* design, was a more complex problem in which the branching trajectory analysis was tightly coupled with other disciplines. The evaluation of all of these analyses was necessary to evaluate the branching trajectory performance.

In addition to their implementation in the selection of the MDO technique chosen for the proposed method, these two testcases were also used to establish the benchmark (the manual iteration method solution) from which comparisons could be made. These comparisons were analyzed with respect to execution times, set-up complexity, and objective values at the solution.

While solving the branching trajectory problem, a significant amount of time was invested in order to understand the details of each method, automate or script many of the analyses in the optimization process, and run thousands of individual analyses needed to generate supporting data. This data was then used to draw conclusions and evaluate any improvements and concurrence with the stated objectives. Based on these conclusions, recommendations for future work were made.

1.6 Organization of the Thesis

The thesis is organized in the following manner. This chapter, Chapter I, introduces the problem of branching trajectories and the contribution of the research. Chapters II and III review background information on trajectory optimization, both in general and for the branching trajectory formulation, and on multidisciplinary design optimization (MDO), respectively. Decomposition methods are the specific methods used for analysis in this thesis. Thus, background information and prior research with respect to MDO decomposition methods are presented in Chapter IV. In Chapter V, the general branching trajectory problem is formulated as MDO problems. This chapter shows specific illustrations of the branching trajectory problem when formed using the decomposition methods of Chapter IV. The first application, the Kistler *K-1* launch vehicle, is described in Chapter VI. Specifically, the vehicle characteristics, trajectory, and objective function are accounted for in detail. The results for the *K-1* analysis are reported on in Chapter VII.

Results for both traditional methods and MDO methods are analyzed. Chapter VIII introduces the second application, *Stargazer*, its design structure, trajectory, and objective function. Results with respect to traditional methods and MDO methods for the *Stargazer* vehicle are examined in Chapter IX. Chapter X closes the thesis with conclusions and recommendations for future work.

CHAPTER II

TRAJECTORY OPTIMIZATION: AN OVERVIEW

Much research has been performed in the area of trajectory optimization [1,2,3]. This chapter presents the background of trajectory optimization with emphasis on that which is necessary for launch vehicle missions. The additional considerations required for branching trajectory optimization with powered flyback, along with past research in that specific area, is discussed.

2.1 Trajectory Optimization in General

Trajectory optimization can be defined as finding the 'best' path from an initial condition to some final condition based on a certain performance index [3]. This is achieved subject to gravitational, propulsive, and aerodynamic forces. The 'best' path is contingent on the performance index, or objective function, to be optimized. The objective function can be to maximize final weight, minimize time, or maximize distance covered. The optimization of the trajectory usually occurs in phases, such as take-off, cruise, and landing. Typically, the phases are optimized given initial and final events, which are subject to path constraints.

2.2 A General Vehicle in Flight

A vehicle in flight can be approximated by a point mass. Figure 3 shows an illustration of a point mass subjected to forces in flight.

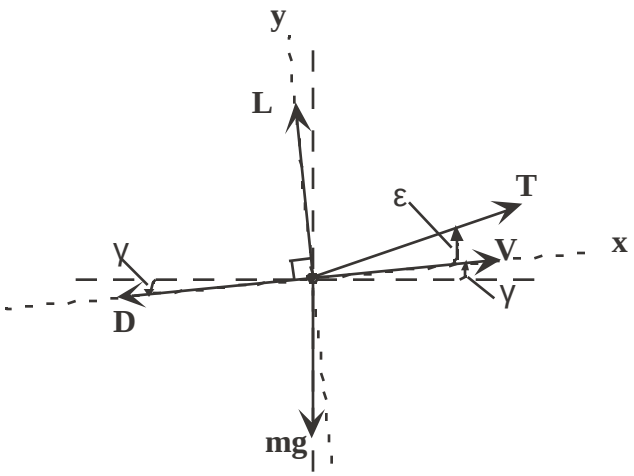

Figure 3: A Point Mass in Flight

Summing about each axis, the dynamic equations for velocity, **V**, and flight path angle, γ, are given in equations 1 and 2.

$$m\dot{V} = -D - mg\sin(\gamma) + T\cos(\varepsilon) \quad (1)$$

$$mV\dot{\gamma} = L + T\sin(\varepsilon) - mg\cos(\gamma) \quad (2)$$

where L is the lifting force, D is the drag force, T is the thrust, or propulsive force, and mg is the gravitational force. These equations can be rearranged to form the general nonlinear longitudinal equations of motion for a vehicle [4], similar equations can be formulated for lateral motion [4]. The general equations are then used to model the flight path. When combined with aerodynamic, propulsive, and weight models, the equations of motion can be

integrated through time to produce the entire trajectory. Once an initial trajectory is obtained, optimization can occur.

2.3 Solution Schemes for Trajectory Optimization

Solution methods for trajectory optimization problems are typically identified as either indirect methods or direct methods [5, 6]. Indirect methods use calculus of variations techniques [7] to characterize the optimization problem as a two-point boundary-value problem [8, 9]. At the initial time, the costate variables, or Lagrange multipliers, must be guessed. Since these variables are just multipliers and have no physical meaning, guessing their initial values is very difficult and may lead to problems with convergence to the optimum. Direct methods discretize the optimization problem through events (distinguishing initial/final conditions) and phases (that part of the trajectory occurring between events.) The subsequent problem is solved using nonlinear programming techniques [10, 11]. Some indirect and direct optimization methods are considered below.

2.3.1 Optimal Control

The optimal control scheme [12] is an indirect method. It has been used to solve many trajectory optimization problems for launch vehicles [13, 14, 15, and 16]. Optimal control uses first variation techniques to determine necessary conditions, for an optimum, and second variation techniques to determine sufficient conditions, to find out what kind of optimum. Optimal control requires analytical differentiation of the equations of motion, including the models for propulsion, atmosphere, weights, etc. In fact, to determine satisfaction of the sufficient conditions, the equations and models must be twice differentiable. The models are usually highly complicated equations and vehicle specific. Thus, optimal control problems are difficult to make modular. Because these problems are posed as two-point-boundary-value problems, *a priori* knowledge of the initial state variables, final costate variables, and occurrence of path constraints is an advantage. Without this knowledge, improper initial guesses can lead to convergence difficulty.

2.3.2 Direct Numerical Methods

The direct schemes which use nonlinear programming include simple shooting, multiple shooting, and transcription, or collocation. In the shooting methods, the control history is discretized as a polynomial, with the trajectory variables a function of the integrated equations of motion. In the collocation method, the vehicle's flight path is discretized, over time intervals, as a set of polynomials for both the trajectory variables and controls. To ensure that a physically feasible to trajectory is calculated, satisfaction of the equations of motion is enforced at discrete points throughout the trajectory.

In both cases, nonlinear programming techniques are used to find the optimal trajectory. These methods require gradient calculations to analyze the sensitivities of the design variables (either controls, or controls and trajectory variables) to the objective and constraints. These gradient calculations usually require many function calls (trajectory simulations). However, numerical optimization schemes of shooting methods and collocation are easily coded and allow for varying models, resulting in their being popular methods for implementation in trajectory optimization software [17, 18, 19]. As with indirect techniques, these methods are sensitive to the weighting scheme and initial guess.

Two popular trajectory optimization codes are described in the next section. Both use direct methods.

2.4 Trajectory Optimization Programs: OTIS and POST

OTIS [17], Optimal Trajectories by Implicit Simulation, is a trajectory simulation program that primarily uses nonlinear programming and collocation, although shooting is an option. OTIS was originally developed by the Boeing Company under contract to the Air Force and is popular throughout the trajectory optimization community. OTIS can accommodate varying models of propulsion, weights, atmospheres, and aerodynamics. As a result of the trajectory variables being parameterized over specific time intervals, constraint boundaries, such as a dynamic pressure boundary, are easily simulated in OTIS.

The Program to Optimize Simulated Trajectories — POST I [18] was developed by Lockheed-Martin under contract to NASA and is widely used for trajectory optimization problems in advanced vehicle design. POST is a generalized event-oriented code that numerically integrates the equations of motion of a flight vehicle given definitions of aerodynamic coefficients, propulsion system characteristics, atmosphere tables, and gravitational models. Guidance algorithms used in each phase are user-defined. Numerical optimization, specifically nonlinear programming and direct shooting, is used to satisfy trajectory constraints and minimize a user-defined objective function by changing independent steering and propulsion variables along the flight path. POST runs in a batch execution mode and depends on an input file (or input deck) to define the trajectory event structure, vehicle parameters, independent variables, constraints, and objective function.

Both the OTIS and POST codes have various limitations and approximations associated with their trajectory models. Table 1 lists the various options offered by these codes. POST and OTIS each offer three- and six-degree-of-freedom simulations and point mass approximations of the vehicle being simulated.

More intricate differences occur between the table modeling options and guidance and steering algorithms employed. Table inputs are linearly interpolated in POST. In OTIS, tables are modeled more complexly. Table data is curve fit with the choices of a linear fit, cubic or quintic spline fits, or, in the most recent version of the code, a chamfered spline fit. In addition, steering in OTIS is essentially achieved open-loop and a ramp steering option acts as guidance for the simulations. Guidance and steering options for POST are more varied and include: vehicle body rates, aerodynamic angles, euler angles, and pitch plane steering; open/closed loop guidance; generalized acceleration steering; and predictor-corrector guidance.

Table 1: Modeling Options for OTIS and POST

Model	OTIS	POST
Atmospheric Model	17 model options, including options for wind models and user-defined models	17 model options, including 4 for winds, 3 for turbulence, and 2 for gusts and user-defined models
Aerodynamic Model	Tables for Axial & Normal or Lift & Drag Coefficients	Tables for Axial & Normal or Lift & Drag Coefficients
Gravity Model	2^{nd} –4^{th} harmonics in the gravity potential function Oblate and spherical planet options	2^{nd} –8^{th} harmonics in the gravity potential function Oblate and spherical planet options
Numerical Integration Methods	6 options including 4^{th} order Runge-Kutta, variable step methods, and implicit integration.	7 options including 3 Runge-Kutta methods, variable step methods, and methods specialized for orbit simulations

POST and OTIS are being improved and additions are made regularly. In addition, users have the option to write their own supplemental algorithms. The options and approximations listed in Table 1 are only highlights of some choices that are common in trajectory simulation models. Ultimately, the main difference occurs in the optimization methods employed, as previously mentioned.

2.5 The Optimization of Branching Trajectories

As explained in Chapter I, there are many different TSTO mission profiles that exhibit branching trajectories. Future RLV's depend on this type of trajectory because the reusability of the vehicle is furthered by it. In the previous sections, the motivation for trajectory optimization was reviewed. Branching trajectories are no different in that they must also be optimized.

Branching trajectories can be posed as non-distributed or distributed simulations. Non-distributed problems require one simulation that can accommodate multiple vehicle models, which would be needed after staging. The optimizer for this problem will be large, as it contains all the design variables and constraints for the entire branching trajectory. This has the potential to lead to long simulation times. Distributed problems simulate the branching trajectory as two or three separate simulations. They can be decomposed at the staging point to result in an ascent trajectory and an upper stage trajectory and/or a flyback trajectory. Optimization can occur at the trajectory level, at an overall system-level, or at both levels. These solutions are explained below and in Chapter V. Simulation, or CPU, time can be saved by posing the branching trajectory in this distributed manner.

2.5.1 Branching Trajectory Optimization for this Research

In the public domain, research is lacking with respect to branching trajectories with powered flyback. In the same domain, it is nonexistent for such trajectories solved in a distributed manner with an overall objective and consistent data between subproblems.

For the research presented in this thesis, branching trajectories with powered flybacks were decomposed into distributed problems. POST, described in the previous section, is the program that was used to simulate the trajectories. POST is currently used for launch vehicle trajectory simulation in the Space Systems Design Lab at Georgia Tech and is the code of which the author is intimately familiar. The use of POST dictated that the branching trajectory optimization be achieved in a distributed manner. Branching trajectories cannot be modeled in POST as a non-distributed problem.

The fact that there are now two, or even three, different parts of the overall branching trajectory makes the optimization more complex. The existence of the staging point means that compromises must be made between the orbital and flyback branches. An example is that typically the upper stage wants a larger flight path angle at staging. This helps it achieve its orbit goals in a shorter amount of time (than with a smaller flight path angle) and thus aids in minimizing its fuel consumed during the orbital portion of the trajectory. At the same time, the booster desires a smaller flight path angle. The closer the velocity vector is to

the horizontal, the faster the booster can achieve that negative flight path angle that is needed to aim the vehicle back to the earth. This also helps to minimize fuel. It is evident that a compromise is needed when the overall trajectory is considered.

Another important aspect of the branching trajectory is the feedback of the flyback fuel and the upper stage fuel. Figure 4 illustrates the fuel locations for a typical TSTO. Unnecessary extra fuel in the booster or the upper stage means that either extra payload can be taken to orbit or smaller vehicles (booster and upper stage) can be used. Not enough fuel means that orbit conditions may not be met and the booster does not return to its designated landing site. Thus, the feedback of these fuels is required.

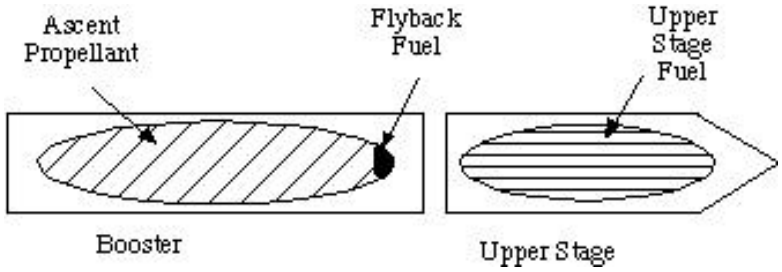

Figure 4: Example of a TSTO's Stages with Fuel

2.5.2 The 'One-and-Done' and Manual Iteration Methods

Unfortunately, a common method currently used in industry for optimizing a branching trajectory problem (henceforth the *'One-and-Done' Method*), while recognizing the coupling of the ascent trajectory and orbital branch, ignores the flyback fuel dependency from the flyback branch to the ascent trajectory. The ascent trajectory, orbital branch, and flyback branch are treated as separate, but sequential optimization subproblems. A reasonable guess at upper stage mass, flyback fuel, and associated structure is made to establish an initial booster weight. Then, the ascent is optimized for maximum weight at staging (or some other similar criteria). The ascent trajectory will produce a staging state vector used to initiate the orbital branch and the flyback branch. This vector includes altitude, velocity, flight path angle, velocity azimuth, latitude, longitude, and sometimes staging weight. The orbital branch will typically be optimized with respect to maximizing

the upper stage burnout weight, while the flyback branch will typically be optimized with respect to minimizing the flyback fuel consumed.

There are a number of deficiencies in the 'One-and-Done' method. A major deficiency is that the final solution is not 'internally consistent,' in other words, it is not guaranteed to be converged between the subproblems. The feedback is not there; the problems that this creates have been discussed above.

This aforementioned deficiency can be eliminated through iteration between the ascent, upper stage, and the flyback branches. From this point on, this method will be referred to as the Manual Iteration method. A significant deficiency still exists with this method as with the 'One-and-Done' method.

At a fundamental level, these methods are inherently flawed. The objective functions of the subproblems are not the same; therefore, they can be in conflict. If the system-level objective is to deliver a certain payload to orbit with a minimum weight booster, then why expect an optimum solution from a method that first maximizes the payload to orbit for the orbital branch, then minimizes the flyback fuel for the flyback branch? A compromise in the staging conditions can be made such that it reduces the flyback fuel and thus decreases the booster weight. A proper solution to this problem requires simultaneous and coupled treatment of all branches of the trajectory, and the establishment of a single, consistent objective function between them (i.e. a system-level optimization).

A mathematical example of conflicting objective functions can be seen in equations 3 – 8. F is the overall equation that is to be optimized.

$$F = f_1 + f_2 = 2(x-1)^2 + x \tag{3}$$

Decomposed, F can be written as two equations, f_1 and f_2. When optimized separately, equations 6 and 7 are produced and x results in two differing answers that optimize each decomposed problem individually.

$$f_1 = (x-1)^2 \tag{4}$$

$$f_2 = f_1 + x = (x-1)^2 + x \tag{5}$$

$$\frac{df_1}{dx} = 0 = 2(x-1) \qquad x = 1 \tag{6}$$

$$\frac{df_2}{dx} = 0 = 2(x-1) + 1 \qquad x = .5 \tag{7}$$

The overall optimization of F in equation 8, however, shows that a compromise in x was made so that the true optimum was found. Table 2 summarizes the end products of this simple example. An example of a compromise that could be made in the branching trajectory problem was discussed in Section 2.5.1.

$$\frac{dF}{dx} = 0 = 4(x-1) + 1 \qquad x = .75 \tag{8}$$

Table 2: Results for Mathematical Conflicting Objective Functions Example

Function	Optimum x	Optimum F
f_1	1	1
f_2	.5	1
F	.75	.875

2.5.3 Branching Trajectory Optimization in the Launch Vehicle Community

Many in industry have recognized the deficiencies of the 'One-and-Done' and manual iteration methods. Some have employed optimizers that solve the branching trajectory problem as a non-distributed problem. OTIS has the ability to simulate the entire

branching trajectory [20], in this manner, as a single simulation. Descriptions and results for applications of branching trajectory research with OTIS are not currently available in the public domain.

Shuttle-IUS trajectories with branches have been simulated at the Aerospace Corporation [21]. An ascent trajectory was attained for the orbiter from launch to a 100 nmi park orbit. From this orbit, trajectories required for the Shuttle deorbit and upper stage (IUS) mission were generated. The overall problem was a parameter optimization problem with variables that were the STS and IUS burns and constraints for the mission requirements. An overall optimization using a sequential quadratic programming algorithm was performed to satisfy the mission constraints of the two branches while maximizing the payload weight of the IUS. Although these trajectories differ from the branching trajectory definition of Chapter I, the solution with an overall optimizer found that compromises, in shuttle deorbit requirements and IUS performance, were necessary to find the desired system optimum of maximum payload. Feedback of the fuels was not considered.

At NASA Langley, POST has been used to solve some branching trajectories. Branching trajectory research has included investigations of a bimese-type vehicle [22] with a glideback, or non-powered, return to the launch site. Separately optimized ascent and glideback POST decks were used for the simulation.

A Sänger-like vehicle with an orbiter and a ramjet-powered return to the launch site is discussed in [23]. The study was used to analyze the effects of various amounts of airbreathing and rocket propulsion during ascent. Thus, optimization for an overall objective was not the goal of the analysis and thus not addressed. The trajectory simulations for the ascent, orbiter, and flyback were run separately with the staging conditions (including altitude, velocity, and flight path angle) fixed for staging at Mach 6. The sizes of the booster and the orbiter were also fixed. Propellant volume in the booster could vary however. While trying to find the booster gross weight needed to lift the orbiter, cruise-back propellant weight was estimated. Feedback of the flyback, or cruise-back, fuel weight was not modeled, but would have been beneficial since the cruise distance and booster staging weight changed for each different gross weight.

POST I's sequel, POST II [24], is currently being tested and is not yet available to the general public. POST II can simulate multiple vehicles and thus branching trajectories as one non-distributed trajectory simulation. At this time, fuel feedback is not an option specific to the code, but has the potential to be included as user-defined calculations.

2.5.4 Summary

The solution methods of the 'One-and-Done' and manual iteration methods rely on at most three separate POST input decks — one for the ascent to staging trajectory subproblem, one for the orbital branch subproblem, and one for the flyback branch subproblem. Each subproblem has its own independent variables, constraints, and objective function. The current research has retained the POST code and the use of at most three separate input decks (one job for each part), but also eliminated any objective function conflict and lack of data consistency between them. Feedback of the flyback fuel weight (and varying upper stage weight) was modeled in this research. This has produced a solution that resulted in internally consistent data (the fuels' feedback is reflected in the initial gross weight, etc.) and a single system-level objective function (without conflicting objective functions for each subproblem).

CHAPTER III

A BRIEF SYNOPSIS OF MULTIDISCIPLINARY DESIGN OPTIMIZATION

This chapter reviews background information concerning the multidisciplinary design optimization. The significance of optimization with respect to design is explained and a standard representation of the coupling in a design process, the design structure matrix, is illustrated. Two classes of multidisciplinary design optimization, parametric and stochastic methods and decomposition methods, are briefly reviewed.

3.1 The Standard Optimization Form

Numerical optimization can be defined as the process that arrives at the best possible solution to a problem with respect to an objective function and constraints. The objective function, F(**x**), is the goal of optimization; it is the quantity that must be maximized or minimized. The objective function is dependent on the inputs, **x**, called design variables. The constraints are the limitations of the design. They may be given as equalities, h(**x**), or inequalities, the bounded function g(**x**).

There exists a standard form in which the optimization problem is stated [25]. Equations 9 – 12 define the standard optimization form.

$$\text{Minimize: } F(\mathbf{x}) \qquad \mathbf{x} = x_1, x_2, \ldots x_n \qquad (9)$$

$$\text{Subject to: } g_j(\mathbf{x}) \leq 0 \qquad j = 1, m \qquad (10)$$

$$h_k(\mathbf{x}) = 0 \qquad k = 1, l \tag{11}$$

$$x_i^l \leq x_i \leq x_i^u \qquad i = 1, n \tag{12}$$

where x_i^l and x_i^u are the lower and upper bounds of x_i, respectively. Given this form, the mathematical equivalent to maximizing the objective function is to multiply $F(\mathbf{x})$ by negative one. Similarly, if an inequality constraint is given as being greater than or equal to zero, the constraint is multiplied by a negative one so that it follows the standard optimization form.

3.2 Design and Optimization

3.2.1 Design

Finding the optimal analytical answer to a simple mathematical equation of one dependent variable is relatively trivial when compared to finding the optimal solution to a design problem. Typically, the root to the first derivative of that equation is found and substituted into the original equation, giving the extremum (maximum or minimum). Within the design set-up, that simple analysis can become thousands of independent variables with numerous constraints.

A typical design structure is shown in Figure 5 in the form of the Design Structure Matrix (DSM) [26]. Blocks A, B, and C represent design analyses, or disciplines, and may themselves contain several sub-analyses. The lines to the right of the analyses represent feedforward loops, while the lines to the left represent feedback loops. Typically, when such loops are present, coupling exists in the design. The circles at each intersection represent coupling of the design variables between the analyses. For a design coupled as in Figure 5, iteration must occur to ensure compatibility among the analyses.

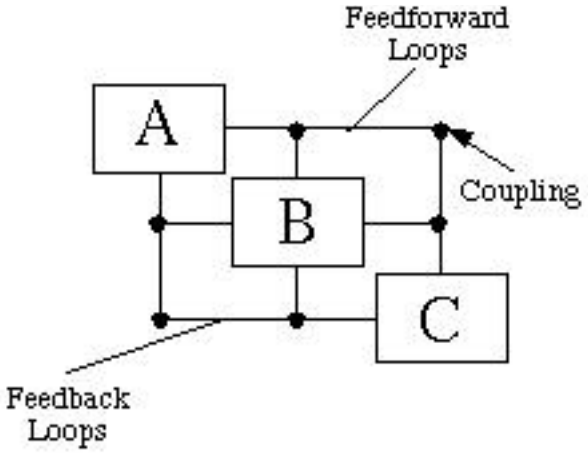

Figure 5: Design Structure Matrix

Design teams, or organizations, can be modeled by DSM's similar to that of Figure 5, although many more analyses usually exist. These teams are typically tightly integrated, or coupled, and designs are produced by iteration. Members of the teams execute the analyses and are referred to as 'disciplinary experts.' These experts usually have a store of knowledge pertaining to the analysis he or she controls. Communication of the coupled design variables between the disciplinary experts can be as simple as yelling across the room or as complicated as transferring files across the country. A converged design, one whose inputs to the analyses and outputs from them are considered the same, may take anywhere from minutes to years to complete, depending on the complexity of the design and the level of detail required.

3.2.2 Optimization of Designs

An algorithm can be used to find the optimal design as evaluated by the DSM. In this design scenario, numerical optimization may reduce design time. It can easily be automated and applied to large design problems, and it is not biased by subjective intuition. However, these advantages may be counteracted by significant set-up times and numerical noise within the analyses. Many numerical optimizers require a continuous, or 'smooth' (first-order or second-order differentiable) design space (that n-dimensional region in which potential designs lie). This is a disadvantage because some of the design variables may be

discrete (e.g., number of engines, TPS type, etc.) or piecewise linear. Typically, in optimization, analyses must be evaluated quickly and numerously, a disadvantage because many design analysis programs can take days to run. Often, these obstacles can be overcome in order to obtain the valuable optimal solution.

The question remains as to the arrangement of the optimizer with the design structure. An introduction to various types of formulations is given in the following sections. Techniques for setting up the optimization problem fall under the category of Multidisciplinary Design Optimization (MDO) methods.

3.3 Multidisciplinary Design Optimization

Multidisciplinary Design Optimization (MDO) is a branch of research dedicated to the formulation of optimization techniques, algorithms, and improvements for the many-disciplined design problem such as that shown in Figure 5. A relatively new field, MDO has its roots in structural optimization [27, 28]. Among many other applications, MDO techniques have been used to optimize numerous vehicle design problems, to the extent of which survey papers have been written for launch vehicle design [29], aircraft design [30], and helicopter design [31].

For the purpose of this introduction, MDO formulations are presented in the next sections by the way in which the optimization is performed: through use of parametric and stochastic methods or through use of decomposition techniques. The crux of the research proposed in the following chapters is in the use of the latter techniques; the former is included for completeness.

3.4 Parametric and Stochastic Methods

Parametric MDO methods use domain spanning techniques to formulate equations that approximate the analysis to be optimized. These methods include Taguchi and Design of Experiments (DOE) methods that are usually combined with response surface methods (RSM). Taguchi methods [32] and DOE methods [33] span the entire design space

through a selection of values for each design variable within a user-defined lower and upper range. Commonly, the representation of each design variable is by its maximum, minimum, and mean values. Through combinations of each of these values for every design variable, a arrays can be established to represent the whole design space. For each array combination, a response, or design objective, is obtained if a feasible design exists for the given values. Once the objective functions are known, RSM can be used to fit the Taguchi or DOE analysis to an equation that can be quadratic, cubic, etc., in order. Subsequently, the design analysis is now modeled by an equation that can easily be used for optimization.

Taguchi/RSM methods have been used successfully in the design of a single-stage-to-orbit, rocket-based combined cycle launch vehicle [34, 35]. DOE/RSM methods have been used to successfully design that same vehicle [35] and an aeroelastic wing [36, 37]. When the probabilistic nature of the design variables is added through Monte Carlo simulation, even more robust results can be obtained [38, 39].

Stochastic methods are those that offer the most advantages to optimization problems that have discontinuous or discrete design variables. Random walk [25], genetic algorithm (GA), and simulated annealing are examples of such methods. They find problem solutions for various combinations of the design space, the optimized answer being that which has the lowest objective function. The GA uses processes from evolution, a survival of the fittest scheme, to optimize a design. A GA has been used successfully in interplanetary trajectory design [40]. Combined with RSM, a GA performed well for launch vehicle design as well [41].

One advantage of these methods is that no gradients are required. However, disadvantages occur due to the approximate and random nature of parametric and stochastic methods. Only near-optimum solutions can be guaranteed by these methods. In addition, problems may occur when trying to meet constraints, producing infeasible designs.

3.5 Decomposition Methods

In terms of optimization, decomposition methods change the iterative or coupled structure of the DSM of Figure 5 by breaking the feedforward/feedback loops and adding a numerical optimizer to the new structure [42, 43]. The optimizer is now at what is referred to as the system-level, while the contributing analyses are at a sub-level. The breaking of the feedback loops poses the original problem as a noniterative problem in which the analyses are evaluated in a sequential order. A noniterative parallel problem results with the additional breaking of the feedforward loops.

Given that the design space is continuous, the analyses can be integrated into a decomposition scheme with no loss of fidelity in the analysis. Since the analyses are not approximated, the optimal solution of the system-level problem can be found. The numerical optimizer controlling the system-level problem is often gradient-based, which may lead to many function calls of the analyses being required as gradients are calculated. As a result, discrete and piecewise linear design variables are not allowed and are typically fixed in the analyses. Despite these obstacles, the advantages of decomposition methods are enough to warrant their usefulness in design optimization.

Basically, two categories exist for decomposition methods: single-level decomposition and multi-level decomposition. The difference between the two being that for single-level decomposition, optimization occurs on the system-level and for multi-level, optimization occurs at the system and subsystem levels.

Single-level decomposition techniques include optimization-based decomposition, also referred to as "simultaneous analysis and design," SAND, or all-at-once, approaches. In these schemes, analysis iteration is avoided by giving all the control to the system-level optimizer. This leaves the analysis as a function call only. These methods have been used successfully in wing and trajectory design [44, 45], launch vehicle design [46], aircraft design [47], building design [48], and common mathematical problems [49]. These applications are discussed in detail in the next chapter.

The multi-level decomposition technique of collaborative optimization allows the subsystem (or analysis) level control and optimization of its own analysis and the system-level optimizer ensures compatible design variable choices for all analyses. This method has been used successfully in building design [48], launch vehicle design [50, 51, and 52],

aircraft design [45, 53], lunar ascent trajectory optimization [50, 54], bridge design [55], and satellite constellation design [56]. Investigations of the combination of collaborative optimization and response surface methods (to model the optimal subsystem) have been performed for an oil tanker, a tailless unmanned aircraft, the High Speed Civil Transport (HSCT) [57], and wing designs for the HSCT [58]. These applications are detailed in Chapter IV. Other approaches for multi-level decomposition have been proposed and used in structural and helicopter design, in common mathematical problems, and for launch vehicle trajectory design [49, and 59 - 62]. These other multilevel methods differ from collaborative optimization with respect to how the coordination between the system and subsystem levels is performed and how the coupling variables are accounted for.

The research detailed in this thesis will incorporate both single and multi-level decomposition. Optimization-based decomposition will be the single-level decomposition method used. Collaborative optimization will be the method representing the multi-level decomposition methods. These methods are explained in greater detail in Chapter IV.

CHAPTER IV

MDO DECOMPOSITION METHODS IN DETAIL

Multidisciplinary design optimization techniques are expounded upon in this chapter. The methods of fixed-point iteration, optimization-based decomposition, and collaborative optimization are illustrated in detail; in addition, reviews of previous research in this area are included. Constraint gradient formulation for the collaborative optimization method, with regard to post-optimality analysis is discussed. The first MDO method listed, the fixed-point iteration method, is not a decomposition method. It is illustrated in this section so that the decomposition methods, optimization-based decomposition and collaborative optimization, can be better understood.

4.1 Fixed-Point Iteration

A diagram of the fixed-point iteration (FPI) method [63], also known as "nested analysis and design," NAND, is shown in Figure 6 for the generic DSM of Figure 5. The optimizer has control of all the system-level design variables, **x**, which are fed to the analyses, A, B, and C. A, B, and C are still allowed to iterate through use of their feedforward and feedback loops. From the analyses, the system-level constraints are sent to the optimizer. The standard optimization form, equations 9-12, can be used to represent the job of the optimizer for this method.

The major advantage of the FPI method, over the 'One-and-Done' method, is that it will find the true system optimum without conflicting objectives from the subproblems. It

has several disadvantages. The disciplinary experts running the analyses do not have much say in the optimization process. The system optimizer can become large due to the fact that it controls *all* system-level design variables and constraints. A, B, and C must execute iteratively, consuming more real time than if they executed in parallel. Also, noisy gradients occur due to the presence of an iteration tolerance, which causes convergence problems.

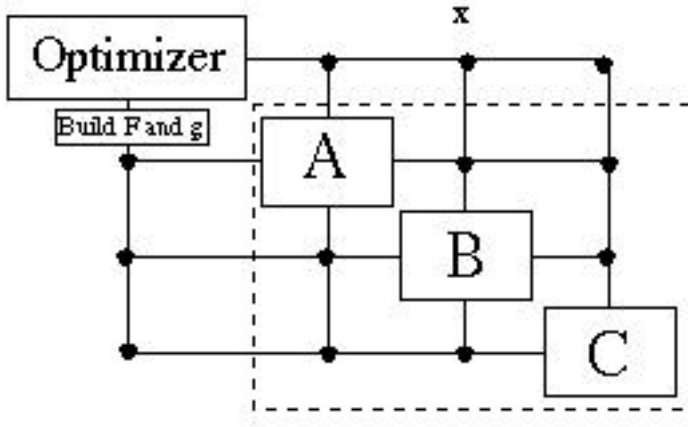

Figure 6: Generic FPI Diagram

4.2 Optimization-Based Decomposition

The single-level decomposition method, optimization-based decomposition (OBD) [63], is illustrated in Figure 7. In this method, the feedforward loops and the feedback loops of the DSM have been broken. Since there is no longer any iteration between the analyses, the system-level optimizer must take over an additional job of ensuring compatibility between A, B, and C. The variables that once were represented by the feedforward and feedback loops, intermediate variables **A**', **B**', and **C**', are now controlled by the system-level optimizer as additional design variables. Along with the system-level constraints, the coupling variables calculated by the analyses, **A**, **B**, and **C**, are also passed to the optimizer. To ensure compatibility between the inputs, **A**', **B**', and **C**', and outputs, **A**, **B**, and **C**, new constraints, called compatibility constraints are formed. These are additional constraints on the system level.

The optimizer's job for OBD can be written in the standard form as follows:

Minimize: $F(\mathbf{x}, \mathbf{A}', \mathbf{B}', \mathbf{C}')$ $\mathbf{x} = x_1, x_2, \ldots x_n$ (13)

Subject to: $g_j(\mathbf{x}, \mathbf{A}', \mathbf{B}', \mathbf{C}') \leq 0$ $j = 1, m$ (14)

$h_k(\mathbf{x}\ \mathbf{A}', \mathbf{B}', \mathbf{C}') = 0$ $k = 1,l$ (15)

$x_i^l \leq x_i \leq x_i^u$ $i = 1, n$ (16)

$\mathbf{A}^l \leq \mathbf{A}' \leq \mathbf{A}^u$

$\mathbf{B}^l \leq \mathbf{B}' \leq \mathbf{B}^u$

$\mathbf{C}^l \leq \mathbf{C}' \leq \mathbf{C}^u$

where **g** includes the compatibility constraints, an example of which is given by equation 17.

$$g_j(\mathbf{x},\mathbf{A}) = ||\mathbf{A}' - \mathbf{A}|| \leq 0 \quad (17)$$

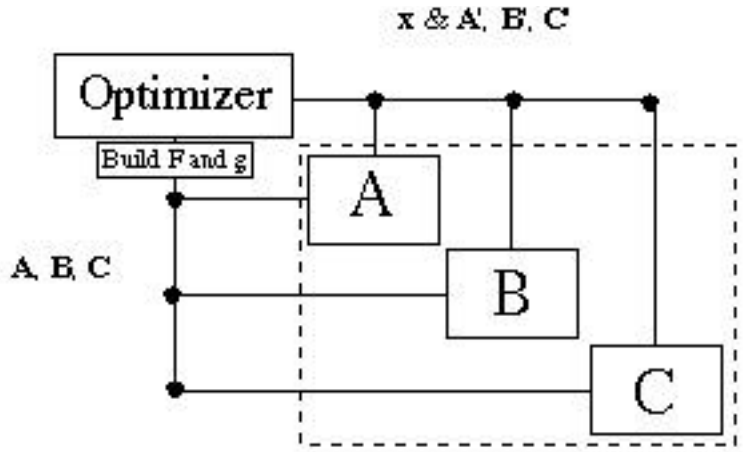

Figure 7: Generic OBD Diagram

Note that the OBD scenario illustrated in Figure 7 is a completely parallel method with respect to execution of the analyses. Another scenario for OBD is when only the feedback loops are broken. This is a partial decomposition (POBD) as opposed to the full decomposition in Figure 7.

An advantage of this parallel scheme is that A, B, and C can be run simultaneously, reducing the execution time even more. This is because there is no iteration (between A, B, and C) for this method. That coupling is handled by the compatibility constraints. Disadvantages are that the size of the optimizer can become quite large and system experts have little say in terms of optimality in their respective analyses.

As stated before, the OBD MDO method has been investigated for various problems, ranging from mathematical problems to launch vehicle design. In [44], fully parallel OBD was used to simultaneously optimize an aircraft and its flight path. Decomposition was achieved on two levels, the flight segments and the disciplinary analyses. This type of decomposition is referred to as '2-dimensional decomposition.' Specific details for that problem appear in [45]. Fixed-point iteration and the partial OBD method were used to solve a single-stage-to-orbit launch vehicle in [46]. Comparisons of the results are included in Section 4.5. In [47], different formulations of the compatibility constraints are listed and each is used to solve a fully parallelized aircraft design problem. With a sequential quadratic system-level optimizer, a compatibility constraint posed as in equation 18 had the highest percentage of converged solutions, while that posed like equation 19 gave the fastest solutions in terms of CPU time.

$$\frac{x}{x'} = 1 \pm \varepsilon \tag{18}$$

$$\left(x - x'\right)^2 \leq \varepsilon \tag{19}$$

In [48], single-level optimization was used to solve the overall minimization of the weight of the exterior frame of a 50-story building subject to structural constraints. Approximately12.5 hours of CPU time was required for one iteration. The problem was solved using collaborative optimization and those results are listed in the next section.

4.3 Collaborative Optimization

The collaborative optimization (CO) [50] method, which is illustrated in Figure 8, is a multi-level decomposition method. For the design represented in the DSM of Figure 5, the application of the CO method would require optimization at the analysis level (indicated by the dashed lines in the analysis boxes) and the system level. In this type of decomposition, the system-level optimizer's job is to coordinate the subsystems' optimization while minimizing the overall objective. In addition to the system-level design variables, the design variables for the system include the coupling variables, now termed targets, $\bar{\mathbf{A}}$, $\bar{\mathbf{B}}$, and $\bar{\mathbf{C}}$. Each analysis is sent a complete set of its targets, regardless if these variables are an input or output of the analysis. Each analysis has a local version of the targets that are selected by the local optimizer or calculated by the analysis.

The system constraints are the sum-squared errors, J_A, J_B, and J_C, between the targets and the local values from each analysis and any system-level constraints. The objective of the subsystems is to minimize its respective error, J_A, J_B, and J_C, while satisfying all its subsystem level (or local) constraints.

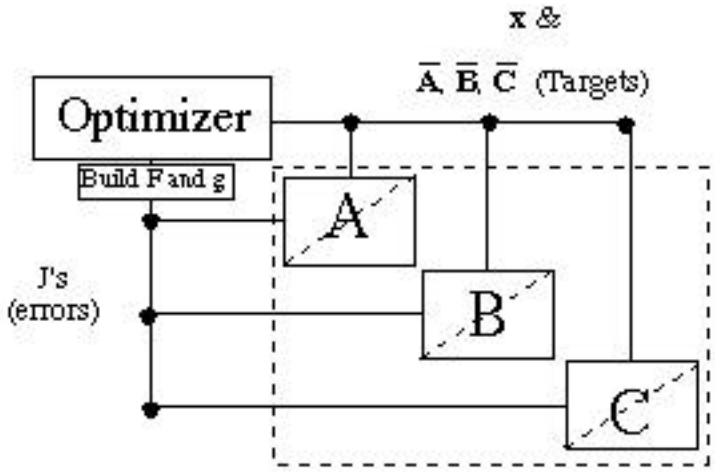

Figure 8: Generic CO Diagram

Because the optimization in this method is on two levels, the goals of the collaborative optimization method can be stated by two standard forms. The system-level optimization is given by equations 20 – 22.

$$\text{Minimize: } F(\mathbf{x}) \qquad \mathbf{x} = x_1, x_2, \ldots x_n \qquad (20)$$

$$\text{Subject to: } g_j(\mathbf{x}) \le 0 \qquad j = 1, m \qquad (21)$$

$$x_i^l \le x_i \le x_i^u \qquad i = 1, n \qquad (22)$$

where **x** includes any system-level design variables and the targets ($\overline{\mathbf{A}}$, $\overline{\mathbf{B}}$, and $\overline{\mathbf{C}}$), and **g** includes the errors, $J_j(\mathbf{x})$, and any system-level constraints required, an example of which is given in Chapter IX. In this case, the errors are given by equations 23 - 25; ε is a small tolerance.

$$J_{\mathbf{A}} = ||\mathbf{B_A} - \overline{\mathbf{B}}||^2 + ||\mathbf{C_A} - \overline{\mathbf{C}}||^2 + ||\mathbf{A} - \overline{\mathbf{A}}||^2 - \varepsilon \le 0 \qquad (23)$$

$$J_{\mathbf{B}} = ||\mathbf{C_B} - \overline{\mathbf{C}}||^2 + ||\mathbf{A_B} - \overline{\mathbf{A}}||^2 + ||\mathbf{B} - \overline{\mathbf{B}}||^2 - \varepsilon \le 0 \qquad (24)$$

$$J_{\mathbf{C}} = ||\mathbf{A_C} - \overline{\mathbf{A}}||^2 + ||\mathbf{B_C} - \overline{\mathbf{B}}||^2 + ||\mathbf{C} - \overline{\mathbf{C}}||^2 - \varepsilon \le 0 \qquad (25)$$

$\mathbf{B_A}$ and $\mathbf{C_A}$ represent A's version (a local version) of the target coupling variables, $\mathbf{C_B}$ and $\mathbf{A_B}$ are B's version, and $\mathbf{A_C}$ and $\mathbf{B_C}$ are C's version. **A**, **B**, and **C** are the output vectors. These values are calculated by analyses A, B, and C, respectively.

The subsystem optimization is given by equations 26 – 29.

$$\text{Minimize: } F(\mathbf{x}_{ss}, \mathbf{c}_l) = J_l \qquad \mathbf{x} = x_1, x_2, \ldots x_n, \; l = \text{A, B, or C} \qquad (26)$$

$$\text{Subject to: } g_j(\mathbf{x}_{ss}) \le 0 \qquad j = 1, m \qquad (27)$$

$$h_k(\mathbf{x}_{ss}) = 0 \qquad k = 1,l \qquad (28)$$

$$x_i^l \le x_i \le x_i^u \qquad i = 1, n \qquad (29)$$

where $\mathbf{x}_{ss}$ is the vector of the subsystem's local design variables, $\mathbf{c}_l$ is the vector of the local versions of the coupling targets, both inputs and outputs (like $\mathbf{A}$, $\mathbf{B}_\mathbf{A}$ and $\mathbf{C}_\mathbf{A}$ in equation 23), and **g** is the vector of local constraints.

A main advantage of the CO method is that disciplinary experts can control their own analyses so that the local objective functions (minimizing the errors) and constraints are met. The system optimizer is relatively small (containing only the target variables, system-level constraints, and the overall objective function) and A, B, and C execute simultaneously, conserving time. CO lends itself well to the design process since the experts' knowledge is still a part of the subsystem optimization processes which is run in a time-saving parallel manner. This method, too, finds the true system-level optimum.

Collaborative optimization has some disadvantages as well. There may be coding or robustness problems given that the analyses have their own optimization problem. This will also contribute to a greater execution time at the local level.

As previously stated, the CO MDO method has been used in the solutions for various problems. Just like for OBD methods, these range from mathematical problems to launch vehicle design problems. References [50] and [54] discuss the development of the collaborative optimization architecture. In addition, lunar trajectory designs and design of an SSTO launch vehicle with cost analysis are solved with this architecture [50, 54]. The lunar trajectory solution was segmented into increasing numbers of paths. When compared to solutions from a standard approach, the CO method was found to perform better, from a CPU and objective function standpoint, as the number of segments was increased.

In [51], the comparisons of the different decomposition methods that were used to solve the SSTO design of [46] are summarized. The addition of the cost analysis is summarized in [52]. Summaries of these comparisons are given in Section 4.5.

The optimal solution of the sizing of the medium range transport aircraft of [44] is solved with collaborative optimization in [53]. The aircraft problem of [47] was also solved with the CO method and comparisons are listed in Section 4.5. CO was used in the design of a cable-supported bridge in [55]. Two subsystems existed at the sub-level.

Nonlinear subspaces can present problems with solution convergence in the CO method. If multiple solutions exist, the subspace optimizer may 'jump' from one solution to the next creating invalid gradient information at the system-level, thus leading to poor performance at the system-level. This problem of design space solution sensitivity was addressed with the introduction of slack variables as the most applicable potential solution to this problem [50].

Since it is a multilevel decomposition scheme, the CO method results in many function call and long CPU times at the subsystem level. In more recent years, research has been performed to reduce these function calls and CPU times. A promising way to achieve this is through use of response surfaces methods to approximate the optimization at the subsystem level. This was implemented in the vehicle designs of [57] and HSCT wing designs of [58] with results incorporated significantly reduced function calls and CPU times.

All of the previously mentioned solutions with the collaborative optimization method used the sequential quadratic programming optimization scheme for the system-level optimization. In [56], CO was used for space based infrared system constellation design. The system-level optimization scheme in that case was a penalty function method. This was due to the fact that gradients were not available for the subsystem analysis solutions, which involved grid search and heuristics in their optimization. However, results were successfully obtained with this system-level optimization that differed from earlier work.

4.4 Post-Optimality Conditions for Collaborative Optimization

Post-optimal sensitivity analysis can be used to investigate trade-offs in design and it can also be used in optimization to aid in finding the optimal solution [64, 65]. Basically, given an optimal solution, post-optimality sensitivity analysis is a useful tool for investigating the effects, on that solution, of varying a parameter that plays a role in the analysis. In general, the crux of the analysis is given by Equation 30. The first term represents the change in the optimal objective function, F*, due to a change in the parameter, p. The second term is the change in F due to a change in p evaluated at the optimum. In the third term, **g** is the constraint vector, **x*** is the set of design variables at the optimal solution,

λ is the Lagrange multiplier vector used to satisfy the Kuhn-Tucker necessary conditions [25], and **r** is the set of constraint boundaries, or ε in the previous equations.

$$\frac{dF^*}{dp} = \left(\frac{\partial F}{\partial p}\right)\Bigg|_{x^*} - \lambda^T \frac{\partial \mathbf{g}(\mathbf{x}^*, \mathbf{p}, \mathbf{r})}{\partial p} \tag{30}$$

The use of post-optimality sensitivity analysis has been successfully demonstrated for collaborative optimization [50, 55, 57, and 58]. Expensive gradient function calls can be eliminated through the knowledge that the subsystems (analyses A, B, and C above) give optimal solutions at each system-level iteration. These optimal solutions, the sum-squared errors, J_l, from Section 4.3, are the constraints for the system-level problem. Thus, the constraint gradients for the system-level optimization problem can be formulated using post-optimality sensitivity analysis. Equation 31 gives the result when equation 30 is applied to the subsystem optimal solutions and is true for each optimized subsystem analysis. For this case, **c*** is the vector of the local versions of the coupling targets, **x**, at the optimum J, and **g** represents the vector of subsystem constraints.

$$\frac{dJ^*}{dx_i} = \frac{\partial J^*}{\partial x_i} - \lambda^T \frac{\partial \mathbf{g}(\mathbf{x}_{ss}, \mathbf{c}^*, \varepsilon)}{\partial x_i} \tag{31}$$

Since the subsystem constraints, **g**, are explicit functions of the subsystem variables ($\mathbf{x}_{ss}$ and **c***) only, the second term of equation 31 becomes zero and equation 32 results [50]. This result is true for all subsystems and target variables, **x**.

$$\frac{dJ^*}{dx_i} = \frac{\partial J^*}{\partial x_i} = -2(c_i^* - x_i) \tag{32}$$

where the generic form of J is

$$J = \sum_{i=1}^{n} \left(c_i^* - x_i\right)^2 \tag{33}$$

Post-optimality sensitivity analysis will be used for the solutions of the collaborative optimization schemes of the problems detailed in Chapters VI and VIII. Equation 33 will be used to calculate the system-level constraint gradients.

4.5 Summary of Decomposition Methods

Several comparisons of decomposition methods exist for aircraft wing design [44, 53], SSTO design [46, 51, and 52], common mathematical problems [49], a civil engineering building problem [48], and ten coupled problems from diverse design fields [66, 67]. Not all methods worked for all design problems, so broad generalizations can be made, but may not be entirely accurate.

For the multidisciplinary wing design problem of [44] and [53], comparisons between the OBD and CO methods revealed that each solution resulted in the same optimum. For that problem, the CO method took several hours to complete while the OBD method was finished in several minutes. In [46], FPI was found to be less computationally efficient than OBD, which had a smoother design space. For the same problem, CO was applied in [51]. Lack of subsystem smoothness in the trajectory discipline created obstacles. That optimizer was taken out and the entire problem was solved in a much greater amount of time than the solutions of [46]. For a similar problem, [52], which added cost to the weights and sizing analysis, the CO method was solved with the trajectory subsystem optimization. It was less computationally efficient than OBD with, on average, many more function calls. However, computationally, it was at the same level with the FPI method. For the problem of [52], the CO method exhibited a much faster set-up time than either the FPI or OBD methods and the communication requirements between the system and subsystem levels were the least for the CO method.

For some problems, CO was found to have fewer function calls than single-level decomposition methods and was found to be less robust [67]. In [49], single-level decomposition techniques were found to be an order of magnitude more computationally efficient than multi-level techniques for ‘trivial’ problems. However, for a ‘non-trivial’, highly coupled problem found in building design, collaborative optimization more computationally efficient [48]. The authors propose that this was due to the facts that the

large problem was segmented info many smaller problems, like that of the lunar trajectory of [50], and that 'engineering intuition' was included to simplify the design. More applications should be tested before any general conclusions can be made regarding the later reason as this result could be problem dependent.

Table 3 summarizes the characteristics of the four proposed MDO solution techniques — fixed-point iteration (FPI), two variations of optimization-based decomposition (OBD), and collaborative optimization (CO). In addition, an entry labeled 'Manual Iteration' is included for comparison. Manual Iteration is simply the 'One-and-Done' (sequential) method iterated to ensure that the coupling variables are internally consistent between the two analyses. The Manual Iteration method is not a preferred solution however, since the conflict between the competing objective functions of the contributing analyses is not resolved. The second column of Table 3 refers to whether the coupled variables are consistent between the analyses at the solution, as is true for all the methods listed. The fourth and fifth columns are interdependent in that if the system-level optimizer is not present conflicting objective functions may occur and vice-versa.

Table 3: Proposed MDO Solution Techniques

Method	Internally Consistent Data	Iteration Required Between Analyses	Potential for Conflicting Objective Functions	Requires System-level Optimizer	Contributing Analysis Execution	Optimizer Strategy
Manual Iteration	Yes	Yes	Yes	No	Sequential	Distributed
Fixed Point Iteration (FPI)	Yes	Yes	No	Yes	Sequential	System Level (large)
Partial OBD	Yes	No	No	Yes	Sequential	System Level (very large)
Full OBD	Yes	No	No	Yes	Parallel	System Level (extremely large)
Collaborative	Yes	No	No	Yes	Parallel	Distributed

CHAPTER V

THE BRANCHING TRAJECTORY PROBLEM FORMULATED USING MDO

Since its structure consists of at least two highly coupled subproblems, the branching trajectory problem resembles more common multidisciplinary problems such as the coupling between structures and aerodynamics (even though, in this case the subproblems are actually of the same discipline!). For that reason, solution techniques from the field of Multidisciplinary Design Optimization (MDO) can be advantageously applied to its solution. MDO methods have been successfully proposed for and/or used in the solutions to highly coupled subproblems from a single discipline. These disciplines include: wing design of the HSCT [58], fluid dynamics [68], and propulsion with respect to the linear aerospike [69].

This study utilized the Program to Optimize Simulated Trajectories (POST I) in order to simulate the branching trajectories. In the following figures, the orbital branch will be designated as 'Orbit.' The flyback branch will be denoted as 'Flyback.' The ascent trajectory will be labeled 'Ascent.' When the internal optimization capability in POST is enabled, a box with a diagonal line will indicate that POST is being used for trajectory analysis *plus* local optimization. A plain box will indicate that POST is simply being used to integrate along a given trajectory.

5.1 The Fixed-Point Iteration Method

In the FPI method of Figure 9, the system optimizer has control of *all* trajectory variables and constraints. Each trial step from the system optimizer requires a series of iterations between Ascent, Orbit, and Flyback. Given guesses for upper stage and flyback fuel weights and its initial trajectory variables from the optimizer, Ascent runs in non-optimizing mode (i.e. it simply integrates the equations of motion along the given trajectory and returns the results). The resultant staging vector ($\mathbf{P}_s$) is then input to Orbit and Flyback. With these initial conditions as a starting point and their subset of trajectory variables from the system optimizer, Orbit runs in non-optimizing mode, followed by Flyback. The new upper stage weight, w_{us}, and the new flyback weight, w_{fb}, are fed back to Ascent through a resizing process. The iterations between Ascent, Orbit, and Flyback continue until the convergence criterion is met to within a certain tolerance. After the iteration process is completed, the outputs from each POST analysis are fed back to the system optimizer to determine the objective function and system constraints. The control variables are then changed in order to minimize/maximize the system-level objective.

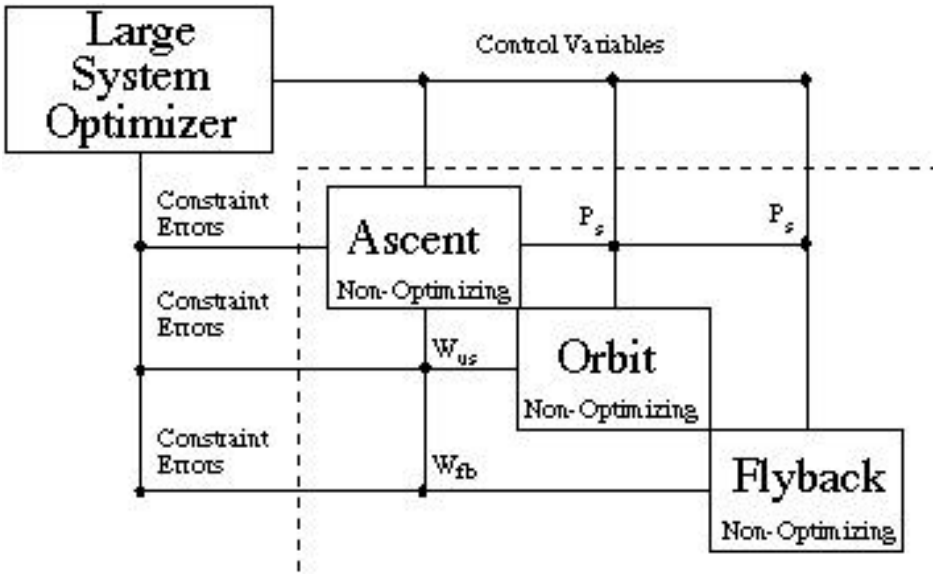

Figure 9: FPI for Branching Trajectories

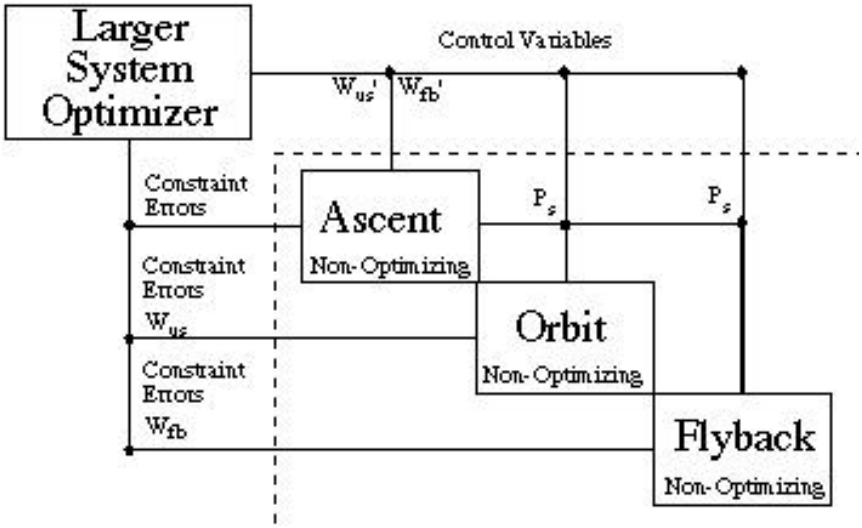

Figure 10: POBD for Branching Trajectories

5.2 The Optimization-Based Decomposition Methods

The optimization-based decomposition methods also require a system optimizer with an objective function to optimize the system-level objective. In the partial OBD method, the feedback loops from Orbit and Flyback to Ascent in the FPI method are broken. Two additional design variables for Ascent are now needed to replace the weights, which were originally fed back. These are the prescribed upper stage weight, w_{us}', and the prescribed flyback fuel weight, w_{fb}', which are controlled by the system-level optimizer. Two compatibility constraints added to the system optimizer are used to ensure agreement between the prescribed weights and the true weights output from Orbit and Flyback at the solution. As a result, iteration is no longer required between Ascent, Orbit, and Flyback to ensure data consistency. A diagram of this method can be seen in Figure 10. The booster will be resized, as a function of the flyback fuel requirement, during the optimizer's execution.

In the full OBD method of Figure 11, both the feedback and the feedforward loops that can be seen in the FPI method diagram are broken. In addition to the new design variables and compatibility constraints from the broken *feedback* loops (defined in the previous paragraph), a set of intermediate variables representing the prescribed staging

conditions is created at the system level ($\mathbf{P}_s$') to be provided directly to Orbit and Flyback. This effectively breaks the *feedforward* loops as well, and creates a parallel set of subproblems. Compatibility constraints are also added to the system optimizer to ensure that, at the final optimum, the intermediate variables ($\mathbf{P}_s$') match the actual conditions ($\mathbf{P}_s$) produced by Ascent.

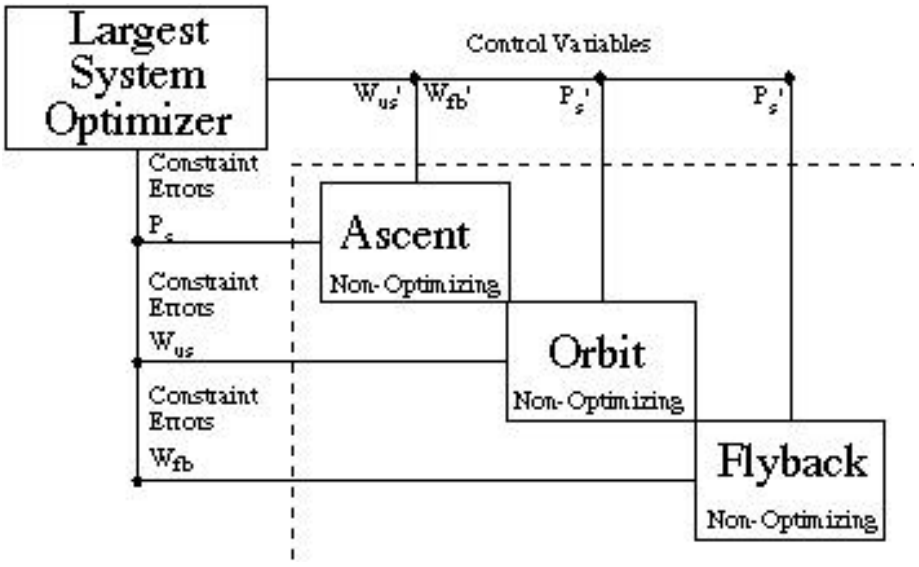

Figure 11: FOBD for Branching Trajectories

5.3 The Collaborative Optimization Method

In the collaborative optimization technique, a system optimizer is incorporated with an objective function of optimizing the system-level objective (Figure 12). The system optimizer chooses target initial condition vectors and weights ($\bar{\mathbf{P}}_s$, $\bar{w}_{us}$, and $\bar{w}_{fb}$ targets) which are to be used in Ascent, Orbit and Flyback which are all run in *optimizing* mode. Each tries to satisfy its own (local) constraints (ascent, orbital, or landing) with its own trajectory variables while minimizing the error between its local versions of the staging variables and the system optimizer's targets. The sum of the squares of the local errors (J_A, J_O, and J_F) become additional constraints for the system optimizer. The system optimizer changes the new target staging conditions until the errors are zero and the system-level

objective function is optimized. In this method, the resizing event will occur during the system optimizer execution.

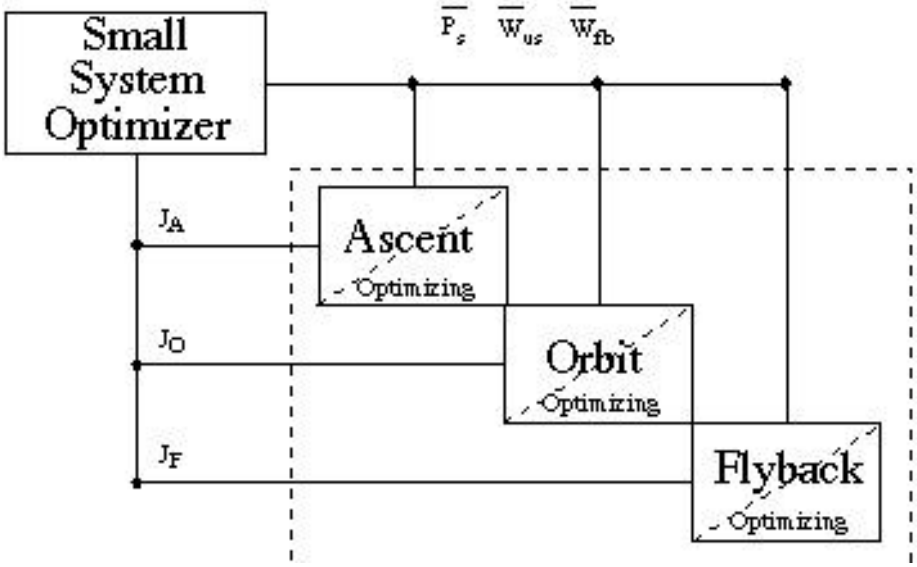

Figure 12: CO for Branching Trajectories

CHAPTER VI

THE FIRST APPLICATION: THE KISTLER *K-1* LAUNCH VEHICLE

To provide applicability to this research, the missions of two candidate TSTO launch vehicle designs have been chosen to serve as reference missions. In this chapter, the Kistler *K-1* launch vehicle is described. The results for this application are analyzed in Chapter VII. In Chapters VIII and IX, the second application and its results, respectively, are reported.

6.1 The Kistler *K-1* Launch Vehicle

Many launch vehicles are currently being developed by commercial industries with the goal of capturing a profitable share of the growing satellite launch market. Such is the case of the Kistler *K-1* launch vehicle [70, 71]. The *K-1* (Figure 13, [72]) will be a fully reusable, two-stage vehicle that incorporates branching trajectories. The vehicle's booster will use three Aerojet modified NK33 engines [73, 74]. The *K-1's* upper stage will be propelled by one Aerojet modified NK43 engine [73, 74]. There will be different versions of the vehicle to accommodate various payload classes. One of its missions will be to deliver a certain payload to a 50 nmi x 846 nmi x 51˚ orbit. This is the mission that will be analyzed in this study.

The data (weights, trajectory constraints, engine data, etc.) pertaining to the aforementioned mission was provided directly by Kistler Aerospace [75]. An outline of the weights used, dry and propellant weights, for both stages are listed in Appendix A.

As mentioned in Section 2.4, POST requires inputs to evaluate the aerodynamics of a vehicle. The tool, Aerodynamic Preliminary Analysis System, APAS [76], was used to generate the aerodynamic data for this problem. In particular, for this case, three sets of aerodynamic data were generated. A table of lift, drag, and moment coefficients, as a function of Mach number and angle of attack, was created for each of the three configurations for the *K-1*: the vehicle as a whole, the booster by itself, and the upper stage by itself. Appendix B lists more detailed information about the aerodynamics for the *K-1*. POST also requires propulsion data input. Also contained in Appendix B is information about the engines' performance for the *K-1*.

Figure 13: The *K-1*

Figure 14: The *K-1* Flight Profile

6.2 The Kistler *K-1* Trajectory

The trajectory of the *K-1* launch vehicle can be seen in Figure 14 [72]. It will consist of an RTLS type branching trajectory as in Figure 1. After launch from the site at Woomera, Australia, (1) the entire *K-1* will fly until staging approximately 120 seconds later (2). After staging, the booster performs a pitcharound maneuver that will guide itself back to within 10,000 ft of the launch site, to land with airbags and parachutes. The upper stage will continue on to the designated orbit (3). For the purposes of this study, the simulation will end when the orbital targets have been attained. In reality, after expulsion of the payload (4) the *K-1's* upper stage will deorbit (5) and return to the launch site (6).

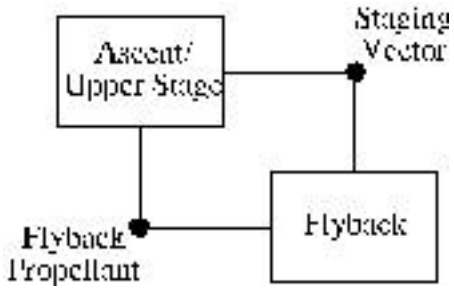

Figure 15: The DSM for the *K-1*

The trajectory is simulated through two POST decks as indicated by the DSM for the *K-1*'s trajectory as shown in Figure 15. The first POST deck follows the vehicle from launch to orbital injection of the upper stage. Note that this specific simulation combines the Ascent and Orbit jobs. The second, or flyback branch, follows just the booster from staging to its return to the launch site. In addition to a three-degree-of-freedom simulation, each POST deck uses the following modeling options: 1976 standard atmosphere, lift and drag aerodynamic coefficients, fourth order Runge-Kutta integration with a one second integration step size, and a spherical Earth approximation.

Table 4: POST Controls and Constraints for the *K-1*

POST Deck	Number of Independent Variables	Number of Constraints
Ascent	13	5
Flyback	6	2
Total	19	7

Table 4 lists the number of controls and constraints used by the ascent and flyback trajectory decks. The reference *K–1* ascent trajectory deck's independent variables are twelve pitch angles and payload weight. The ascent has five constraints involving orbital insertion criteria and dynamic pressure boundaries. The vehicle is steered by a table look-

up of inertial pitch angles. Nominally, the objective of the orbital branch is to maximize the payload for a given set of propulsion characteristics, vehicle aerodynamics, *K-1* weights, and ascent propellant.

The reference flyback trajectory deck uses six independent variables: four pitch angles, azimuth of the pitcharound maneuver needed to initially head the vehicle in a direction back to the launch site, and engine burn time. The two constraints guarantee a smooth rocket pull-up and landing within a certain downrange distance. Given a set of engine propulsion characteristics, aerodynamics, and a staging point, the flyback trajectory nominally tries to minimize flyback fuel weight. The required staging point data from the ascent branch includes altitude, flight path angle, latitude, longitude, velocity, and velocity azimuth. The booster is steered initially by an angle of attack of 180 degrees used to head the vehicle back to the launch site. The turnaround maneuver is achieved with pitch angle steering.

6.3 The Objective Function for the Kistler *K-1*

Note that there are many ways to optimize the trajectories of both the upper stage and the booster. Should the booster ascent propellant be resized if necessary? Should all inert weights remain fixed? Should the system-level objective be maximum orbital payload or minimum booster weight?

For the *K-1* simulation, fixed weights were used for all weights except for booster ascent propellant weight, flyback fuel weight, and payload weight. Consequently, the exterior of the vehicle stayed the same throughout thus did the aerodynamics as well. The constant total propellant weight, given by equation 34, was the sum of the booster ascent propellant weight and the flyback fuel weight used. (Note that pre-liftoff propellants are subtracted from the total propellant.) This equation was very easily coded into the system-level optimizer. The payload weight was the objective to be maximized.

$$487{,}823 \text{ lbs} = \text{ascent\_propellant} + \text{flyback\_propellant} \qquad (34)$$

CHAPTER VII

RESULTS FOR THE *K-1* LAUNCH VEHICLE

Results for solutions to the Kistler *K-1* branching trajectory problem are presented in this chapter. Solutions for the 'One-and-Done' method, manual iteration method, and the distributed method using MDO techniques are analyzed. All executions of the POST decks, system-level optimization code, and any associated codes were performed on the Silicon Graphics Octane platform with a 300 MegaHertz IP30 processor using an R12000 processor chip.

7.1 Methods with Conflicting Objective Functions

7.1.1 'One-and-Done' Method

The solution for the 'One-and-Done' method for the *K-1* is outlined in Figure 16. The method does not account for the iterative, coupled nature of the ascent and flyback branches. The data extraction/insertion from one POST deck to the next was performed manually. The results for this method appear in Table 5. The solution for this method will be the starting point for all the methods following this one. As a result, computational time is not listed for this method. The main reason to show this method's results is to see the large difference in the objective function (recall that the goal is to maximize payload weight) that can be achieved when iteration occurs.

Table 5: ‘One-and-Done’ and Manual Iteration Method Results (*K-1*)

Method	Payload Weight (lbs)	POST Computational Time	Number of Iterations
‘One-and-Done’	3314.7881	-	0
Manual Iteration	3528.7911	201.4 sec (3.36 min)	6

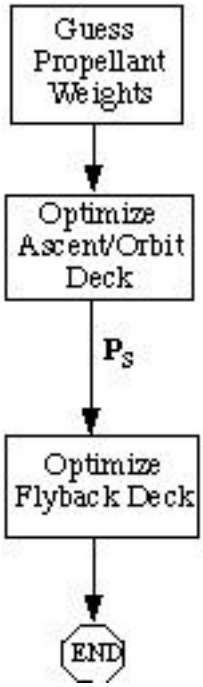

Figure 16: ‘One-and-Done’ Method Flowchart, *K-1*

For this method, the initial guess for booster ascent propellant is significant. The percentage of booster ascent propellant, with respect to the total available, used for this simulation was 92.88%. This left a little more than 7% for the flyback fuel. After the serial execution of the two POST decks, it was found that 14.6% of the initial flyback fuel was left over, or not used. If the guess for booster ascent propellant percentage was too high, then the possibility of not having enough flyback fuel would have existed. In that case, as far as the flyback simulation is concerned, the constraints would have been met, however, negative propellant would be used. In other words, the POST deck would have used the dry weight

as propellant, resulting in an obviously wrong answer. That scenario highlights an example of one of the many deficiencies of this method.

As stated previously, the next method and the MDO methods will all begin with the solution to the 'One-and-Done' method. Thus, the initial guesses are as follows: percentage of flyback fuel – 6.08% (the original initial guess less 14.6% of that guess, resultant percentage of booster ascent propellant – 93.92%, and payload weight – 3,314.79 lbs.

7.1.2 Manual Iteration Method Results

The manual iteration method uses two subproblem optimizers and no system-level optimizer. A flowchart of the method can be seen in Figure 17. Execution is sequential and iterative between the ascent deck and the flyback deck. The flyback weight is updated as the iterations occur. Again the data extraction/insertion is manual. Iteration information and execution time results are shown in Table 5. For this case, iteration was performed between the two basic subproblems to ensure data consistency (unlike the 'One-and-Done' method), however the conflicting objective functions were not addressed. The convergence criterion for the manual iteration method was flyback fuel weight. The *K-1* was considered converged when this variable came within .01% of the result from the previous iteration. This result will be used as a comparison case in the MDO method assessments. The final design variables used for this method are listed in Appendix C.

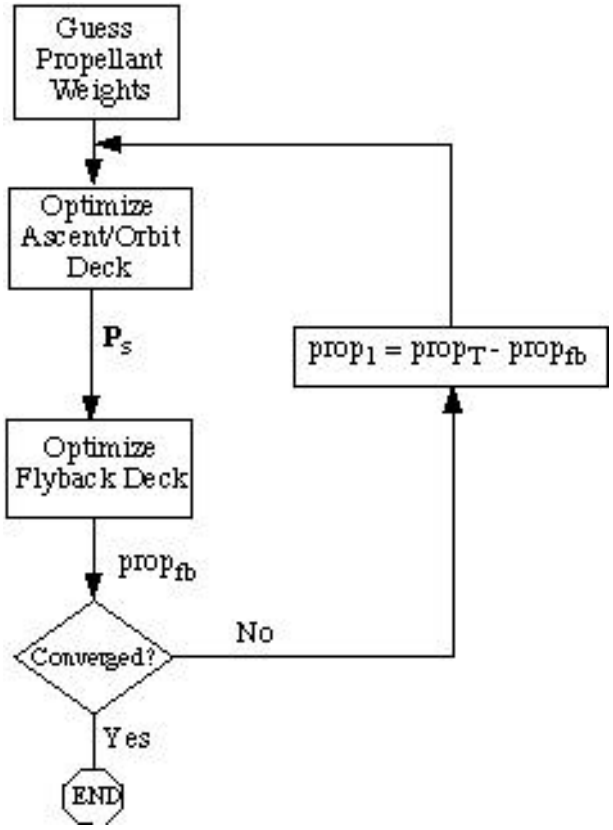

Figure 17: Manual Iteration Method Flowchart, *K-1*

7.2 The System-Level Optimizer

The Design Optimization Tool, DOT™ [77], is a commercial optimization program that is supplied without charge for academic research. It provides several algorithms for optimization that have been used to generate the results for the MDO methods. The program contains optimization methods for constrained and unconstrained problems. For branching trajectories, the MDO methods used result in constrained problems. The available algorithms are: modified method of feasible directions (MMFD), sequential linear programming (SLP), and sequential quadratic programming (SQP). Each uses gradient information to find a new direction to look for the optimal solution. The new direction for MMFD, or search direction, is based on lowering the constraint violation while minimizing the objective function. For the SLP and SQP methods, Taylor Series approximations of the objective function and constraints are used in optimization. The SLP method solves the

linear approximate optimization problem. The SQP method solves the optimization problem using a search direction based on the quadratic approximate problem optimization problem with linearized constraints.

7.3 Multidisciplinary Design Optimization Results

Table 6 shows the system optimizer size for the *K-1* case. DOT™ requires that equality constraints be formulated as inequality constraints. The equality constraints for all the POST decks were posed as two inequality constraints. Three of the constraints from Table 4 were equalities; formulated as inequality constraints, this brings the total number of constraints for the FPI method to ten. Note that for the POBD method, there were either one or two more constraints in addition to those of the FPI method. The compatibility constraint can be posed as either a squared inequality constraint (eleven total constraints, equation 35) or two inequality constraints (twelve total constraints, equation 36.) The compatibility constraints for the full OBD method were posed as seven pairs of inequality constraints, thus the total number of constraints was twenty-four. Note that the compatibility constraints, like all the other constraints, are normalized to aid in the numerical conditioning of the problem.

Table 6: Size of System Optimizer for Kistler *K-1* Cases

	Variables	Constraints
Manual Iteration	-	-
FPI	19	10
Partial OBD	20	12/11
Full OBD	26	24
Collaborative	8	2

$$g_i = \left(\frac{fb_w - fb_w'}{10{,}000} \right)^2 \leq 0 \qquad (35)$$

$$g_{i,i+1} = \pm\left(\frac{fb_w - fb_w'}{10{,}000}\right) \leq 0 \qquad (36)$$

It is imperative to note that while the number of target variables for the collaborative optimization scheme is expected to be seven (flyback fuel weight plus the six staging vector components), eight appear in Table 6. This will be expounded upon in Section 7.3.4.

7.3.1 Fixed-Point Iteration Method

The flowchart for the FPI method can be seen in Figure 18. The entire process, including data extraction/insertion and gradient calculation was automated. The 'grayed' boxes in the figure represent those parts of the process that were coded in C++ such as the main execution program of the optimizer. Data extraction/insertion was achieved with PERL (Practical Extraction and Report Language) and is represented, in the figure, by dashed arrows. The system-level optimizer used was the Modified Method of Feasible Directions.

The Fixed Point Iteration method involves use of a system-level optimizer and POST deck iterations. The POST decks are not optimized for this method. They are used to integrate the equations of motion using the set of controls given by the system-level optimizer. The POST deck iterations were considered converged when the flyback fuel weight was within 0.01% of itself, just like in the manual iteration method. The gradients for the system-level optimizer were calculated using central finite differences with varying perturbation sizes that were dependent on the size and type of the original design variable.

Quantitative results for this method were obtained using the optimization scheme of the Modified Method of Feasible Directions and detailed results can be seen in Tables 8 & 9 in Section 7.4. The FPI method gave an optimized solution of 3,544 pounds of payload weight in 16.3 minutes with eighteen system-level iterations. Appendix C lists the final set of design variables for this method. Figure 19 shows how the payload weight varied with function call. In addition, the plot shows the number of MMFD iterations, the line searches needed to define the search direction, per function call. Figure 20 shows the log of the

active constraints at each MMFD iteration. Active constraints are those that were either violated or greater than –0.5.

In Figure 20, the line denoting the 'feasible solution' was found by calculating the log of the 2-norm of the accepted tolerances of the active constraints. For example, all of the constraints for the FPI method were scaled such that a single tolerance, ε, of 0.0001 was used for all the constraints. If 'n' constraints were active, the equation used for the feasible solution at iteration one would be that of equation 37. The 'feasible solution line for all MDO methods was similarly calculated based on the number of active constraints, n, and acceptable tolerances, ε.

$$\log\sqrt{\left(n\varepsilon^2\right)} \tag{37}$$

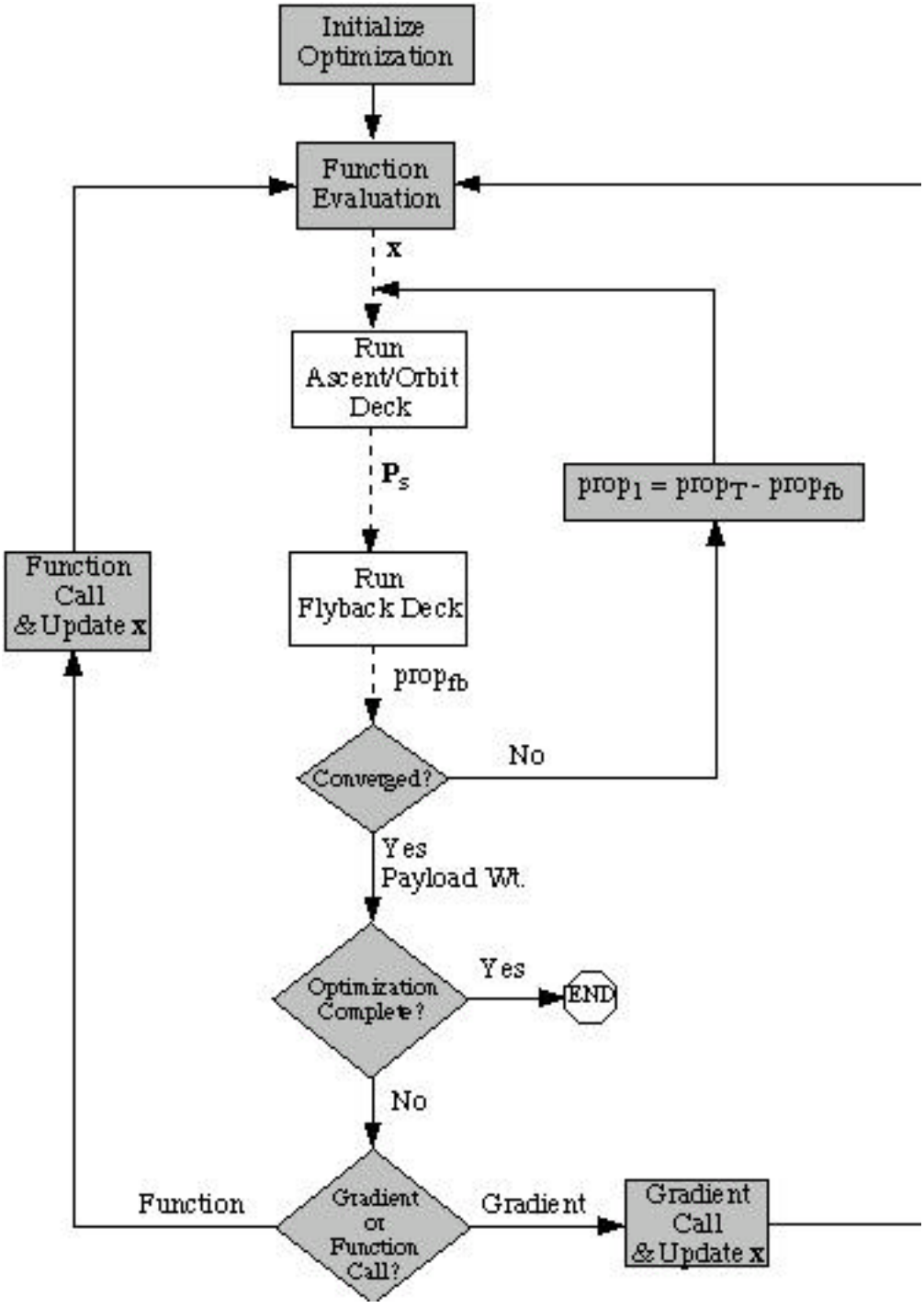

Figure 18: FPI Flowchart, *K-1*

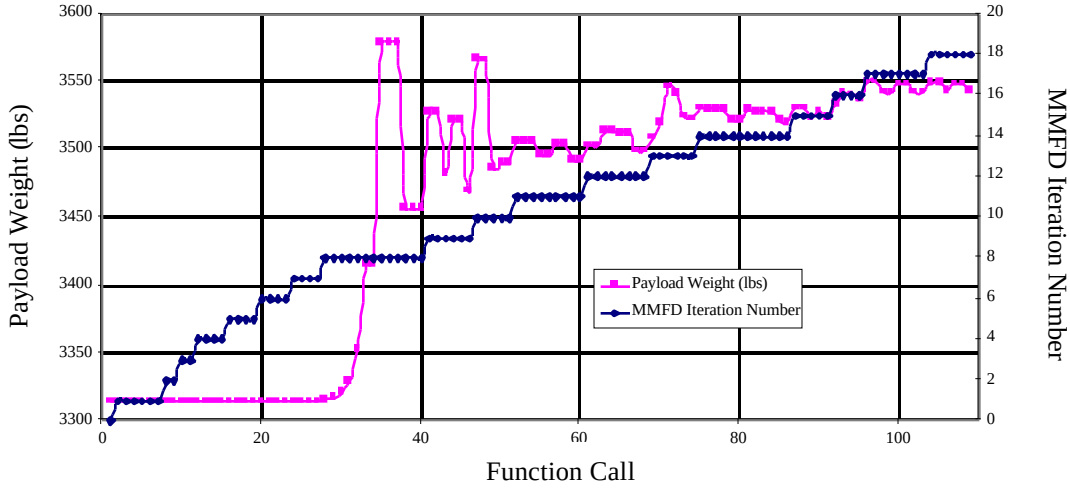

Figure 19: Payload Weight Tracking for FPI Method

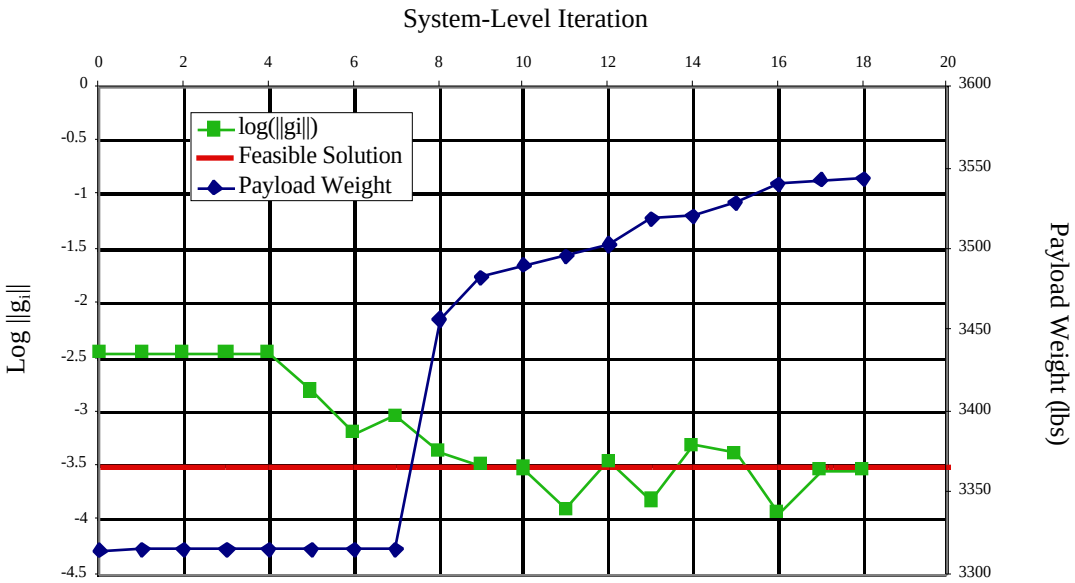

Figure 20: Active Constraint History for the FPI Method

7.3.2 Partial Optimization-Based Decomposition

The flowchart for the POBD methods, with the compatibility constraint posed as either one or two inequalities as described in Section 7.3, can be seen in Figure 21. For these methods, the compatibility constraint is needed for the flyback fuel weight only.

Like the FPI method, the POBD methods involve use of a system-level optimizer and POST decks that are not optimized, however, feedforward of the staging vector still exists. The gradients for the system-level optimizer for these methods were also calculated using central finite differences with a varying perturbation size. Again, the entire process, including data extraction/insertion and gradient calculation was automated. Those parts of the process that required a C++ program are shown as gray boxes in Figure 21. Data extraction/insertion was achieved with PERL and is indicated by dashed arrows in the figure.

The system-level optimizer was the MMFD for these methods as well. The POBD methods resulted in an optimized payload weight of 3,567 pounds in twenty system-level iterations requiring 15.7 minutes. Detailed numerical results are listed in Tables 8 & 9 in Section 7.4. Appendix C lists the final set of design variables for this method. Figure 22 shows how the payload weight changed at each function call. Additionally, the plot shows the number of MMFD iterations per function call. Figure 23 shows the log of the active constraints at each MMFD iteration. Data for the POBD method that had the flyback fuel weight compatibility constraint posed as two inequalities is shown in Figures 22 & 23; the data for the POBD method that had the flyback fuel weight compatibility constraint posed as one inequality was nearly identical.

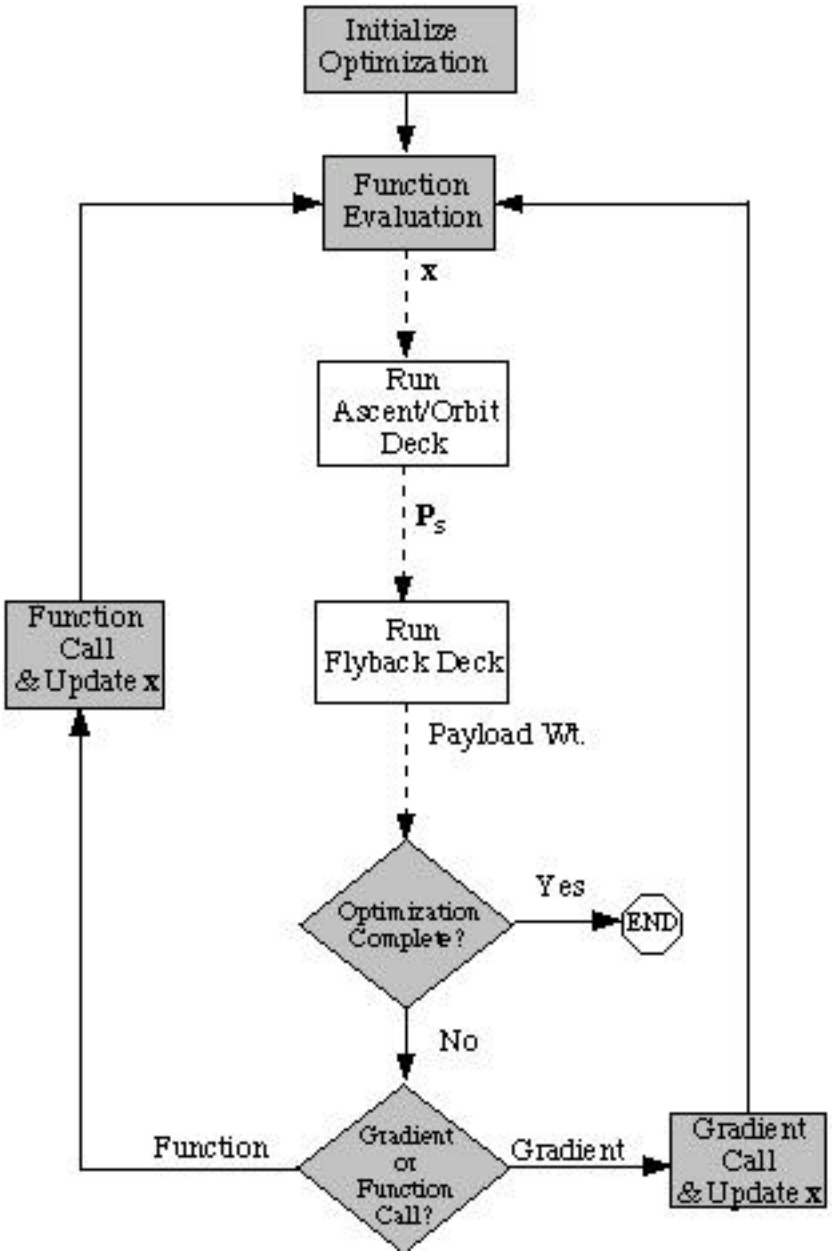

Figure 21: POBD Flowchart, *K-1*

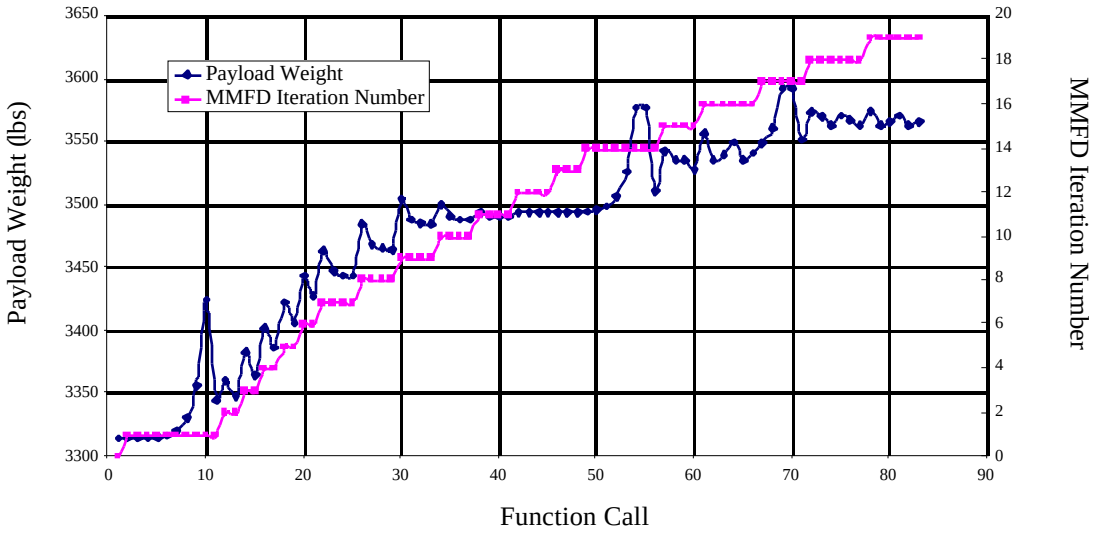

Figure 22: Payload Weight Tracking for POBD Methods

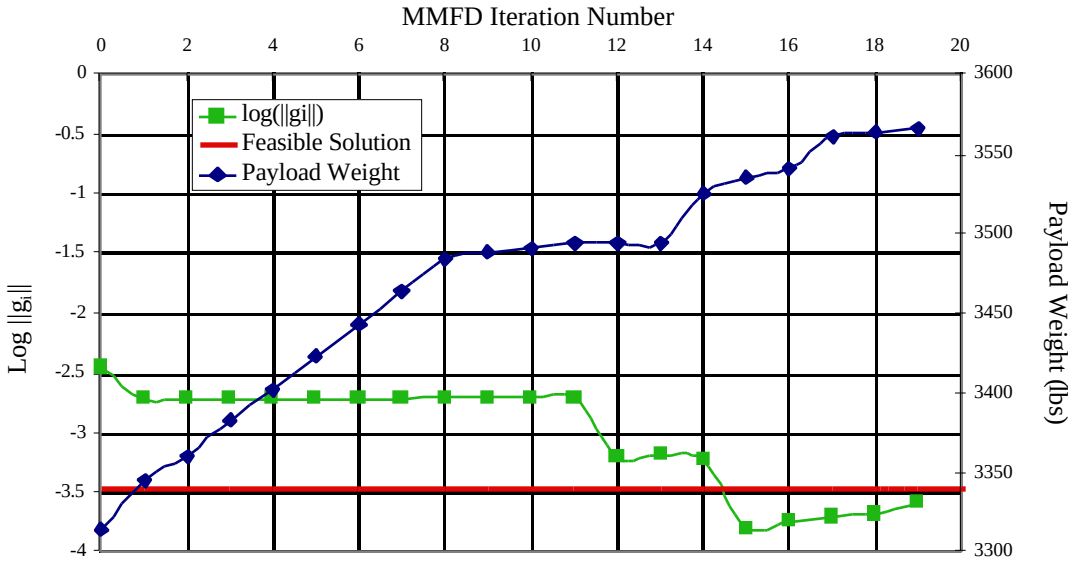

Figure 23: Active Constraint History for the POBD Methods

7.3.3 Full Optimization-Based Decomposition

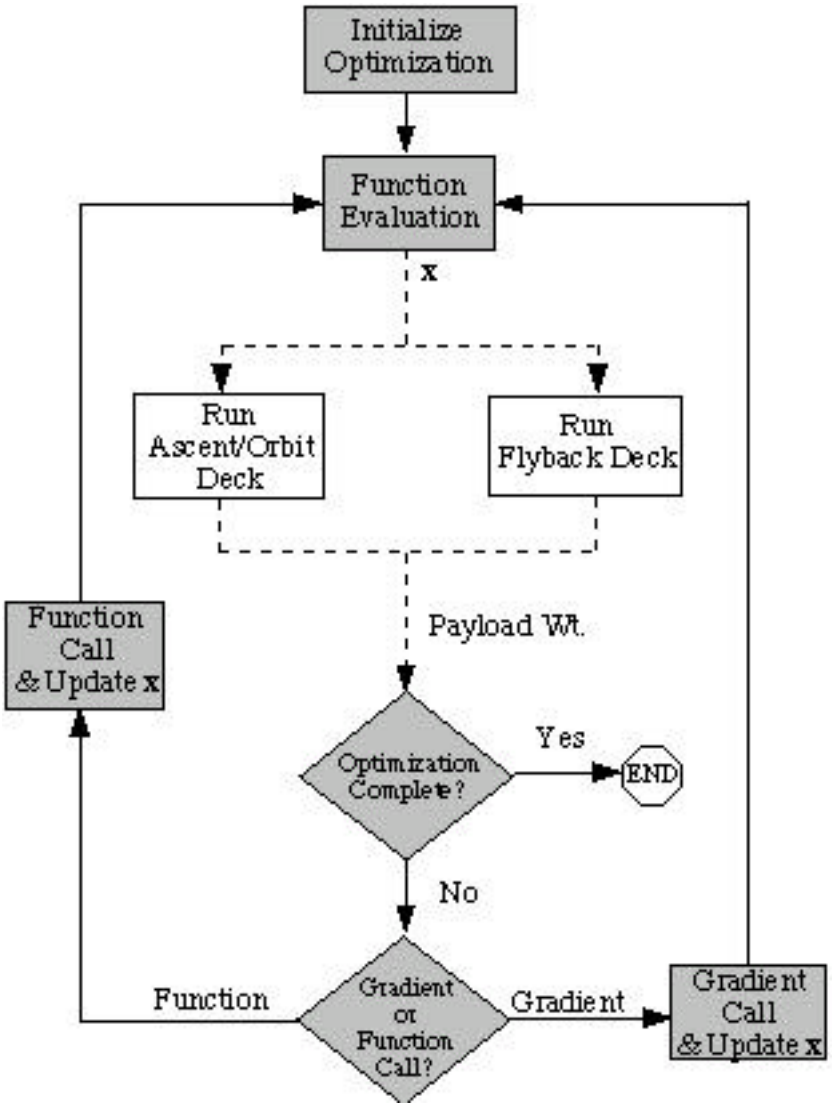

Figure 24: FOBD Flowchart, *K-1*

The flowchart for the FOBD method, with the compatibility constraints posed as pairs of inequalities as described in Section 7.3, can be seen in Figure 24. There are seven compatibility constraints needed for this method: flyback fuel weight and the staging vector

of altitude, velocity, azimuth velocity, flight path angle, latitude, and longitude. All of these constraints are normalized in the problem set-up.

The FOBD method requires the use of a system-level optimizer and POST decks that do not themselves optimize. For this method, there is no feedback *or* feedforward and the POST decks are executed in parallel. The gradients for the system-level optimizer for this method were also calculated using central finite differences with a varying perturbation size. The entire process, including data extraction/insertion and gradient calculation was automated. Those parts of the process that required a C++ program are shown as gray boxes in Figure 24. Data extraction/insertion was achieved with PERL and is indicated by dashed arrows in the figure.

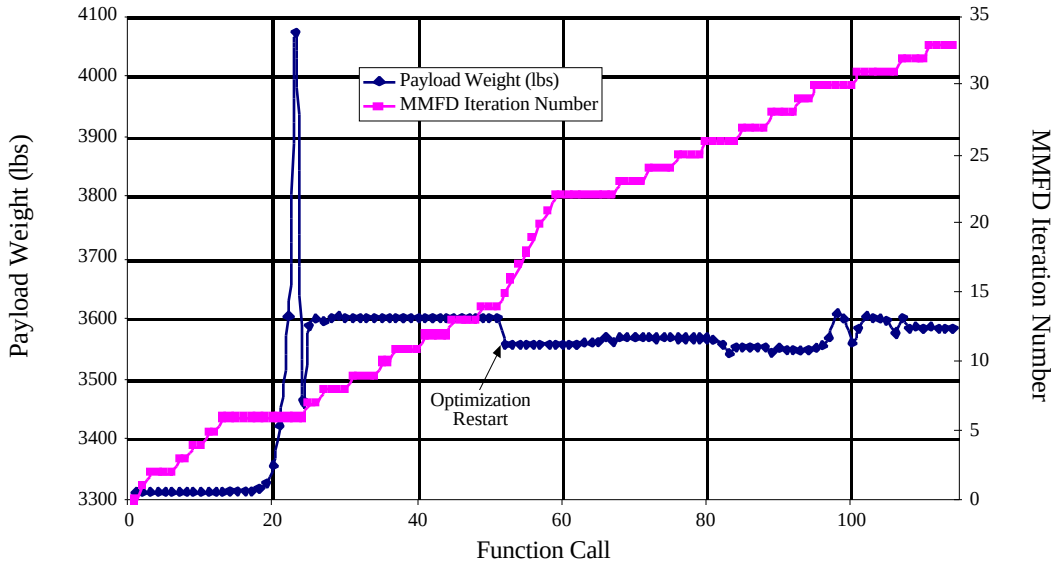

Figure 25: Payload Weight Tracking for the FOBD Method

The system-level optimizer was the MMFD for the FOBD method. The optimization had to be restarted once due to a lack of progress the first time. After this restart, an optimal solution of 3,585 pounds of payload weight was found. This took about sixteen minutes total in thirty-four system-level iterations for the entire problem. Quantitative results are listed in Tables 8 & 9 in Section 7.4. Appendix C lists the final set

of design variables for this method. Figure 25 shows how the payload weight changed at each function call. Additionally, the plot shows the number of MMFD iterations per function call. Figure 26 shows the log of the active constraints at each MMFD iteration.

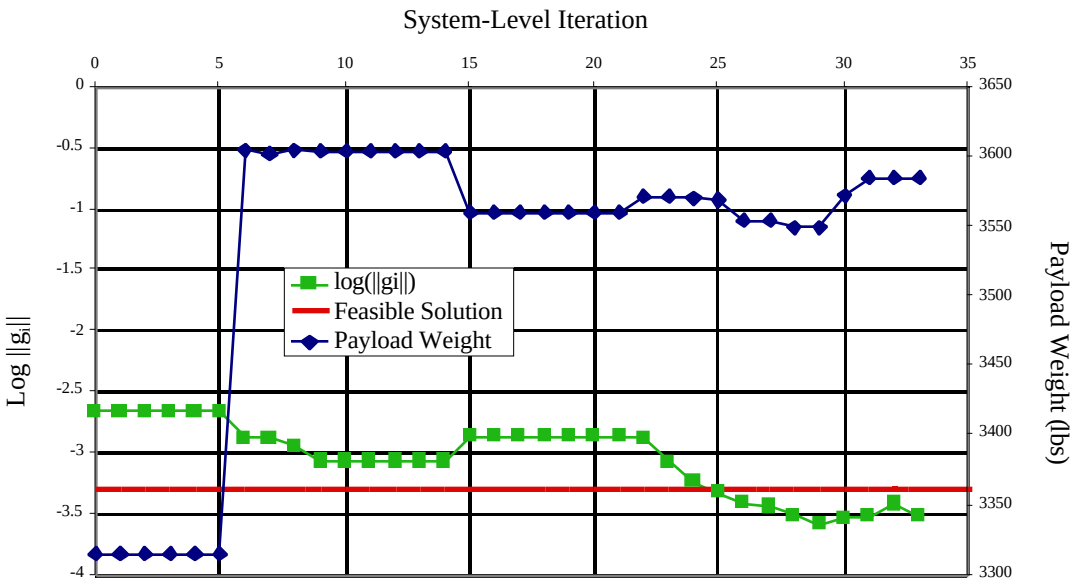

Figure 26: Active Constraint and Objective History for the FOBD Method

7.3.4 Collaborative Optimization

Figure 27 shows the flowchart for the CO method. The CO method involves the use of a system-level optimizer and a parallel analysis structure. However, for this multi-level decomposition scheme, the POST decks *are* optimized using the NPSOL optimizer included in the POST software.

The entire process, including data extraction/insertion and gradient calculation was automated. Those parts of the process that required a C++ program are shown as gray boxes in Figure 27. Data extraction/insertion was achieved with PERL and is indicated by dashed arrows and box lines in the figure. The dashed lines in the analysis (POST) boxes indicate that the POST optimizer is in use. After each gradient call, the local POST design

variables are copied into the corresponding POST decks as the new controls. This was done in an effort to minimize the number of function calls required at the subsystem level. The CO method gave an optimal solution of 3,569 pounds of payload weight. This was attained in seven system-level iterations requiring 1.84 hours. More results are given in Section 7.4.

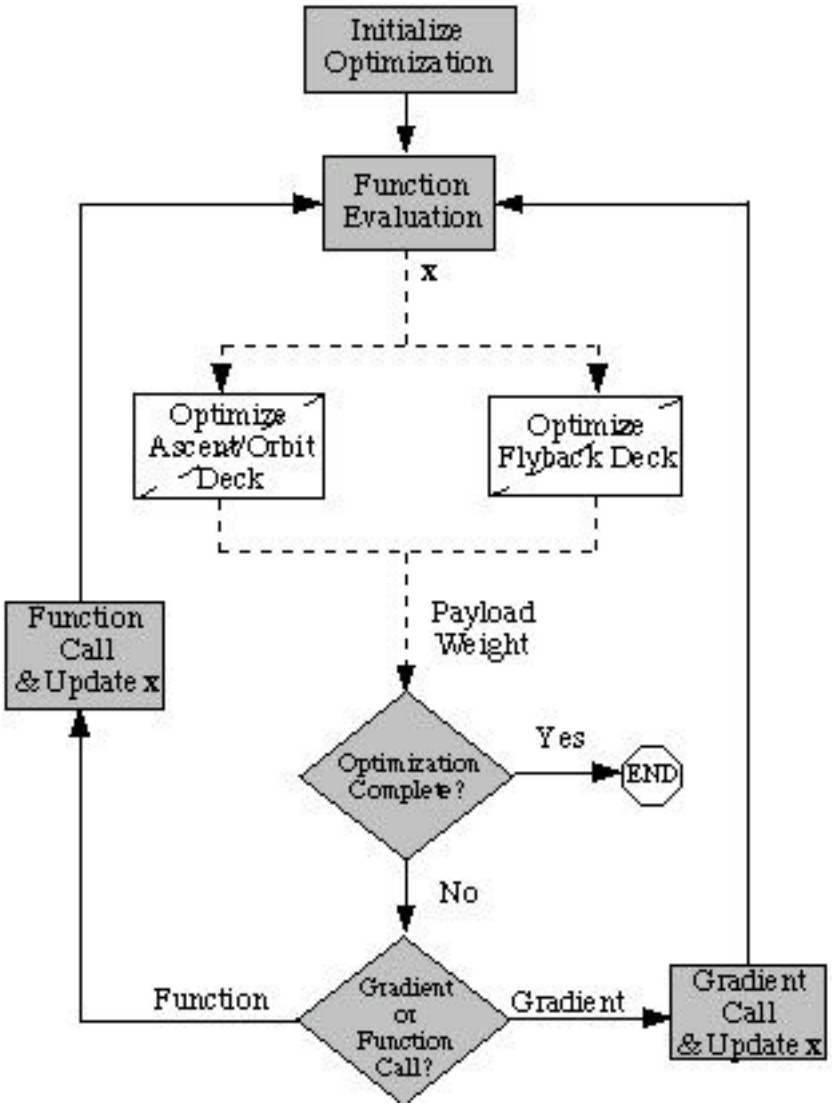

Figure 27: CO Flowchart, *K-1*

There were eight target variables required for this method. These included the payload and flyback fuel weights and the six variables that composed the staging vector. Table 7 shows how these target variables were perceived by the ascent and flyback POST decks, as either inputs or outputs. The system-level constraints, or J's, were calculated accordingly.

Table 7: Targets' Relationship to POST Decks for *K-1*

	Ascent Deck	Flyback Deck
Payload Weight	Input	-
Flyback Fuel Weight	Input	Output (as a function of Eqn. 26)
Staging Altitude	Output	Input
Staging Velocity	Output	Input
Staging Azimuth Velocity	Output	Input
Staging Flight Path Angle	Output	Input
Staging Latitude	Output	Input
Staging Longitude	Output	Input

Constraint gradient calculations were performed using the post-optimality sensitivity analysis introduced in Section 4.4. The benefit from this analysis, in that numerous analysis calls can be eliminated, is exploited if the objective function gradient can also be calculated analytically. This can be achieved by adding the objective function, in this case, payload weight, to the vector of targets. In addition, it is now included in the error, J, for the ascent deck and is perceived as an output *from* the ascent deck (but an input/control *in* the ascent deck). Consequently, the objective function gradient can now be easily and analytically derived. This target's inclusion in the flyback deck is not required since it is neither an input nor an output for that analysis.

Figure 28 shows how the payload weight varied per system-level function call. This plot also shows how the payload weight from the ascent deck follows the payload weight target. They are matched almost exactly because the payload weight is a control, or

dependent variable, in the POST deck and it can easily be changed to meet the target requirement.

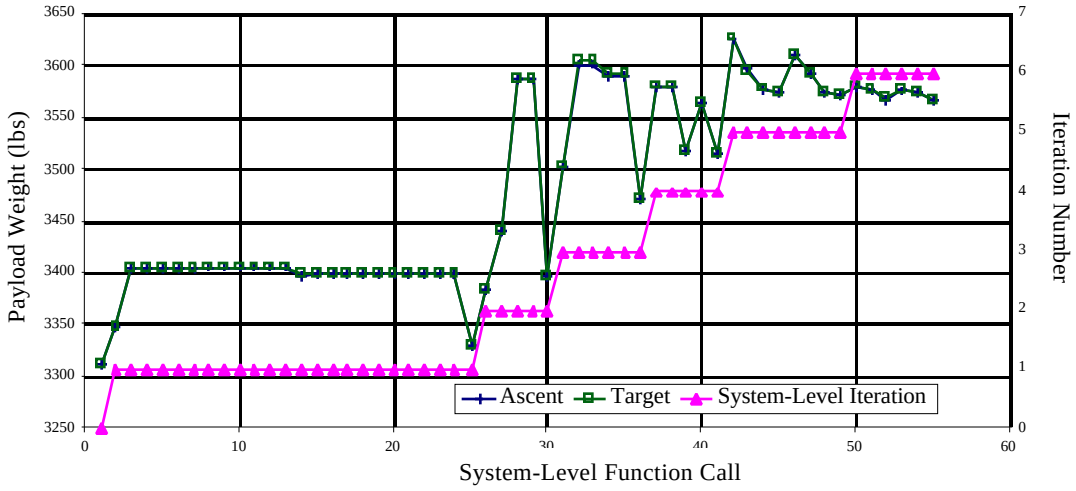

Figure 28: Payload Weight Tracking for the CO Method

Figure 29 illustrates the active constraint history for the seven system-level iterations needed to solve this problem. Because the initial targets came from the solution to the 'One-and-Done' method, the first iteration (zero on the graph) was a feasible solution at the system level. After this iteration, all other iterations then had a feasible solution.

Figures 30 and 31 show the subsystem level target achievement for the first three system-level iterations (0, 1, and 2) for the ascent propellant and payload weight, respectively. . The number of subsystem iterations is indicated by the number scale on the x-axis. The flyback deck was usually very flexible in finding a feasible solution. In Figure 30, the ascent propellant weight was matched at the beginning of the flyback deck's iterations and is difficult to see in the plot. In Figure 31, it is shown that the payload weight increased at every iteration. This was allowed because the ascent deck optimization matched the target at each iteration.

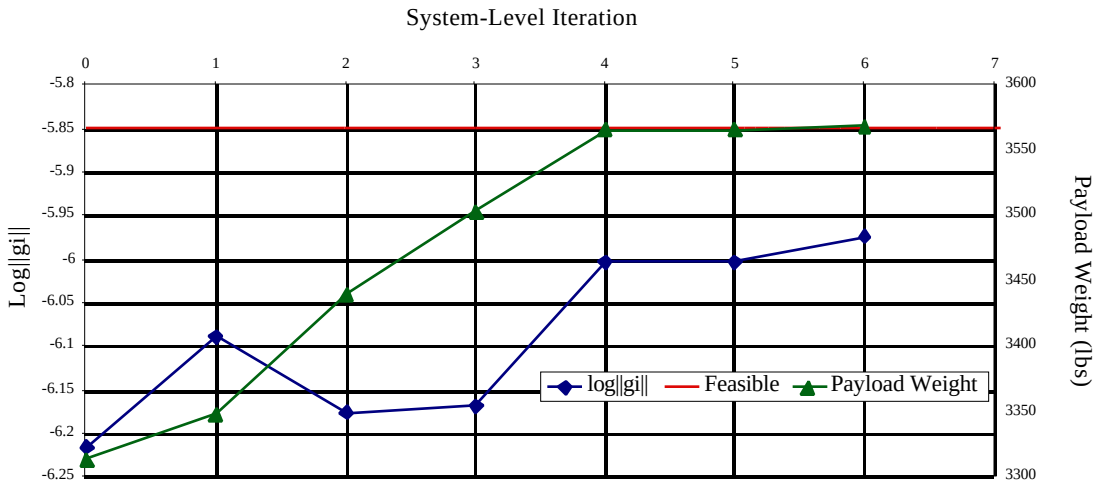

Figure 29: Active Constraint History for the CO Method

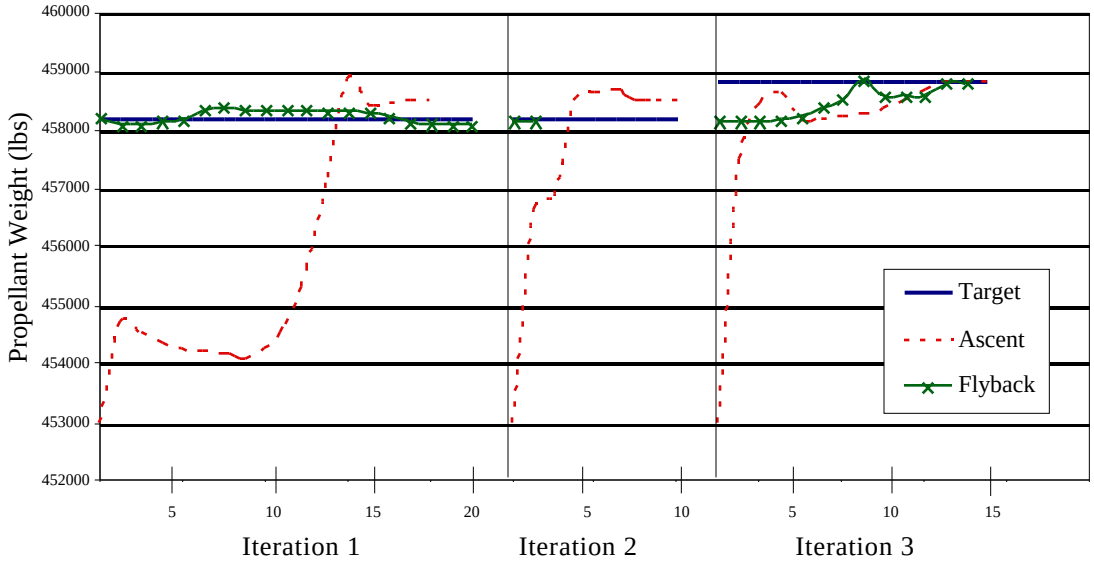

Figure 30: System-Level Coordination for Ascent Propellant

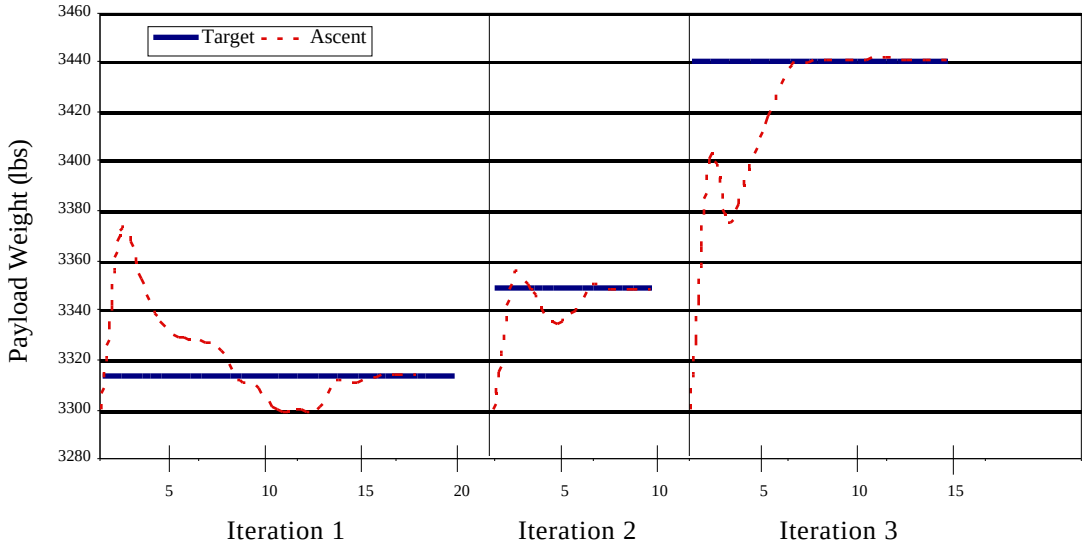

Figure 31: System-Level Coordination for Payload Weight

7.4 Summary

Tables 8 and 9 give quantitative results for the Kistler *K-1* MDO methods. In Table 8, POST computational time refers to the total amount of time to run the POST decks for all calls, including function calls and gradient calls. Although the actual method executions were performed with one processor, the CPU time results are reported as if two processors had been available (for example, in the FOBD and CO results, times are given as if the ascent POST deck ran on one processor while the flyback POST deck ran on another processor).

As indicated in Table 8, all methods increased the payload weight of the *K-1*. The fixed-point iteration method improved the payload weight by about 15 pounds. The partial optimization-based decomposition improved the payload weight of the *K-1* by approximately 23 pounds over the FPI method. The full optimization-based decomposition results in about a 42 pound increase in the payload weight over the FPI method. Use of the collaborative optimization method increased the payload by approximately 32 pounds. The decomposition methods gave an approximate 40 – 55 pound increase over the manual

iteration method, a 1.6% increase, which is relevant considering the high costs per pound to launch payloads.

Table 8: *K-1* Results Comparison (MDO)

Method	Optimized Payload Weight (lbs)	POST Computational Time
FPI	3,543.64	976.8 sec (16.3 min)
POBD 1	3,566.82	939.52 sec (15.7 min)
POBD 2	3,566.85	941.44 sec (15.7 min)
FOBD	3,585.06	968.33 sec (16.1 min)
CO	3,569.04	5,008 sec (1.39 hr)

It was expected that the FPI, POBD, FOBD, and CO methods would result in the same objective function; however, the lack of performance by the FPI method may be attributed to the numerical noise introduced by the flyback fuel weight convergence tolerance on the internal POST iterations. This noise also affects the gradient calculations for the engine-on time design variable because for that gradient, internal POST iterations occur. This tolerance then affects the flyback fuel weight and consequently the optimized payload weight. The marked difference in the FOBD method may partially be attributed to the existence of tolerances for the staging vector since the feedforward no longer existed. These tolerances would have affected the final payload weight. The variance in optimum design variables can be seen in Appendix C.

Some definitions for the columns in Table 9 are required. The third column, 'POST calls,' refers to how many times an analysis evaluation occurred, including system-level, gradient (except for the CO method), and line search evaluations. For the FPI and POBD methods one 'POST call' is a sequential execution of both POST decks. For the FOBD method, one 'POST call' is a parallel execution of the two POST decks. Note that there are two numbers given for the CO method. The first is the number of simulation function calls for the ascent deck, the second is for the flyback deck. As would be expected the number of

'POST calls' for the collaborative optimization method is significantly larger than that for the other methods because many function calls were needed for optimization. While the number of system-level iterations is smaller for CO, many function calls with the subsystems at each iteration were required.

Table 9: *K-1* Detailed Results Comparison (MDO)

Method	System-Level Iterations	POST Calls	Average CPU Time per POST Call	Gradient Calls
FPI	18	884	1.105 sec	17
POBD 1	20	843	1.114 sec	19
POBD 2	20	843	1.117 sec	19
FOBD	34	1622	0.911 sec	29
CO	7	2271/4745	1.326 min	5

In the fourth column, CPU time refers to the average time it took for one POST call to run, be that iteratively, sequentially, or in a parallel manner. At first glance, the average CPU times per function call listed in Table 9 are not what one would expect. The average time for the FPI method is usually larger than that for the OBD methods because the internal iterations for convergence are many. For the Kistler case, internal convergence occurred in zero or one iteration, usually zero for gradient calculation (this is because the flyback fuel weight is controlled by 'engine-on' time, one of the design variables). Thus for the majority of 'POST calls', one POST call for the FPI method would take approximately the same amount of time as one POST call for the POBD method. This is the case as shown in Table 9. The time for the FOBD method was smaller since the POST decks were executed in a parallel manner. The Ascent POST deck required a longer amount of execution time than that of the Flyback deck. Even though the POST decks for the CO method were executed parallelly, the CPU time was longer because the optimization of the POST decks required a longer amount of time than a simple integration of the equations of

motion did. Gradient calls' refers to how many times the objective and constraint gradient vectors were calculated in their entirety.

Note that the results for the POBD method were the same regardless of which way the compatibility constraints were posed. This was not the case, however, for the FOBD method. When the compatibility constraints were formed as one inequality per design variable, a feasible solution was not found.

More quantitative results can be seen in Table 10, which shows the difference in staging vectors for the methods. Included for comparison is the staging vector for the manual iteration method. Since the results for the two POBD methods were almost exactly the same, just one is included in the table. Assuming that convergence tolerances affect the FPI method staging vector, the results from the other MDO methods imply that a smaller flight path angle can lessen flyback fuel weight consumed and thus, the increase the payload weight. (In the FOBD case, the lower staging altitude also has a similar effect.) The returning booster desires this lower angle so that it can perform its pitcharound maneuver more efficiently.

Table 10: Staging Vector Results for the *K-1*

	MIM	FPI	POBD 2	FOBD	CO
Altitude, ft	138,028	138,019	138,014	137,542	138,028
Velocity, ft/s	4,172.28	4,169.27	4,166.92	4,160.34	4,171.15
Gamma, deg	33.337	33.520	33.272	32.892	32.667
Vel. Azimuth, deg	43.519	43.517	43.520	43.527	43.526
Latitude, deg	-30.893	-30.893	-30.893	-30.900	-30.902
Longitude, deg	137.029	137.028	137.027	137.020	136.996

Figures 32, 33, and 34 show plots of the trajectory data for the different MDO methods. Through the ascent, the trajectories are very similar with regards to altitude and velocity. In fact, as can be seen in Table 10, the staging points are relatively close to one

another. The angles of velocity azimuth, latitude, and longitude are expected to be identical considering there are no yawing movements during the ascent and the results of the table recognize that fact. In Figure 32, it is shown that the flyback altitudes, especially, exhibit differences. Differing pitch angles during the flyback pitcharound maneuver affect the flyback trajectory seen in Figure 33, as does the staging altitude.

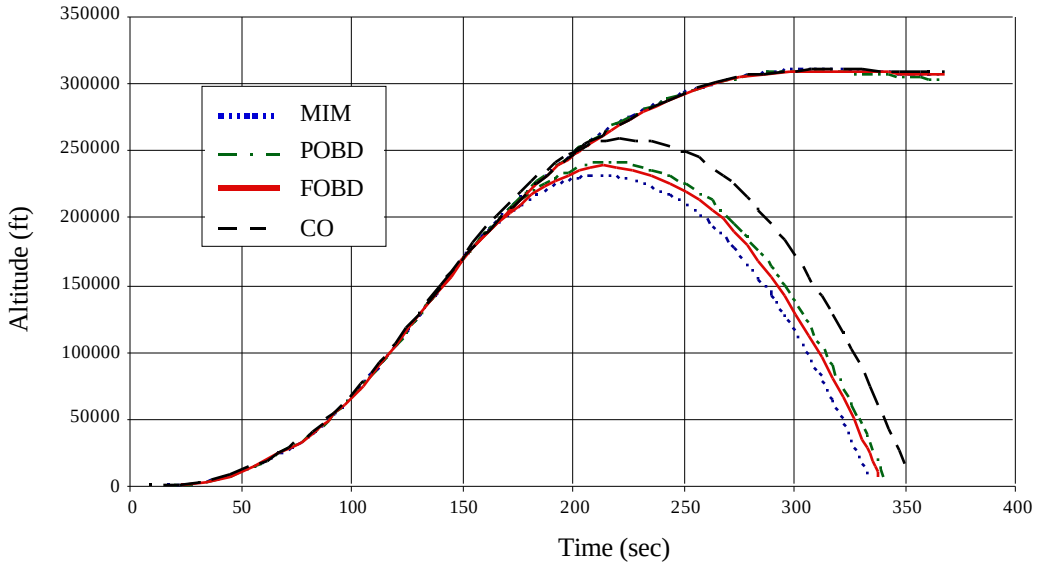

Figure 32: Altitude versus Time for the *K-1*

The velocity plot of Figure 34 illustrates the flyback engine-on phase well. For all methods, from about 130 seconds to 155 seconds the engine is on and the pitcharound to the launch site occurs. A slight dip in the velocity after the pitcharound occurs as the vehicle attains a zero degree angle of attack for its ballistic entry. The lowest velocity corresponds to the highest altitude, after which point the vehicle speeds up as it is aided by gravity as it descends. Terminal conditions on velocity for the flyback were not imposed.

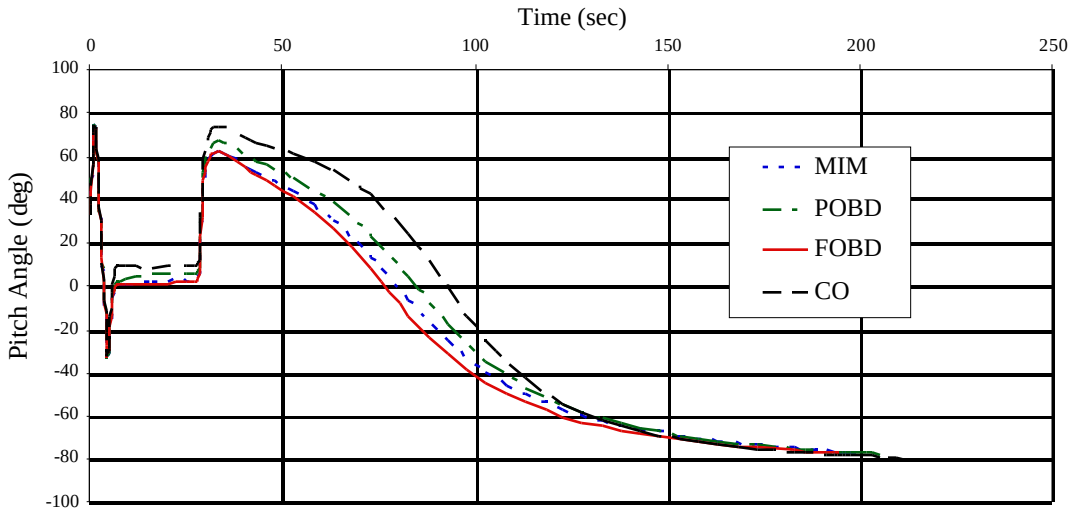

Figure 33: Flyback Pitch Angle versus Time for the *K-1*

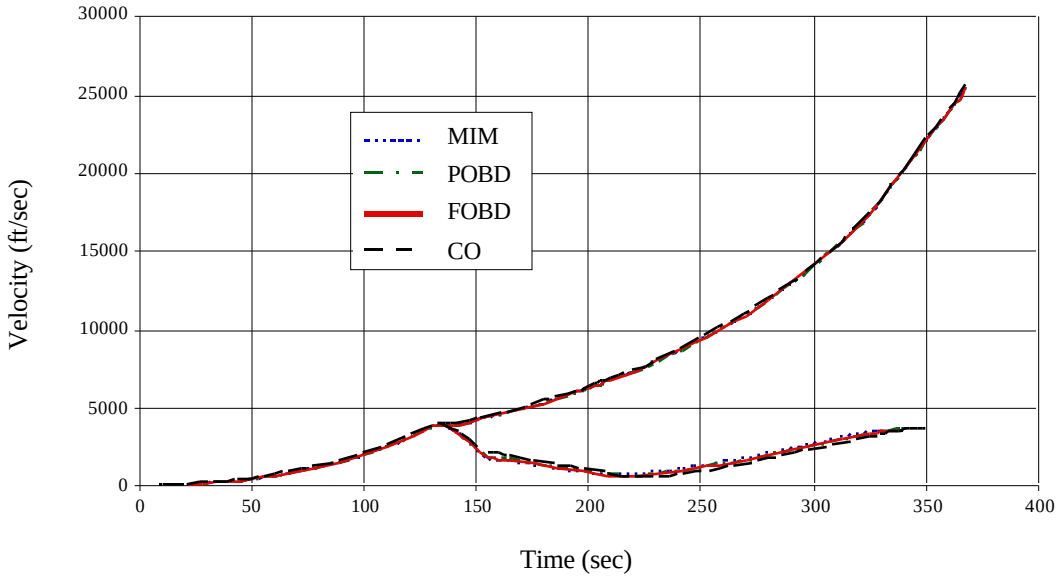

Figure 34: Velocity versus Time for the *K-1*

CHAPTER VIII

STARGAZER: THE SECOND APPLICATION

8.1 *Stargazer*

Figure 35: *Stargazer* Concept

The second application, which uses branching trajectories, is the *Stargazer* launch vehicle (Figure 35, [78]). The mission for this vehicle is to deliver a 300 pound payload (of

a university Explorer class) to a 200 nautical mile circular low-earth orbit at 28.5˚ inclination (Figure 36). This is to occur at a flight rate of 24 flights per year and at a price goal of less than $1.5M per flight. *Stargazer* is a concept that was developed by the Georgia Tech Space Systems Design Lab for the mission outlined below.

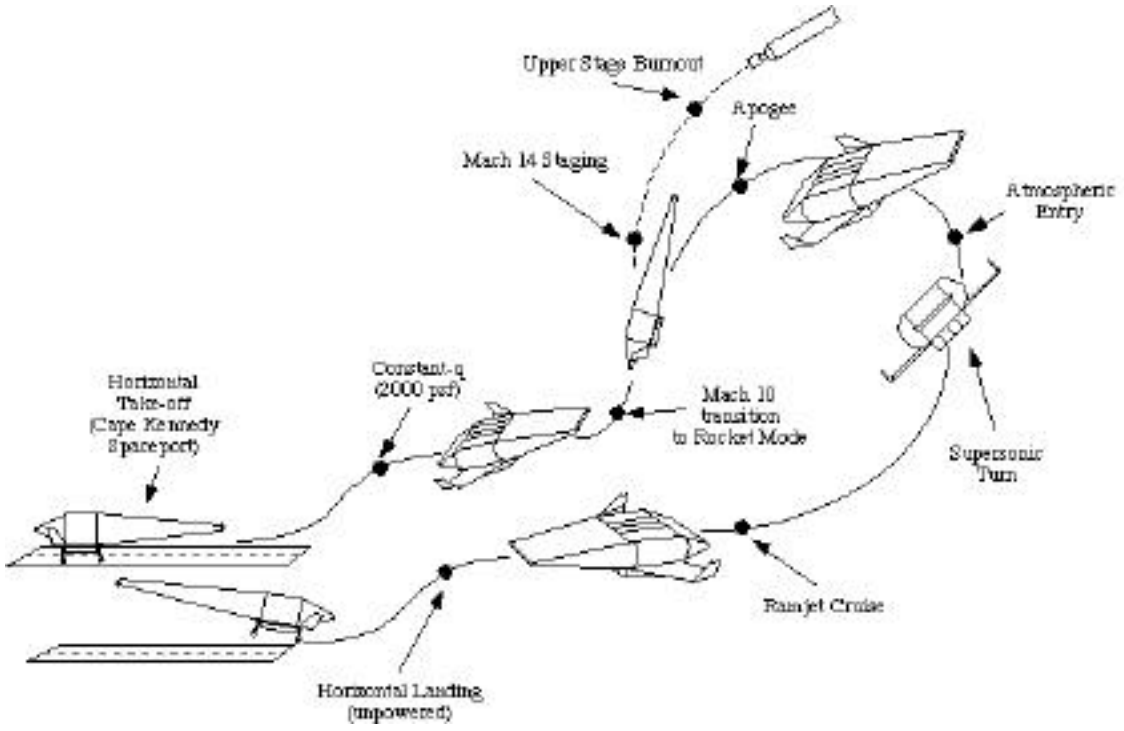

Figure 36: *Stargazer* Mission Profile

Stargazer is a TSTO vehicle with a reusable RBCC booster and an expendable, 'pop-up' upper stage with a low-cost rocket engine. The four RBCC engines are ejector-scramjet engines with four modes consisting of ejector, ramjet, scramjet, and rocket. The vehicle is fully autonomous and uses advanced technologies and TPS. From its horizontal take-off at KSC, the booster, with the upper stage, flies its ascent trajectory until it reaches Mach 14. After a brief coast, the upper stage is then jettisoned to continue on its flight to a 200 nmi. circular orbit. The booster then returns to KSC under ramjet power at an altitude of approximately 70,000 ft. to an eventual horizontal landing. It is clear from Figure 36 that *Stargazer*'s branching trajectory is like that of Figure 1.

8.2 The Design Structure Matrix for *Stargazer*

Stargazer was initially designed using a collaborative, multidisciplinary integrated design team approach. Team members executed individual disciplinary analysis tools in an iterative conceptual design process, exchanging information and data files, for each candidate configuration, until the propellant mass fractions for each mission segment were converged. The overall DSM for the *Stargazer* design process can be seen in Figure 37. The bolded box represents the main disciplinary iteration loop, the details of which are shown in Figure 38.

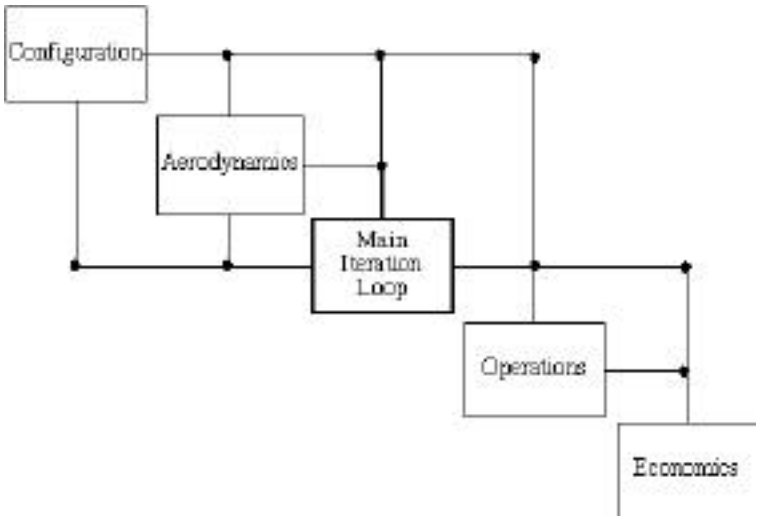

Figure 37: *Stargazer* DSM

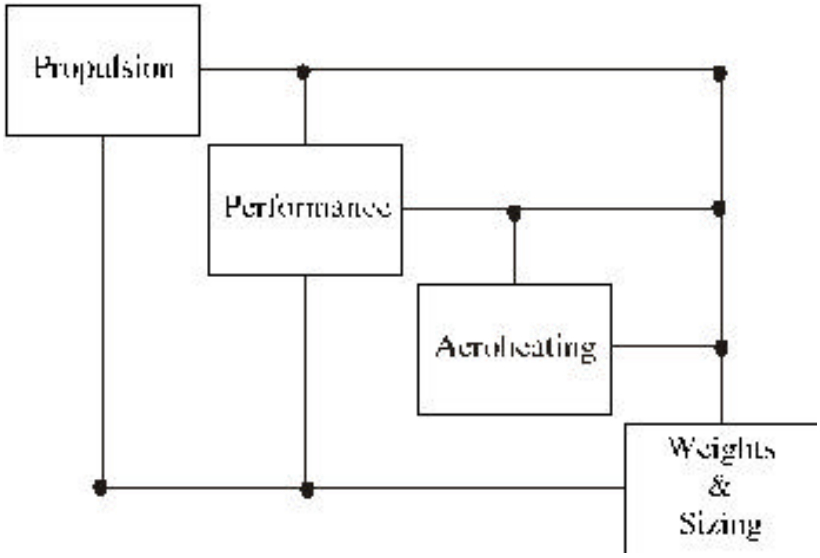

Figure 38: Main Iteration Loop

As introduced in Chapter III, the DSM is a useful mechanism for showing the data interdependencies in a multidisciplinary design process. The main iteration loop exhibits strong coupling among the propulsion, performance (trajectory optimization) and weights & sizing disciplines. The aeroheating (thermal protection system) discipline is rather weakly coupled with the other three beyond the first iteration.

Traditionally, the first two disciplines in Figure 37 iterate to find a feasible packaging and aerodynamic configuration. Once a feasible configuration is determined, the analyses in Figure 38 iterate to find a converged, properly scaled design to deliver the 300 lb. payload. (Note that photographic scaling is used such that the aerodynamic coefficients are the same for a single configuration, only scaled by wing planform area.) The operations and economics disciplines in Figure 37 are analyzed after a converged design is created.

For this research, however, the emphasis was on the performance discipline alone. Nonetheless, the other disciplines still play a role. In order to focus on the trajectory, an initial vehicle had to be baselined. The baseline packaging and configuration is that which is described in [78]. Figure 39 shows the vehicle layout from an isometric viewpoint. The hydrogen tanks are red with the oxygen tanks being blue. The payload bay occupies the top

center of the vehicle. The aerodynamic coefficients used were those of the baseline configuration; this could be done since photographic scaling was used.

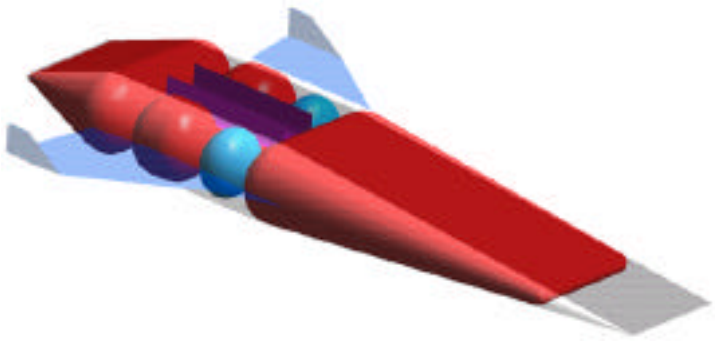

Figure 39: Baseline Packaging for *Stargazer*

The performance analysis occurs in the main iteration loop. Thus, the vehicle needed to be resized and given new engines at each change in performance. Since the propulsion and weights & sizing analyses have to be performed with different codes, on different platforms, than that of the performance analysis, POST, there needed to be a way to simplify the other codes.

This was achieved through use of linear multipliers and response surfaces. In particular, instead of running the RBCC propulsion code, SCCREAM [79], a web-based code, at every iteration, linear multipliers on each engine mode's thrust were employed. In addition, linear multipliers were also used to find the correct ramjet, scramjet, and rocket mode capture and exit areas along with ejector and rocket mode LOX flow rates. The factors used to scale the engine data were based on engine inputs created by SCCREAM for the engine detailed in [78]. The original engine inputs to SCCREAM can be found in Appendix D. New inputs for the trajectories were based on the iteration's booster and upper stage gross weights. Specific equations for the multipliers can be found in Appendix E.

The weights and sizing analysis for *Stargazer* uses a photographic scaling set of parametric mass estimating relationships that have a NASA Langley heritage. This analysis

is performed on a spreadsheet program. In order to simplify the communications requirements between the spreadsheet and POST, response surfaces were used to parameterize *Stargazer*'s gross weight and wing planform area for both the booster and upper stage. The booster dry weight was also parameterized. (The response surface equations can be found in Appendix F.)

The acreage percentages of various thermal protection systems on *Stargazer* were assumed to be constant, thus an aeroheating analysis did not have to be updated at every iteration. A representative Thermal Protection System (TPS) layout can be seen in Figure 40. These simplifications allowed for equations to be used at each iteration in place of complicated codes.

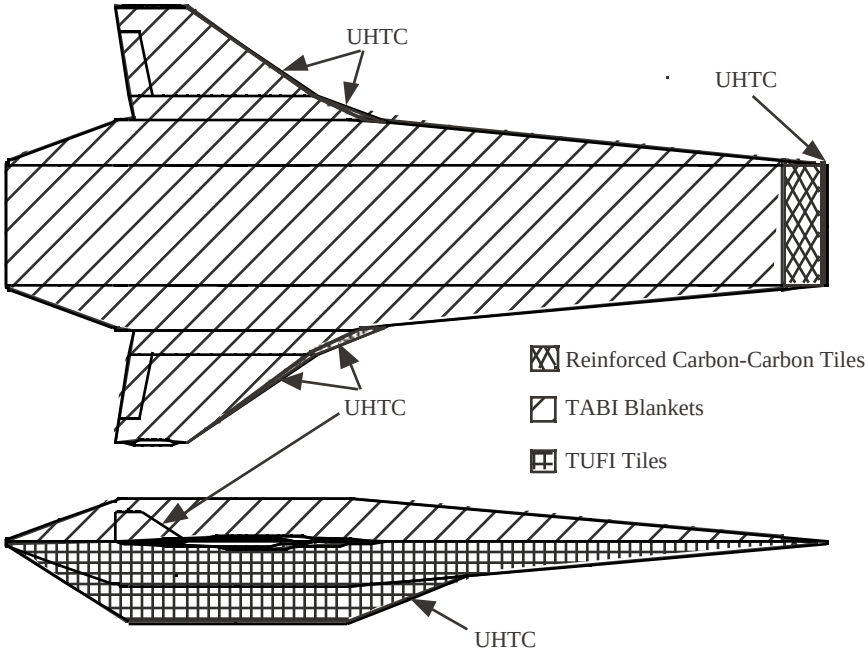

Figure 40: *Stargazer's* TPS Layout

As a result of the modifications made to the *Stargazer* design process, the DSM is altered. Figure 41 shows the new design structure matrix. Booster mass ratio and mixture ratio, flyback mass ratio, and upper stage mass ratio are required in order to calculate the

new vehicle weights and sizing values for the next iteration. Therefore, these are viewed and formulated in the MDO set-ups as feedbacks from the POST decks. For the MDO set-ups, the weights and sizing and propulsion calculations are included in the main program that also executed the system-level optimizer, as opposed to being a separate discipline, just as the weight calculation was for the *K-1* problem. The area of concentration is still the branching trajectory.

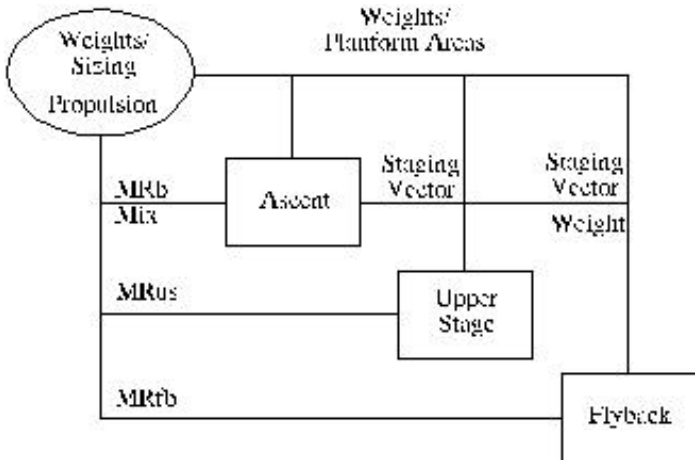

Figure 41: Modified DSM for *Stargazer*

8.3 *Stargazer's* Branching Trajectories

In the Kistler *K-1* branching trajectories, the booster itself was jettisoned. In the current case the upper stage is jettisoned at Mach 14, the staging condition. As a result of this fact and the fact that the turnaround, descent, and ramjet cruise to the launch site is so difficult to simulate, the *Stargazer* trajectory is modeled by three different POST decks. These are the ascent trajectory, the upper stage branch, and the booster flyback branch. The number of controls and constraints for these POST decks are listed in Table 11. In addition to a three-degree-of-freedom simulation, each POST deck uses the following modeling options: 1976 standard atmosphere, lift and drag aerodynamic coefficients, fourth order Runge-Kutta integration with a varying integration step sizes (smaller step sizes, 0.1 second,

for airbreathing ascent and larger step sizes, 5.0 seconds, for ramjet flyback), and a spherical Earth approximation.

The ascent trajectory deck involves the portion of the flight from horizontal take-off to staging at Mach 14. The trajectory is constrained by a maximum dynamic pressure boundary, a 3g acceleration limit in rocket mode to help minimize structural loading, and a wing normal force limit of 1.75 times the gross takeoff weight. The former is used as a surrogate for limiting internal engine pressures and external heating rates. The chosen wing normal force limit represents a compromise between wing structural weight and a more fuel-optimal, sharp pull-up after the at takeoff and at the beginning of rocket mode transition (Mach 10). During ejector and all-rocket modes, the vehicle is steered with pitch angles. The dynamic pressure boundary that *Stargazer* flies is 2000 psf during the ramjet and scramjet modes between Mach 3.5 and 10, during which time a linear feedback guidance scheme is used to steer the vehicle. The transitions between the four engine modes (ejector, Mach 0 – Mach 2.5; ramjet, Mach 3.5 – Mach 6; scramjet, Mach 7 – Mach 10; and rocket, Mach 11 – Mach 14) are modeled as a linear ramp down of the preceding mode and a linear ramp up of the following mode. The staging vector at Mach 14 (weight, altitude, longitude, latitude, velocity, flight path angle, and azimuth velocity) must be supplied to the upper stage and flyback branches. The objective of the ascent trajectory is to maximize the weight at staging.

Table 11: *Stargazer* Controls and Constraints

POST Deck	Number of Independent Variables	Number of Constraints
Ascent	11	7
Upper Stage	7	2
Flyback	17	6
Total	35	15

The upper stage POST deck simulates the expendable upper stage from the staging point to orbital injection. After a five second coast, the upper stage engine is ignited and it

flies a trajectory guided by optimal pitch angles. The engine runs for about 230 seconds and then the upper stage coasts until the apogee of 200 nmi. is reached. At this point, the engine is restarted to provide the instantaneous velocity increment needed to circularize the orbit. During the initial and final coasts, aerodynamic angles are used to steer the vehicle. Angle of attack, bank angle, and sideslip angle are all zero for the second coast phase in order to keep a flight path angle of zero degrees. The trajectory is constrained by a smooth pull-up at rocket ignition and orbital termination criteria. The objective of the upper stage trajectory is to maximize the weight at the end of the trajectory.

The flyback trajectory, which begins immediately after the upper stage is jettisoned and ends near KSC, is controlled by many variables. The variables are: angles-of-attack and bank angles used for the turnaround to KSC, the altitude at which the turn begins, the heading coming out of the turn, and the time at which the ramjet is turned on along with the throttle setting at which it starts. The trajectory is constrained by the termination conditions at KSC and the conditions at which the ramjet can be started. The ramjet flyback itself is constrained to result in flight of a constant heading at a constant altitude of approximately 70,000 ft., while maintaining Mach 3.5. To begin the turnaround to the launch site, the vehicle maintains thirty degrees angle of attack and ninety degrees bank. During the turnaround these angles are changed in value, but they still steer the vehicle. During the ramjet cruise, generalized acceleration steering is used as the guidance scheme to hold the vehicle in straight, level, unaccelerated flight. The objective of the flyback trajectory is to minimize the weight of the fuel consumed.

The rocket mode transition for Stargazer begins at Mach 10. Mach 10 was chosen as a conservative upper end for scramjet propulsion. While there is an advantage in reduced gross weight to be had from higher Mach airbreathing mode operation, disadvantages in terms of higher inlet (engine) weight and reduced propellant bulk density also appear.

The staging Mach number was fixed for this research. Fourteen was chosen as a compromise between booster size and upper stage size. The system-level objective of minimizing booster dry weight contributed to the fact that the staging Mach number was fixed. Had it not been fixed, the lowest Mach number in the range would have chosen to achieve the system-level goal. Fixing the staging Mach number also allows the compromises in the rest of the staging vector components to be emphasized.

8.4 The Objective Function for *Stargazer*'s Branching Trajectories

The system-level objective of the entire *Stargazer* branching trajectory was to minimize booster dry weight. While many metrics could be chosen, dry weight is typically minimized in launch vehicle applications. It was also a product of the trajectory, weights and sizing, and propulsion disciplines and was easily available from these analyses.

CHAPTER IX

RESULTS FOR *STARGAZER*

Results for solutions to the *Stargazer* branching trajectory problem are presented in this chapter. Solutions for the 'One-and-Done' method, manual iteration method, and the distributed method using MDO techniques are analyzed. All executions of the POST decks, system-level optimization code, and any associated codes were performed on the Silicon Graphics Octane platform with a 300 MegaHertz IP30 processor using an R12000 processor chip.

9.1 Methods with Conflicting Objective Functions

9.1.1 'One-and-Done' Method

The solution for the 'One-and-Done' method for the *Stargazer* vehicle is outlined in Figure 42. This method does not account for the iterative, coupled nature of the ascent, upper stage, and flyback branches. The analysis for this method was performed manually and its results appear in Table 12. The only reason to mention this method at all is to point out that the mass ratios and mixture ratio that are guessed are typically far from being those that are output.

For this method, the initial guess for the mass ratios and mixture ratio are crucial. It is quite difficult to guess these inputs and have the outputs match. In this case, the initial

guesses came from educated estimates and those values used for the vehicle described in [78] and were as follows: booster mass ratio—2.162, booster mixture ratio—1.858, upper stage mass ratio, 3.168, and flyback mass ratio—1.333. From these inputs, new weights and engine performance values were computed using the methods explained in Section 8.2 and input to the POST decks. After running the POST decks once, the outputs for mass ratios and mixture ratio, in the same order as before were: 2.281, 1.677, 3.172, and 1.393. Obviously, the inputs and outputs were not the same. In fact, there was an increase of about twenty thousand pounds of gross weight and three thousand pounds of dry weight, the objective function. Obviously, iterations are needed to insure that the vehicle flown corresponds to an internally consistent design.

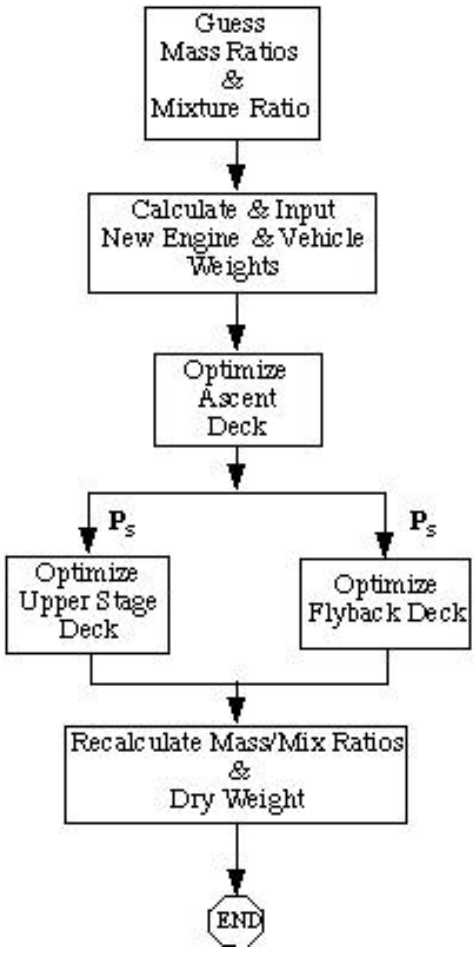

Figure 42: 'One-and-Done' Flowchart, *Stargazer*

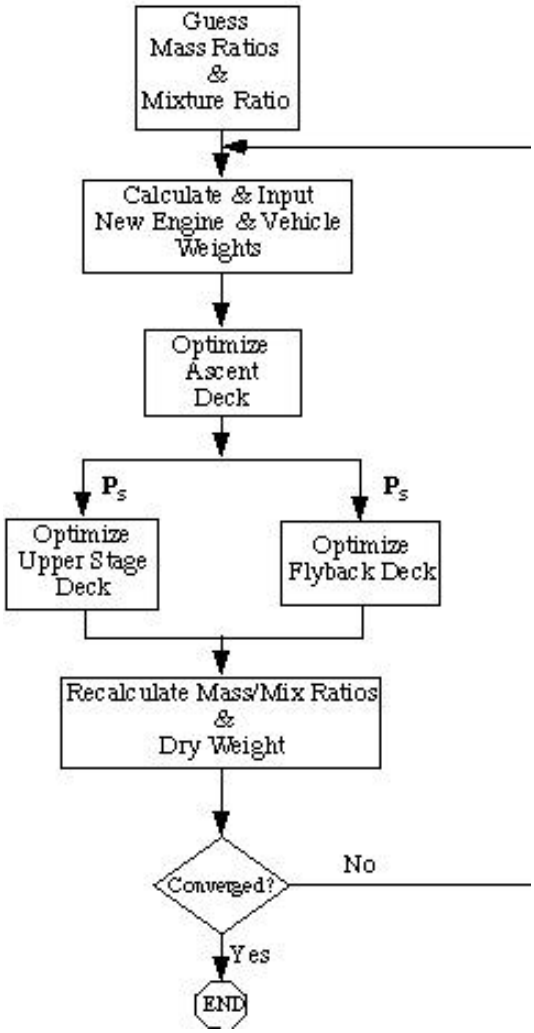

Figure 43: Manual Iteration Method Flowchart, *Stargazer*

Table 12: 'One-and-Done' and Manual Iteration Method Results for *Stargazer*

Method	Booster Dry Weight (lbs)	POST Computational Time	Number of Iterations
'One-and-Done'	31,220.6	-	0
Manual Iteration	25,759.7	1185.6 sec (19.76 min)	19 5 from last restart

9.1.2 Manual Iteration Method

The manual iteration method uses three subproblem optimizers and no system-level optimizer. A flowchart of the method can be seen in Figure 43. Execution is sequential and iterative between the three POST decks. At each new iteration, the initial weights and propulsion data are calculated, as functions of the last iterations' mass ratios and mixture ratio, and input into the new POST decks. Again the data extraction/insertion is manual and took a considerable amount of time considering all the propulsive and weights inputs required. Two restarts of the iteration process were invoked. This means that twice the dry and gross weights were found to be oscillatory. The iteration process had to be restarted with a relaxation factor of one half for the mass ratios and booster mixture ratio. In other words, the mass ratios and mixture ratio for the next restart were the average of those values that created the oscillatory weights of the current iteration process. The MDO methods that follow were started with initial conditions from the last restart.

Iteration information and execution time results are shown in Table 12. For this case, iteration was performed between the three basic subproblems to ensure data consistency (unlike the 'One-and-Done' method), however the conflicting objective functions were not addressed. The convergence criterion for the manual iteration method was booster dry and gross weights. *Stargazer* was considered converged when both booster dry and gross weights came within 1.0% of the results from the previous iteration. In addition, the input mass ratios and booster mixture ratio had to be reasonably close to that output. The results for this method will be used as a comparison case in the MDO method assessment currently being conducted. The final design variables used for this method are listed in Appendix G.

9.2 The System-Level Optimizer

The DOT™ program was used as the system-level optimizer for the *Stargazer* vehicle as well. Table 13 lists the size of the system-level optimizer for *Stargazer*. A fixed-point iteration solution was not achieved due to difficulties in converging the branching trajectory at each system-level iteration. A lack of robustness in the POST deck simulations added to the difficulties of the convergence tolerance noise. Considering the restarts,

staging tolerance issues, and abundant function calls required for the full optimization-based decomposition method solution for the *K-1* vehicle, this solution technique was not considered for this problem.

The *Stargazer* POST decks used nine equality constraints, which when formed as two inequalities, brings the total number of constraints to twenty-four. Additional constraints existed at the system-level and are discussed in the next section.

Table 13: Size of System Optimizer for *Stargazer* Cases

	Variables	Constraints
Manual Iteration	-	-
Partial OBD	39	34
Collaborative	11	5

The variables added to the POBD method are the three mass ratios and booster mixture ratio. Their compatibility constraints were formed as two inequalities per added design variable, resulting in an addition of eight constraints. The eleven design variables for the CO method are the staging vector and weight, the three mass ratios, and the booster mixture ratio. Its constraints are the sum-squared errors, or J's, for each POST deck.

9.2.1 System-Level Constraints for Stargazer

Two constraints are added at the system-level for both the POBD and CO methods. These are the convergence criteria constraints on booster dry and gross weight. Tight tolerances on the three mass ratios and mixture ratio could also satisfy the convergence criteria on booster dry and gross weights. However, it is difficult to know *a priori* what those tolerances should be relative to the values input. Furthermore, dry weight convergence or gross weight convergence alone is not sufficient. These convergence weight constraints can not be added to the individual POST deck optimization of the CO method or to the compatibility constraints for the POBD method because they are functions of outputs from each POST deck.

Table 14 gives examples of slightly varying input ratios and the resulting differences from a set of baseline values given on the first row. In the table, 'Mix' stands for booster mixture ratio, 'MRus' represents upper stage mass ratio, the booster mass ratio is given by 'MRb,' and the flyback mass ratio is given in the 'MRfb' column. As can be seen in rows three and four, a convergence in dry weight does not necessarily mean a convergence in gross weight and vice-versa. In addition, a relatively small change in flyback mass ratio means a large change in dry and gross weights as shown in row two. Thus, the system-level constraints are employed for booster dry and gross weights. Relatively large changes in mixture ratio and upper stage mass ratio may not have a large effect as illustrated in the last two rows. However, the requirement of the original problem, that these four variables be reasonably close upon input and output, would not be satisfied for the upper stage mass ratio input and output in the last row. That difference is 0.016, which is quite significant for a mass ratio difference; the difference in mass ratios and mixture ratio for rows two through four are smaller, within a 0.003 absolute tolerance.

Table 14: Dry and Gross Weight Comparisons

Mix	MRus	MRb	MRfb	Gross Weight	Gross Wt. Variance	Dry Weight	Dry Wt. Variance
1.744	3.332	2.211	1.383	80,309.14	N/A	25,538.31	N/A
1.744	3.332	2.211	1.384	80,655.79	-0.0035	25,629.07	-0.0036
1.744	3.332	2.2115	1.383	80,416.60	-0.0011	25,563.23	-0.00099
1.7465	3.332	2.211	1.383	80,213.94	0.00095	25,509.05	0.0012
1.744	3.316	2.211	1.383	80,214.29	0.00095	25,517.10	0.00085

Equations 38 and 39 define the system-level constraints for the booster dry and gross weight, respectively. An absolute tolerance of 0.005 was used for the mass ratios and mixture ratio feedbacks.

$$\left(\frac{dry_{in} - dry_{out}}{25{,}000}\right)^2 \le .000001 \qquad (38)$$

$$\left(\frac{gross_{in} - gross_{out}}{100,000}\right)^2 \le .000001 \qquad (39)$$

9.3 Multidisciplinary Design Optimization Results

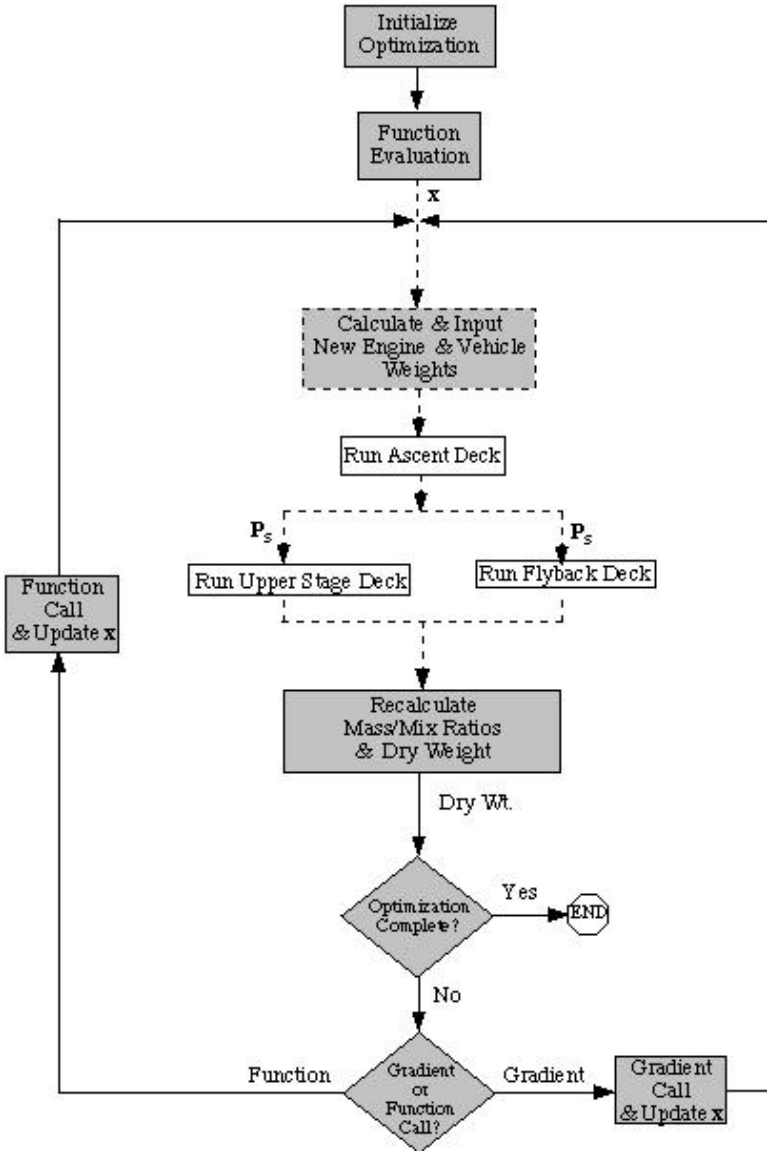

Figure 44: POBD Flowchart, *Stargazer*

9.3.1 Optimization-Based Decomposition

Optimization-based decomposition was used to solve the *Stargazer* branching trajectory. For this case, Partial OBD was employed in that only the feedbacks of the mass ratios and booster mixture ratio were eliminated and posed as compatibility constraints. A flowchart of the process can be seen in Figure 44. As in the flowcharts for the Kistler *K-1*, the 'grayed' boxes represent C++ programs while dashed lines indicate the use of PERL for automated data insertion and extraction.

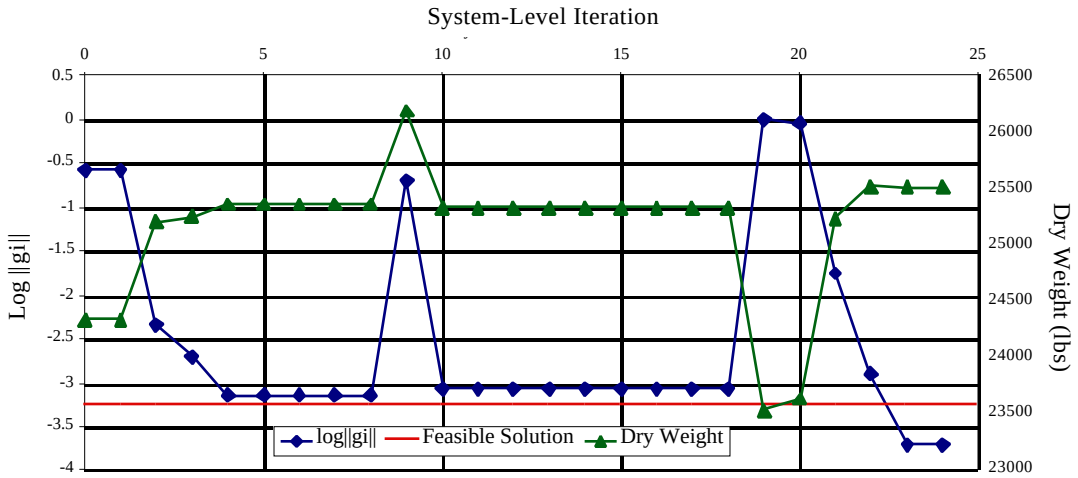

Figure 45: Active Constraint and Dry Weight History for *Stargazer* POBD

This method resulted in a difficult optimization process for the *Stargazer* branching trajectories. Figure 45 shows the active constraint and dry weight history for the branching trajectory solution. The upper stage and flyback design variables could not change significantly without crashing the POST decks (meaning either the booster would crash into the ground or the upper stage would fly off into the far reaches of space.) Thus returning a false mass ratio that was not physically valid or in the range for the response surfaces. Output dry weights for this type of error took values close to 450,000 lbs. Therefore, the upper stage and flyback design variables were not allowed to vary largely.

The method had to be restarted twice due to oscillations in the dry weight. (The restarts can be seen at system-level iterations 8 and 18.) Such oscillations can be viewed in Figure 46 as the function calls are shown for system-level iterations 12 – 16. The restarting process was similar to the procedure described for the manual iteration method. Optimized results for this method include a dry weight of 25,522 pounds of dry weight in 2.8 hours and a total of twenty-four system-level iterations. Additional results are given in Section 9.4.

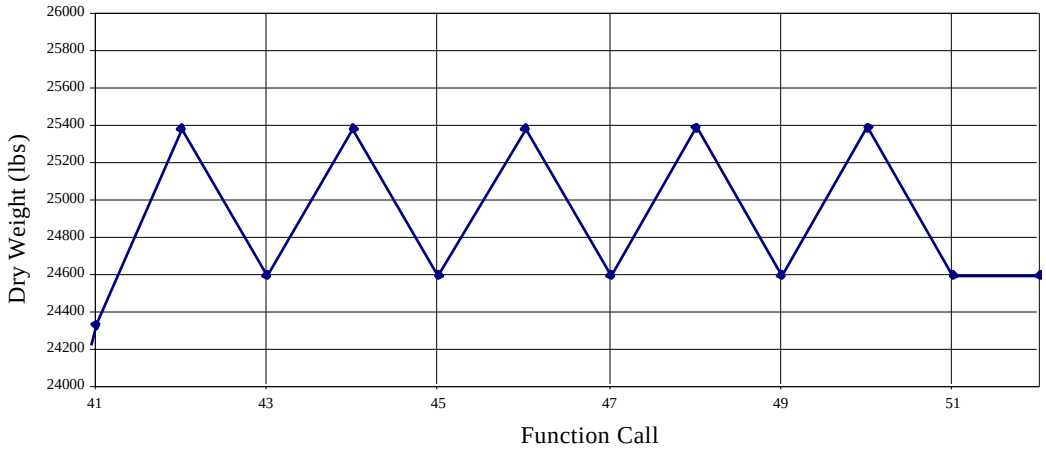

Figure 46: Dry Weight Oscillations for System-Level Iterations 12 – 16

9.3.2 Collaborative Optimization

Collaborative optimization was also used to solve the *Stargazer* branching trajectory. A flowchart of the process can be seen in Figure 47. The 'grayed' boxes represent C++ programs while dashed lines indicate the use of PERL for automated data insertion and extraction. The POST deck optimization is emphasized by the dashed lines through the POST call boxes.

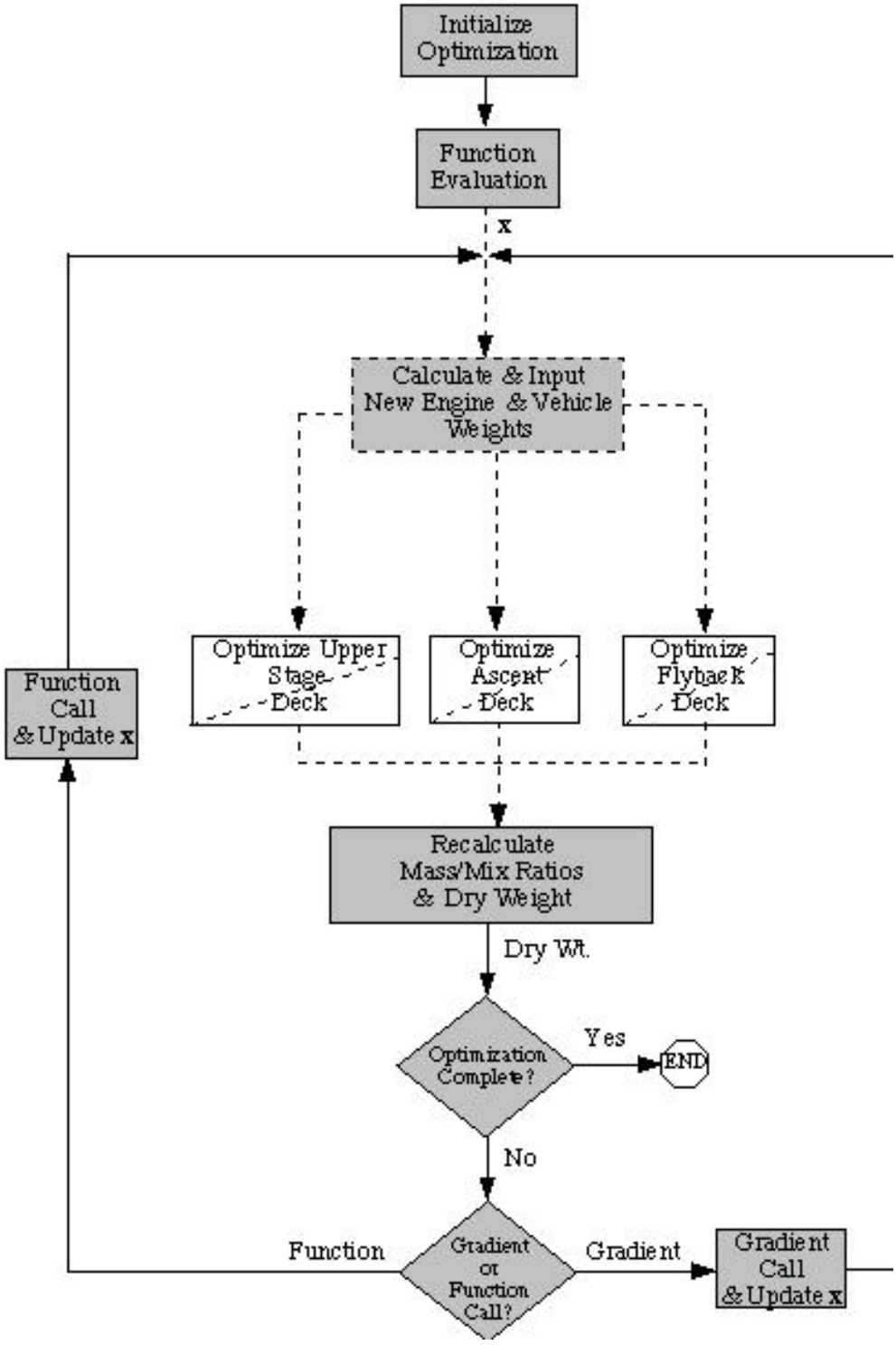

Figure 47: CO Flowchart, *Stargazer*

The target vector for this method is composed of eleven variables: the staging vector (altitude, velocity, azimuth velocity, flight path angle, latitude, and longitude); the initial flyback weight; ascent, upper stage, and flyback mass ratios; and the ascent mixture ratio. These last four variables are included as system-level targets since they were posed as feedbacks from the POST decks. They are indirect inputs to the POST decks through the weights and engine inputs. Table 15 shows which targets are explicit outputs and inputs with respect to each POST deck. The error, J, for each POST deck is calculated accordingly.

Table 15: Targets' Relationship to POST Decks for *Stargazer*

	Ascent Deck	Upper Stage Deck	Flyback Deck
Staging Altitude	Output	Input	Input
Staging Velocity	Output	Input	Input
Staging Azimuth Velocity	Output	Input	Input
Staging Flight Path Angle	Output	Input	Input
Staging Latitude	Output	Input	Input
Staging Longitude	Output	Input	Input
Initial Flyback Weight	Output	--	Input
Upper Stage Mass Ratio	--	Output	--
Flyback Mass Ratio	--	--	Output
Ascent Mass Ratio	Output	--	--
Ascent Mixture Ratio	Output	--	--

Similar to the *K-1*'s CO scenario, post-optimality sensitivity analysis was used to calculate constraint gradients for the *Stargazer* branching trajectory. Unlike the *K-1* analysis, in which the objective function of payload weight was added to the target vector, for the *Stargazer* analysis, the objective function of dry weight was *not* added to the target vector.

As explained in Section 9.2.1, the system-level constraint vector includes two convergence criteria constraints, one for booster dry weight and one for booster gross

weight. Neither of these can be added to the target vector because neither is an explicit output of any of the POST decks. Thus, neither dry nor gross weight could be included in any of the system-level constraints, J. However, these variables *are* explicit functions of the four targets of the three mass ratios and ascent mixture ratio, as evidenced by the response surface equations given in Appendix F. Their constraint gradients can be analytically derived from those equations. In addition, the objective function gradient can also be analytically derived from the same equations.

Figure 48 shows the dry weight history for the branching trajectories of the *Stargazer* CO method. Figure 49 shows the active constraint history. The initial conditions for this case started from an infeasible region and the CO method was successful in finding a feasible solution. The optimized solution that was found resulted in 25,509 pounds of dry weight. This solution took six system-level iterations, with seventeen system-level function calls, in 14.3 hours.

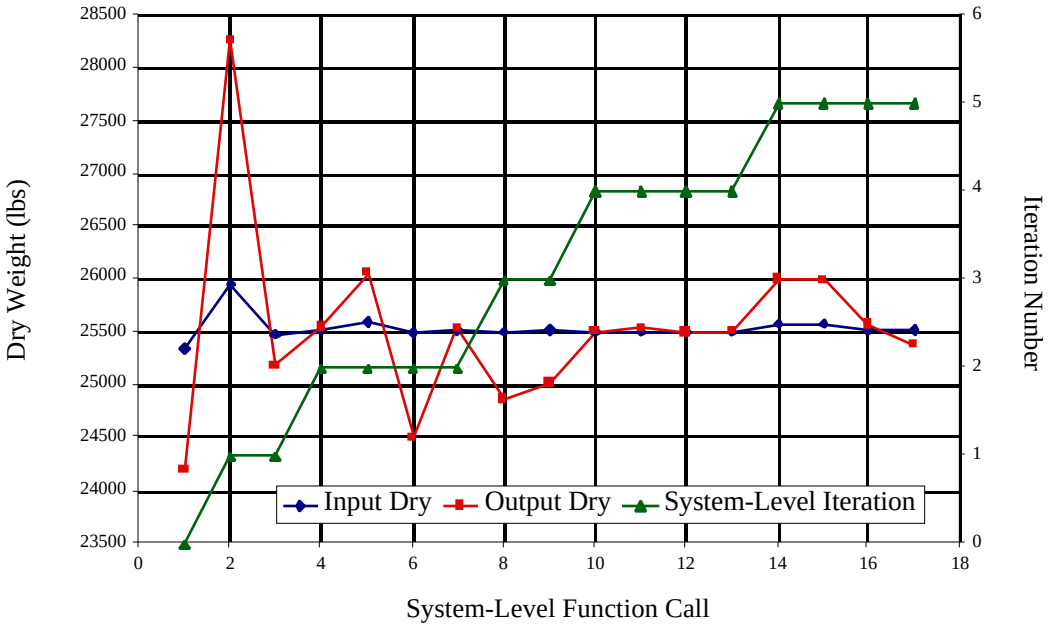

Figure 48: Dry Weight History for *Stargazer* CO

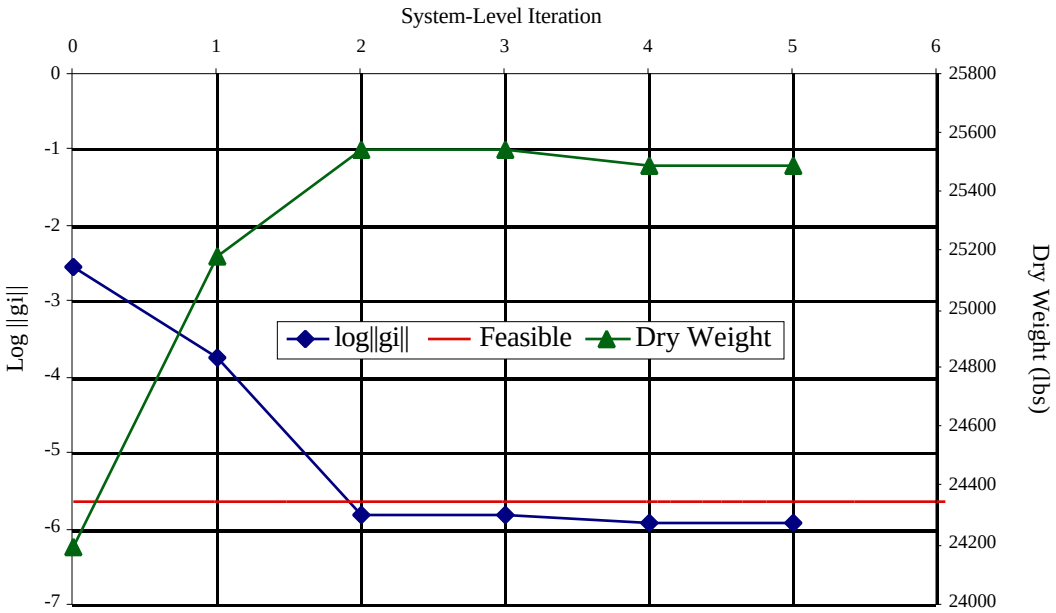

Figure 49: Active Constraint and Objective History for *Stargazer* CO

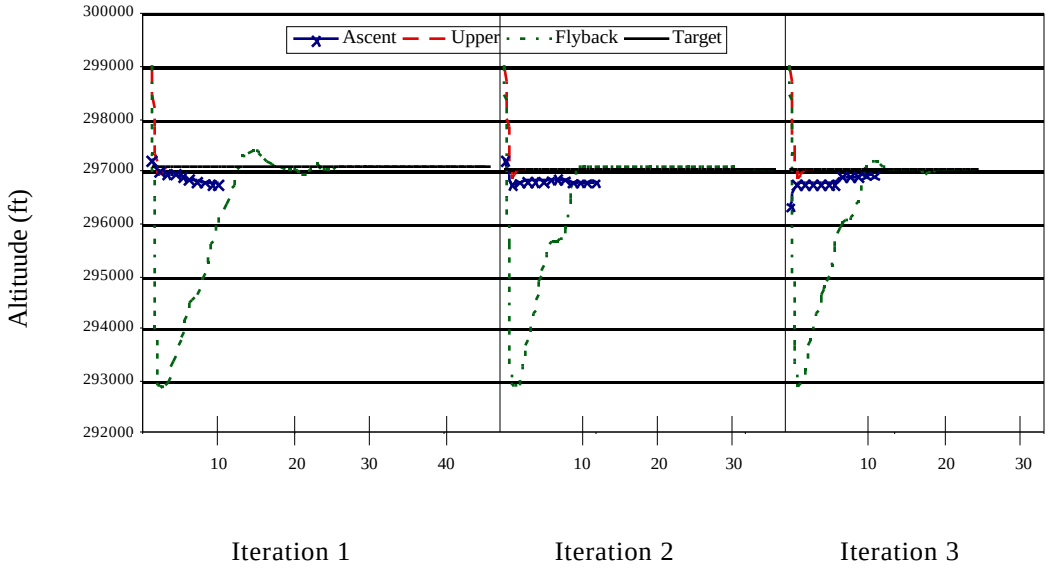

Figure 50: System-Level Coordination for Altitude

Figures 50 and 51 illustrate the system-level coordination for altitude and initial flyback weight, respectively, for the first three system-level iterations. The number of subsystem iterations is indicated by the number scale on the x-axis. The flyback and upper stage POST decks met the target altitudes at each iteration. This is because the altitude is an internal design variable, an input, in these POST decks. The same can be said of the initial flyback weight of Figure 51. For the ascent, however, altitude and initial flyback weight are outputs of the trajectory. Initially, these target variables were not met by the ascent. Figures 50 and 51 show how the system level optimizer reduced these values in order to obtain target agreement from the ascent subsystem.

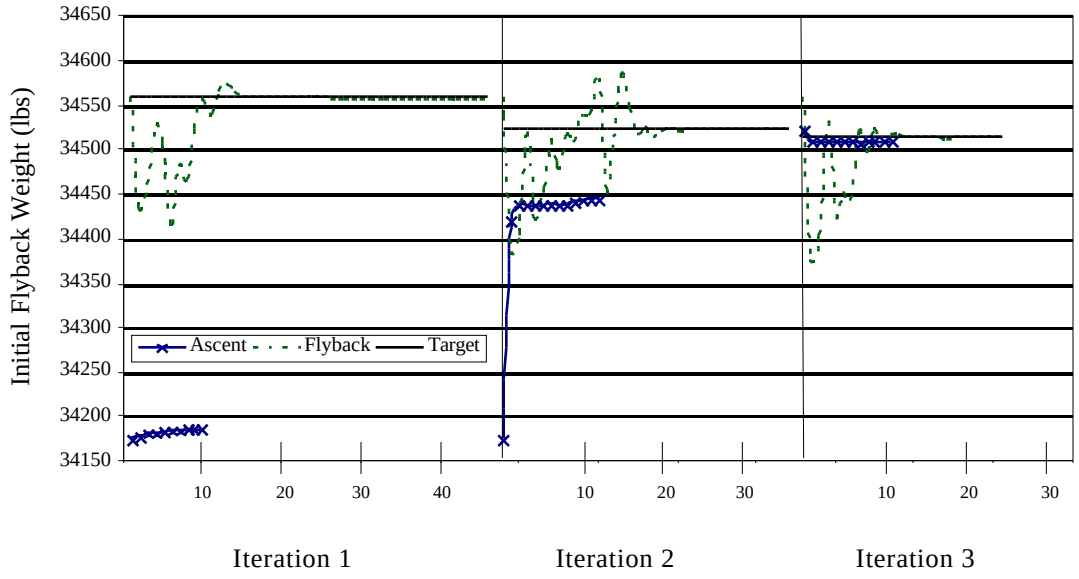

Figure 51: System-Level Coordination for Initial Flyback Weight

9.4 Summary

Qualitative final result comparisons can be made. Optimized dry weight and computational times are listed in Table 16. Although the optimization process for the POBD method encountered difficulties, the final dry weight produced was within 0.1% of that resulting from the CO method. Both dry weights were approximately 200 pounds less

than that obtained with the manual iteration method results. Additionally, even though it had to be restarted, the POBD method took about five times less POST computational time than the CO method. This is a result of the multilevel optimization of the CO method. Similar to the *K-1* results, the actual method executions were performed on one processor. Hoever, the CPU time results are reported as if three processors had been available. (For example, in the CO results, times are given as if the ascent POST deck ran on one processor while the upper stage POST deck ran on its own processor and the flyback POST deck ran on another processor).

Table 16: *Stargazer* Results Comparison (MDO)

Method	Optimized Dry Weight (lbs)	POST Computational Time
POBD	25,521.9	2.793 hrs
CO	25,509.4	14.294 hrs

Table 17 gives more detailed results for the POBD and CO methods. The third column, 'POST Calls,' refers to the number of sequential executions of the POST decks for the POBD method and it includes the gradient evaluations. That definition for the CO method is the number POST function calls to each subsystem (ascent/upper stage/flyback.) Each number includes line searches.

Table 17: *Stargazer* Detailed Results Comparison (MDO)

Method	System-Level Iterations	POST Calls	Average CPU Time per POST Call	Gradient Calls
POBD	24	638	15.758 sec	14
CO	6	1929/114/1785	49.286 min	4

For the CO method, the upper stage POST deck usually solved in about six iterations for 17 system-level function calls. Thus, this results in a small number of POST calls, 114, for that subsystem.

The final mass ratios and booster mixture ratio for the manual iteration, partial optimization-based decomposition, and collaborative optimization methods are listed in Table 18. As expected, these values for the manual iteration method (MIM) are quite different than those for the MDO methods.

The values for the MDO methods compare more favorably. These values for the POBD and CO methods result in about a four pound difference for the upper stage weights (1,784 lbs and 1,788 lbs, resp.) and about an eight pound difference in the gross weights (80,228 lbs and 80,220 lbs, resp.). The upper stage weight difference is a little high relatively and can be attributed to the large effect of the differing upper stage mass ratios for these methods.

Table 18: *Stargazer* Ratios Results Comparison

	Booster Mass Ratio	Booster Mixture Ratio	Upper Stage Mass Ratio	Flyback Mass Ratio
MIM	2.2231	1.7612	3.2988	1.3816
POBD	2.2088	1.7467	3.3256	1.3845
CO	2.2104	1.7482	3.3311	1.3835

Table 19 shows the final staging vectors for the MIM, POBD, and CO methods. The velocity azimuth, longitude, and latitude are all similar in value as expected since the booster performs only longitudinal maneuvers on ascent. The MDO methods gave more similar staging vectors than for the manual iteration method. However, differences in altitude, velocity, and flight path angle were on a slightly larger order than the other variables. These differences are a result of the small tolerances on those variables for the CO methods.

Tables 18 and 19 imply that an increased flight path angle helps to achieve the minimization of the booster dry weight by decreasing the booster mass ratio and mixture ratio, while increasing the upper stage and flyback mass ratios. The last three effects are not intuitive. The effect of increasing the upper stage mass ratio is an increase in the upper stage weight, which indirectly increases the booster dry weight. The effects of decreasing the booster mixture ratio and increasing the flyback mass ratio require more hydrogen tank structure and thus more dry weight for the booster. For these sets of MDO mass ratios and mixture ratio, decreasing the booster mass ratio dominates the dry weight minimization. So, decreasing the booster mass ratio has the strongest effect on minimizing the booster dry weight, while the other effects are weak. The increased staging flight path angle was needed to get the values of mass ratios and mixture ratio that led to the minimum dry weight.

Table 19: *Stargazer* Final Staging Vector Comparison

	MIM	POBD	CO
Initial Flyback Weight, lbs	34,907.9	34,498.8	34,513.3
Altitude, ft	296,360	296,622	297,008
Velocity, ft/s	12,543.5	12,474.8	12,443.2
Gamma, deg	11.879	12.351	12.525
Vel. Azimuth, deg	98.627	98.663	98.647
Latitude, deg	27.609	27.601	27.608
Longitude, deg	291.097	291.157	291.215

The relative pitch angle versus time plot for the ascent trajectories is illustrated in Figure 52. A notable difference in the pitch angles of the manual iteration method and the MDO methods occurred between twenty and one hundred eighty seconds during ejector mode. This difference allowed for decreased drag losses, during the ascent, for the MDO methods, which produced a smaller booster mass ratio.

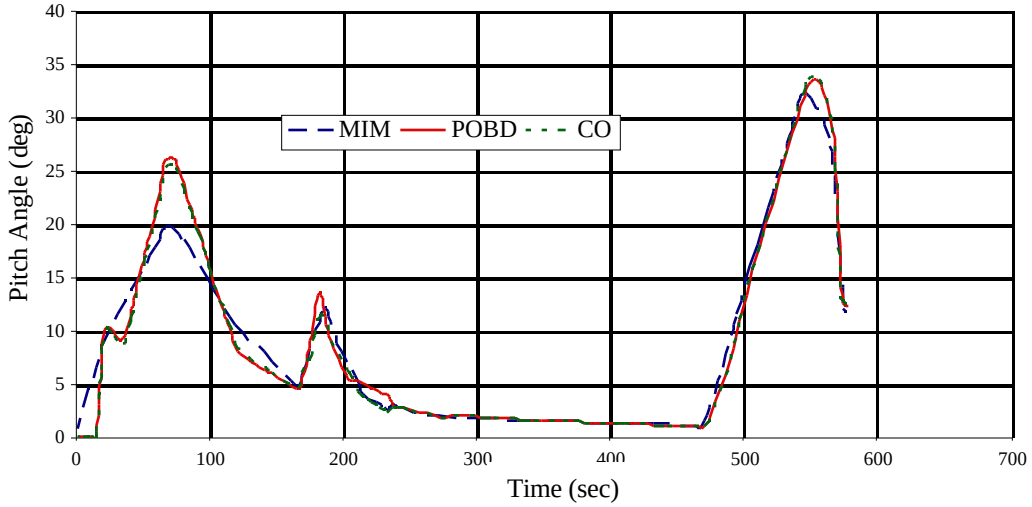

Figure 52: Pitch Angle versus Time for *Stargazer* Ascent Trajectories

Figure 53 shows a typical ascent plot for the *Stargazer* vehicle. The MIM, POBD, and CO methods give similar plots for the ascent, with slightly larger dips in the beginning of the dynamic pressure plots. This initial dip is characteristic of RBCC vehicles. The dynamic pressure boundary discussed in Chapter VIII is apparent in the figure.

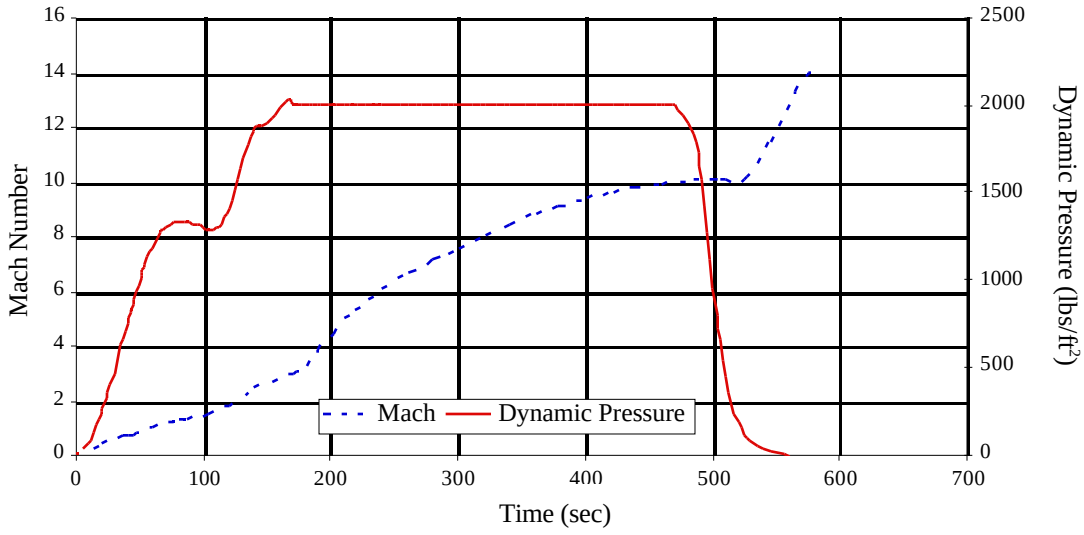

Figure 53: Typical Ascent Trajectory Plots for *Stargazer*

Figures 54 - 58 relate to the flyback trajectories. Figures 54 and 55 are cut off at about 600 seconds, after which point they continue at the same angle of attack and bank angle of 600 seconds until the end of the flyback. The flyback I_{sp}'s for all the methods were within 2 seconds of one another. The mass ratio difference can be attributed to the greater drag losses of the MDO methods. The drag losses are greater because the ramjet is on longer as it is throttled to a lower setting than that of the manual iteration method. The groundtracks of Figure 56 show that the flyback trajectories do indeed return close to KSC launch site. The groundtracks end at when the ramjets are turned off. An unpowered descent, at that point, concludes the flyback, but was not modeled in the POST decks. The flyback for the manual iteration method exhibits a smaller turn radius for the MIM, also evidenced in Figures 54 and 55.

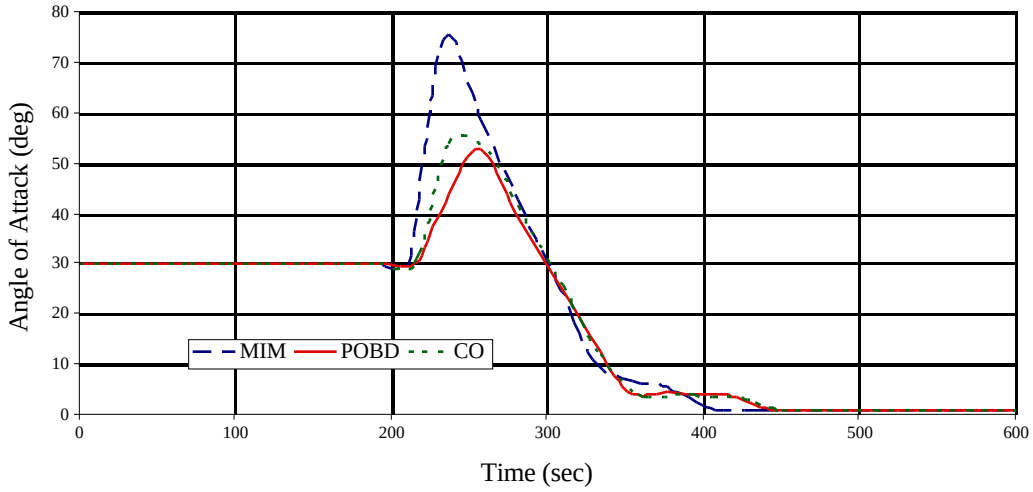

Figure 54: Angle of Attack versus Time for *Stargazer* Flyback Trajectories

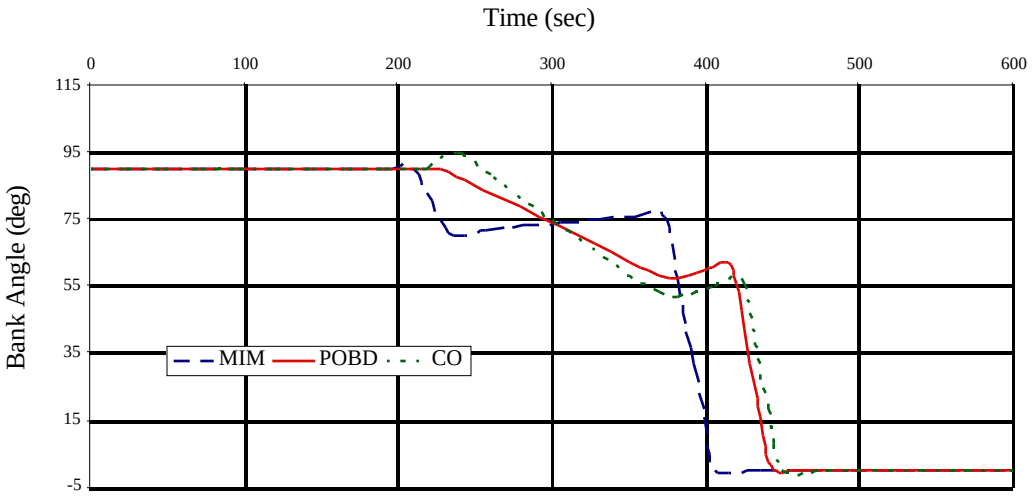

Figure 55: Bank Angle versus Time for *Stargazer* Flyback Trajectories

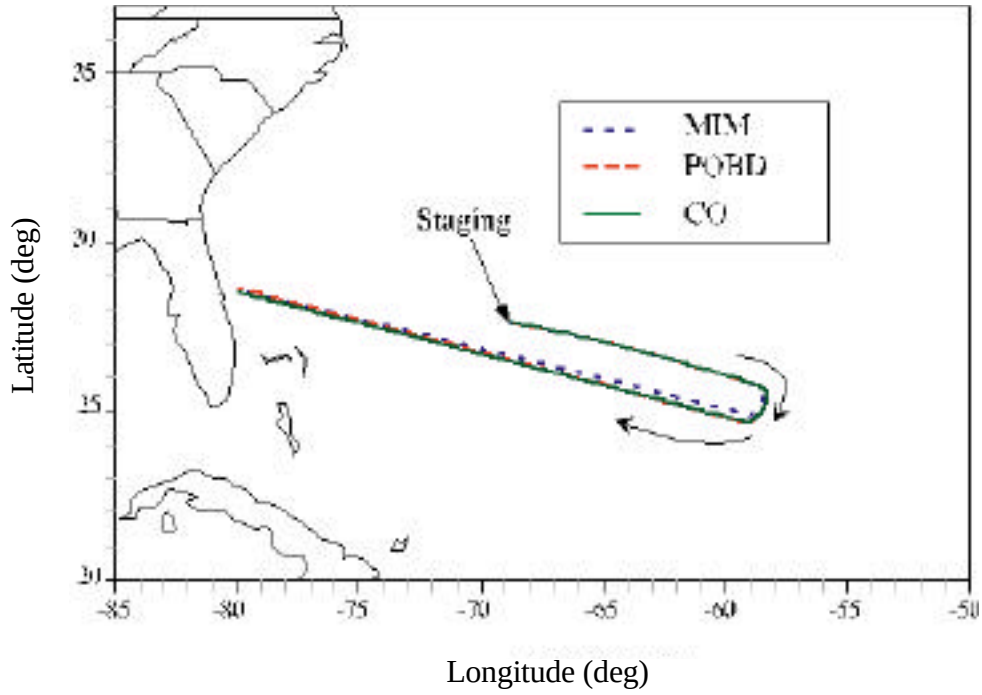

Figure 56: Groundtrack Comparison for *Stargazer* Flyback Trajectories

Figures 57 and 58 respectively show the altitude and velocity plots of the *Stargazer* flybacks. The angle of attack and bank angle turnaround does not begin until the apex of the ascent occurs at about two hundred seconds. It is also at this point that the velocity is at a minimum. The ramjet cruise back to KSC begins at approximately 500 seconds from the staging and ends about thirty-three minutes later.

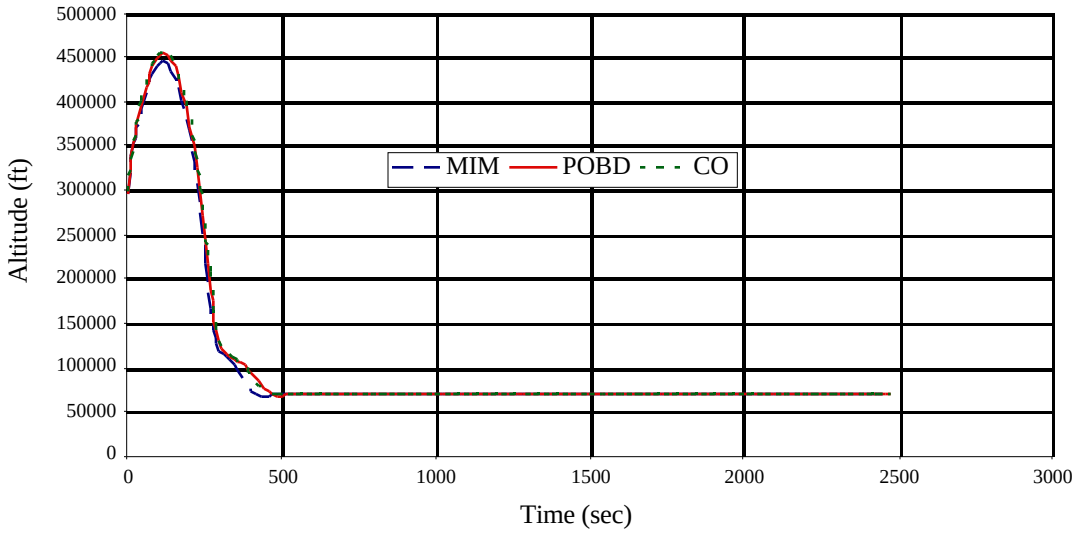

Figure 57: Altitude versus Time for *Stargazer* Flyback Trajectories

The upper stage trajectories are shown in Figure 59. As can be inferred from the plot, the pitch angles are dissimilar between the MIM and MDO methods. At the end of the respective trajectories an instantaneous velocity increment is applied. In the MIM case, this increment is small and gives a smaller upper stage mass ratio.

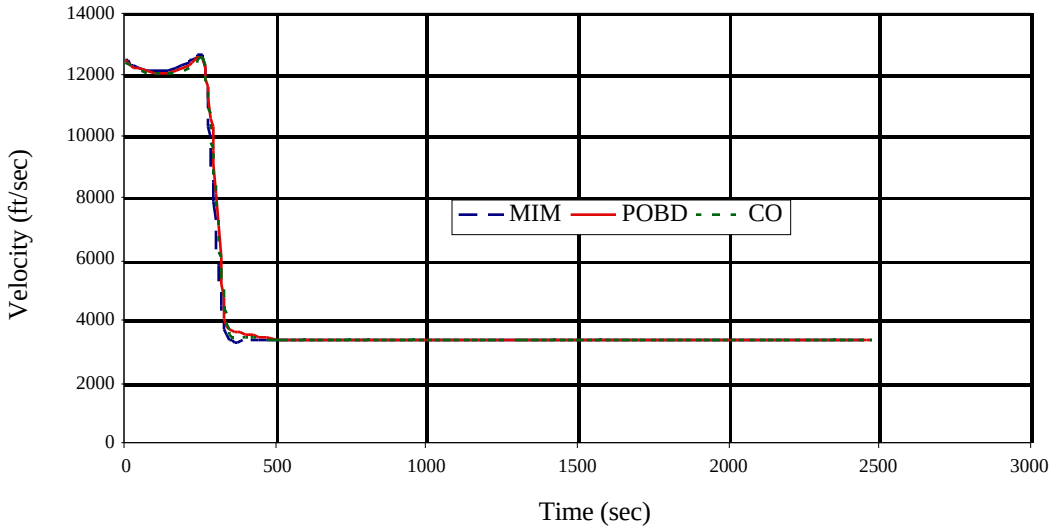

Figure 58: Velocity versus Time for *Stargazer* Flyback Trajectories

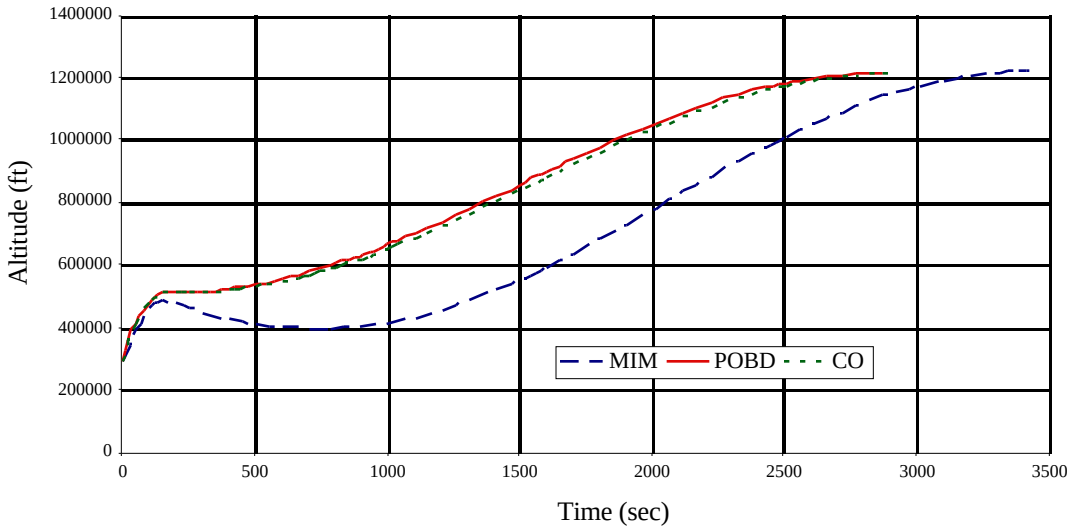

Figure 59: Altitude versus Time for *Stargazer* Upper Stage Trajectories

CHAPTER X

CONCLUSIONS AND RECOMMENDATIONS

10.1 Conclusions and Observations

The main contribution of this research has been the development and demonstration of a method for solving branching trajectories that exhibit feedback data flow. In addition, the method was formed such that the branching trajectory problem was decomposed into trajectory subproblems. These subproblems were executed in a distributed manner that produced an optimal solution with respect to an overall, system-level objective function while retaining agreement of the coupled data that existed between the branches and the ascent.

Solutions to the two branching trajectory testcases of the Kistler *K-1* launch vehicle and the *Stargazer* launch vehicle were obtained. The use of multidisciplinary design optimization techniques was examined in the method solutions for the branching trajectory problem. Based on the conclusions made below, the MDO technique selected for use in the overall method was the partial optimization-based decomposition method. The details for this overall method and reasons for the solution technique of POBD are given at the end of the conclusions section.

10.1.1 Conclusions

Specific objectives were established in support of the goals mentioned and the method developed. These qualitative and quantitative objectives are listed below with respective conclusions for each.

- Demonstrate an efficient computation approach that can be distributed on several computing processors to reduce overall solution time enough such that the solution process would be applicable in a vehicle design framework.

A reasonable time for solution methods depends on the complexity of the branching trajectory being studied. The Kistler *K-1* branching trajectory was not complex as, when decomposed, it was a product of simple rocket trajectories. A CPU time more than thirty minutes would slow the entire design process for that vehicle. CPU times on the order of fifteen minutes were obtained with the FPI, POBD, and FOBD solution techniques. The *Stargazer* branching trajectory is much more complex the *K-1*'s. However, the fastest CPU time obtained was for that of the POBD solution and that was almost three hours. Even though the entire *Stargazer* design is very involved, three hours is much too long for one discipline; one hour would be more acceptable.

For both vehicle branching trajectories, the CPU times for the CO solutions were four to five times longer than those for the other solution techniques. These solutions would not be acceptable, time wise, from a vehicle design standpoint. This illustrates one of the disadvantages of implementing CO with small-scaled problems.

- Demonstrate an improvement of 1% or greater in the objective function relative to the suboptimal solution of the manual iteration method.

The solution of the distributed method for the Kistler *K-1* problem showed that an increase in payload weight of 1%, on average, could be obtained. Similarly, a reduction in *Stargazer*'s dry weight of approximately 0.8% was achieved through the method. These percentages came close to the stated objective, but were not as large as hoped.

These percentages are significant in terms of revenue and vehicle costs. In the case of the *K-1*, more payload can be put into orbit per launch and thus, potentially $5,000,000 of profit to Kistler can be achieved. *Stargazer*'s non-recurring costs total in the billions of dollars. The smaller dry weight achieved implies a crucial amount of savings in non-recurring costs. The recurring costs is also reduced through a decrease in labor and hardware replacement costs.

- Decrease the computing time relative to a fixed-point iteration approach by 10% or more for a single trajectory solution.

The full OBD and CO solutions had decomposed trajectories that could be executed in a parallel manner. No CPU time improvements were made because of the number of additional function calls required for the full OBD solution and the amount of CPU time required by the subsystem optimization for the CO solutions.

- Maintain a reasonable level of method complexity and a set-up time that is no more than 50% greater than the set-up time of a suboptimal method like the manual iteration method.

Set-up times for the branching trajectory solutions varied depending on which vehicle's branching trajectory was being studied. Table 20 gives estimated set-up times for the manual iteration method (MIM) and MDO solution techniques. They are estimated from a non-biased standpoint as if the set-ups for each vehicle started independent of knowledge gained from another set-up for that vehicle. The only standard for the times in the table is the existence of the POST decks. For the *Stargazer* case, creation of the weights & sizing response surfaces and the multipliers for the engine data, taking about two days' time, are not included in each solution method set-up time. The times do not include the amount of time necessary for choosing the correct system-level optimizer or optimization program, DOT, a process requiring months of code manipulations and results examinations for each solution method.

Table 20: Set-up Time Comparisons

Vehicle/Solution Method	Set-up Time
Kistler *K-1*	
MIM	15 min
FPI	35 min
POBD	40 min
FOBD	50 min
CO	30 min
Stargazer	
MIM	30 min
POBD	2 hours
CO	1.73 hours

The times of Table 20 are based on the number of additional scripts needed to automate the solution, the number of design variables and constraints for each solution, and the number and type of modifications required in setting up the POST decks. The manual iteration method's set-up time only involved the amount of time needed to create a results database to monitor vehicle convergence. The MDO solution techniques set-up times were much more similar to each other than they were for the MIM. Even though POST decks and POST code needed modification in the CO solution, there were less design variables and constraints required by the system-level optimizer. Thus, the CO set-up time was less than that for the other decomposition methods, but only by a small amount.

The MDO solutions for the Kistler vehicle averaged 160% more time for set-up than for the manual iteration method. *Stargazer*'s MDO solutions averaged 270% more set-up time than the MIM. This increase is a direct consequence of the automation of the MDO methods; most of the increase is due to the new scripts required for data extraction and insertion. Had the data insertion and extraction for the manual iteration methods been automated as well, the differences in the set-up times for the MDO would have been significantly reduced. Detailed observations about automating and implementing the branching trajectory solutions are given in the last section of this chapter.

- Guarantee internal data consistency between the individual branches at the solution.

Internal data consistency between the individual branches was ensured by iteration (for the MIM and FPI solutions), compatibility constraints, (for the OBD solutions), or system/subsystem level coordination (for the CO solution). It was shown that the 'One-and-Done' method was an invalid method because of the differences between the feedback variables, or outputs, of the flyback and upper stage branches and the corresponding input to the ascent path.

- Demonstrate the scalability and robustness of the new method for small and large branching trajectory problems.

Solutions were found by the distributed method for solving decomposed branching trajectories. The relatively small branching trajectory problem of the Kistler *K-1* launch vehicle and the larger *Stargazer* branching trajectory problem were each solved successfully. The method was robust for the smaller *K-1* problem in that all solution techniques found a relatively similar solution. The method was robust for the *Stargazer* problem in that there were relatively similar solutions found for two solution techniques. The fact that solutions for *Stargazer* were difficult to obtain, as was the case for the POBD method, or unobtainable, in the case of the FPI method, is a product of the lack of robustness, or deficiency, in the MDO solution technique and the *Stargazer* POST decks. In Section 10.3, recommendations are made with the intent to improve this robustness.

- Formulate generalities of staging vector compromises for the branching trajectory problem.

Staging vector trends could not be made for the general branching trajectory problem. The trends observed were specific to the vehicle studied and the system-level objective function minimized.

Kistler *K-1* Branching Trajectories

The results of solving the *K-1* branching trajectory with MDO solutions indicated a trend from the manual iteration method. These results showed that a decrease in the flight path angle at staging aided in reducing the booster's flyback propellant. This allowed more payload weight to flown to orbit.

Stargazer Branching Trajectories

The MDO solutions for *Stargazer*'s branching trajectory showed a trend in staging flight path angle as well. This time, the inclination from that of the manual iteration method was towards an increased flight path angle. This was a result of the compromises made in the vehicle mass ratios and booster mixture ratio to obtain a minimal dry weight.

10.1.2 The New Method for Branching Trajectory Problem Solutions

In order to exploit the benefits of a distributed approach, branching trajectories were distributed into two or three subproblems. The point of separation for these trajectories naturally occurs at staging so that there exists an ascent subproblem and one or two branches, an upper stage branch and/or flyback branch. Once the trajectories were decomposed, the solution was obtained with traditional and multidisciplinary design optimization techniques.

The main deficiencies of the traditional methods of the 'One-and-Done' and manual iteration methods were discussed for the branching trajectory problem. The main deficiency was that conflicting objective functions existed in these methods. Each POST deck had its own objective to fulfil, but compromises in each individual trajectory could benefit the entire trajectory. Multidisciplinary design optimization decomposition techniques introduced a system-level optimizer that resulted in an overall, system-level objective for the branching trajectory problem at the solution.

With this knowledge in mind and that of the conclusions given above, the new method for solving branching trajectories with feedback is outlined below and in Figure 60.

- Distribute the branching trajectory problem into logical subproblems. The partition for the subproblems occurs at staging. For time-consuming upper stage and flyback

simulations, both branches should be separate from the ascent in order to exploit parallel executions and thus save CPU time.

· Invoke a system-level optimizer to ensure satisfaction of an overall objective function.

· Decompose the feedback coupling of the upper stage and flyback branches by breaking the data flow. Retain the feedforward of the staging vector.

· Solve the resulting problem with the system-level design variables being the trajectory simulation's design variables and the constraints being the constraints of the trajectory and the feedback compatibility constraints.

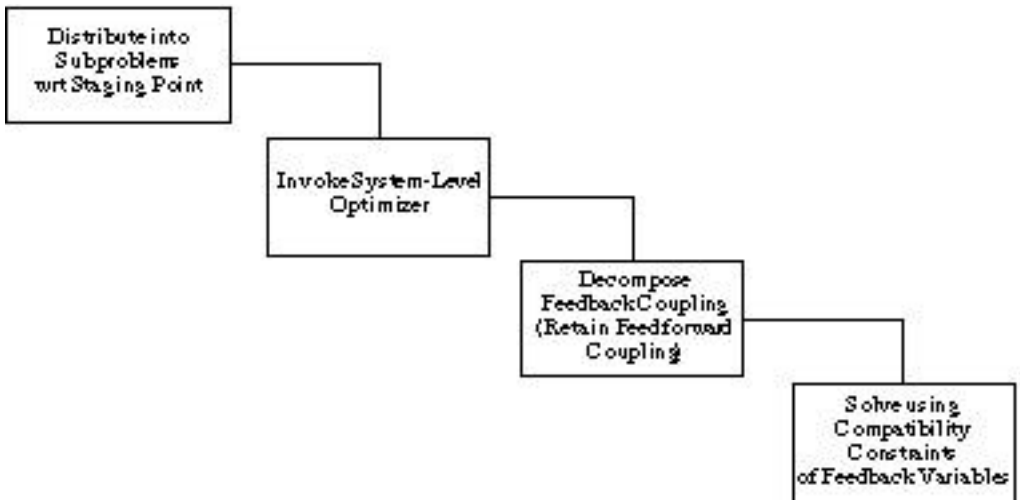

Figure 60: Method Structure for Branching Trajectory Solutions

The new method uses partial optimization-based decomposition in the solution of the optimization problem. This solution technique gave the best results when considering all the previous analysis and conclusions. CPU time was the greatest factor in determining whether the branching trajectory solution would be feasible in a vehicle design environment. Thus, the objective to keep this CPU time reasonable for each vehicle design was considered

to dominate the resultant choice. The POBD solution technique took approximately five times less CPU time when compared with the CO technique. POBD required slightly more time to set up; however, the difference was negligible, especially when compared with the difference in CPU execution time.

The exact staging vector is fed forward to the trajectory branches in the POBD method. Thus, the solution is not subject to the staging vector tolerances of the FOBD method. Also, any convergence tolerances are not an issue in partial optimization-based decomposition as in the FPI method. Although not fully parallel, if there are both flyback and upper stage branches, they can be executed in parallel with one another, saving some CPU time. The automation difficulty of POBD for the *Stargazer* solution is discussed in Section 10.3.

10.1.3 Observations

Multidisciplinary design optimization techniques were employed in the method solution for the branching trajectory problem. Some conclusions regarding their comparative performance at the solution, the system-level optimizer used, and implementation differences were observed.

MDO Methods: CO and OBD

The term ‘multidisciplinary design optimization’ suggests that the optimization problem being solved had many distinct disciplines. The branching trajectory problem, typically viewed as its own distinct discipline, when viewed as a distributed problem is composed of subproblems, thus MDO was a useful way to solve this problem. The MDO solutions presented add to the growing wealth of knowledge that exists currently about these methods.

Expected results were obtained with respect to collaborative optimization and optimization-based decomposition. Similar optimized results were obtained, though with difficulty for the partial optimization-based decomposition method for *Stargazer*. Although the system-level iterations were less for the collaborative optimization method than the optimization-based decomposition methods, the number of analysis calls were much greater

and required five to six times the amount of computational time. Though originally developed for large-scale distributed problems, collaborative optimization was used successfully, if slowly, for the small-scale branching trajectory problem.

System-Level Optimization

Many lessons were learned with respect to inclusion of the system-level optimization scheme for the distributed solutions to the branching trajectory problem. The modified method of feasible directions was the system-level optimization strategy used for each branching trajectory and all solution techniques. As discussed in Section 4.3, past research has typically used sequential quadratic programming as the system-level optimization scheme. For the branching trajectory problem, both the SQP and SLP methods were not able to find valid solutions even after many experiments with scaling factors and gradient perturbations. In addition, a projected gradient system-level optimization strategy was used as a solution technique. This strategy was not capable of solving the branching trajectory problem as well.

Gradient perturbation size was found to be dependent on the design variable size and small perturbations (on the order of 0.00001) were used in the MMFD solutions. All the optimizations performed better (in that feasible solutions were found) with scaled design variables. The scaling used was internal to the DOT™ optimization program.

Implementation

From the standpoint of the person that was required to run all the POST decks, the automation of this process was well received. However, problems occurred with the automation when the optimization did not proceed as desired. Examples of these problems and recommendations for improving the automation process are suggested in Section 10.3.

Some qualitative observations on the implementation for the different MDO methods can be made. The automation of the methods helped a great deal from the time standpoint of executing each method. This did require more coding from the outset. That small disadvantage was outweighed by the fact that each method did not have to be monitored constantly in order to know when to pass the inputs and outputs.

Because it was the first method implemented, the FPI method for the Kistler *K-1* took the greatest amount of time to implement and debug from errors. Although this method required internal iterations, this requirement was not an obstacle because the iteration convergence was based on flyback fuel weight, which was directly linked to the time the flyback engine was on. Since this time was a design variable, internal iteration convergence was met within at most one iteration for every function call.

For the single-level decomposition methods, (POBD and FOBD), different variables had to be put into the POST decks as the breaking of the feedback/feedforward loops necessitated. However, the coding for this was trivial as it was used in the FPI method. The only real addition for the POBD and FOBD methods was the calculation of the compatibility constraints, which occurred at the system level. The communication requirements for the FPI, POBD, and FOBD methods increased with respect to the number of variables in the broken loops.

The collaborative optimization method had different set-up requirements. Not as much calculation was required on the system-level as for the single-level decomposition methods. However, since CO is a multi-level scheme, a lot of modification was required at the analysis level, or for the POST decks. For each POST deck, all of the system-level targets had to be included, a trivial task that required only one additional line of code. Additional internal control variables (the local versions of the system-level variables), had to be added to each POST deck, again, a relatively simple task.

For the CO method, the hardest task was in modifying the actual POST code, but a special calculations subroutine exists for such modification. The errors, J's, had to be calculated in this subroutine since the objective for the POST decks was to minimize these errors. Much of the set-up time for the CO method was spent in insuring that the local variables used to calculate the J's, and the J's themselves, were correct.

Knowledge of the basic set-up for the *K-1* MDO cases helped in the coding for the *Stargazer* cases in that the algorithms and PERL scripting were easier. However, for the *Stargazer* cases, more computations were performed at the system level, because of the

addition of the propulsion and weights and sizing analyses, and more variables were passed to and from an increased number of POST decks.

When compared to the *K-1* cases, the communication requirements were significantly increased for the *Stargazer* MDO processes. The addition of the more complex weights and sizing and propulsion analyses added to the increased number of interactions between the POST decks and the system-level optimizer. Table 21 summarizes the differences in communication requirements for the two vehicles for the POBD and CO methods, respectively. The number of PERL scripts and POST include files are listed in the table along with the number of variables they represent. For example, the *K-1* POBD method's 3 PERL scripts extracted six staging variables and five constraints from the ascent deck, the flyback fuel weight and two constraints from the flyback deck, and inserted nineteen design variables into the POST decks. The include files for this method were two files that contained the twentieth design variable, prescribed flyback fuel weight and the six staging variables from the ascent deck that were needed by the flyback deck. Additional PERL scripts were employed to get CPU times and system-level iterations for the CO method, but these are not included in the totals. The aerodynamic and propulsive tables are not included in the 'Include Files' totals.

Table 21: Communication Requirements Summary

	POBD		CO	
	K-1	*Stargazer*	*K-1*	*Stargazer*
PERL Scripts /Variables Represented	3/33	11/78	4/45	10/88
Include Files /Variables Represented	2/7	10/18	1/8	10/22

10.2 Recommendations for Future Research

A number of recommendations can be made regarding directions for future work on the branching trajectory problem. Even though all the goals of the research were met, some of the objectives were not. The first few recommendations are directly related to those objectives.

CPU Time Reduction

In order to realistically include the optimization of *Stargazer*'s branching trajectory in a design paradigm, the total CPU time must be reduced. Elimination of the restarts in the POBD solution could help reduce this time. Investigation into whether this is a vehicle level characteristic, an RBCC vehicle characteristic, or a scaling problem would be beneficial.

CPU Time Reduction for CO Solutions

CO solutions can not be included in the design process with such large CPU times as evidenced in the *K-1* and *Stargazer* results. CPU time reduction may be achieved for this solution technique by approximating the subsystem optimization with a response surface method as in [57]. This would especially benefit the flyback branch of the *Stargazer* trajectory. Analysis into whether this approximation would significantly reduce the CPU times for this small-scaled branching trajectory problem should be studied.

Another idea that may warrant consideration is the use of collocation trajectory simulations with a sparse optimizer at the subsystem level for the CO solutions. This may reduce overall CPU time, but would one of the industry standards for trajectory optimization – POST. Starting subsequent system-level iterations from the previous solutions' design variables should also decrease CPU time. This was attempted in the *Stargazer* problem, but because of the lack of robustness in the POST decks, invalid trajectories were obtained.

Staging Vector Compromises

Although the FOBD solution resulted in a larger payload weight than for that of the other solution techniques, a part of that success may be attributed to the existence of tolerances on the staging vector variables. Although small, these tolerances introduce error

between the calculated staging vector from the POST deck and the corresponding design variables. This error may slightly benefit the objective function. More investigation into what tolerances are acceptable for each variable should be researched and may make the FOBD solution more desirable, since it can be decomposed into a totally parallel structure.

More branching trajectory applications need to be solved with MDO methods before concrete solutions can be made. In fact, for the branching trajectory problems of this thesis, the results were problem dependent. This may be the case for all branching trajectory problems. One such branching trajectory that could easily be researched with respect to its optimization is that of the Liquid Fly-Back Booster. It is described below.

Liquid Fly-Back Booster

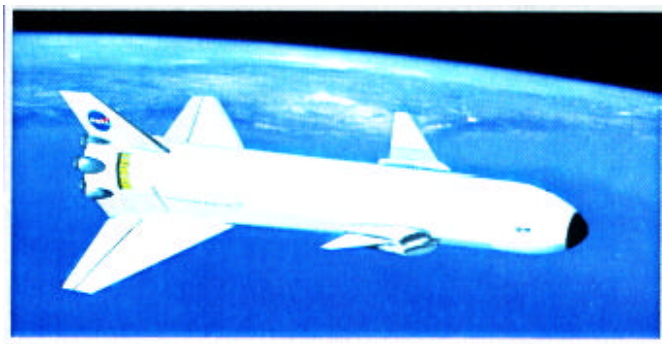

Figure 61: Lockheed Martin LFBB [82]

The Space Shuttle with liquid flyback boosters is a TSTO system that incorporates branching trajectories. An example of a Lockheed Martin concept is shown in Figure 61. To extend the life of the Space Shuttle and reduce launch costs, NASA is considering replacing the current solid rocket boosters with a reusable liquid booster(s) in a single or dual configuration [80, 81]. After staging, the liquid flyback booster(s) (LFBB) would return to KSC under powered flight. Power for the return flight would be provided by conventional turbofan or turbojet airbreathing engines. LFBB concepts typically require deployable or fixed wings.

The LFBB configuration and its characteristics are far from final definition. However, when including the orbiter, its trajectory will certainly be a branching problem (like Figure 1). The orbital branch (the Orbiter and the ET) and the flyback branch of the ascent trajectory must be treated simultaneously to produce an overall system-level objective. Compromises in the orbital branch might significantly improve the flyback branch and vice versa.

Stargazer Branching Trajectory Optimization

The optimization of the *Stargazer* branching trajectory was not possible without the inputs from the weights and sizing and propulsion disciplines. And in this case, the analyses for these disciplines were simplified. Additionally, the vehicle TPS was assumed constant throughout each iteration. These approximations can lead to errors. Thus, a vehicle design optimization without these approximations would make the results more realistic. In addition, though dry weight is certainly a large factor in the recurring cost/price per flight (as its effects appear in the propellant, LRU hardware, and labor costs), the upper stage also contributes a lot to the recurring cost/price. Subsequently, an entire vehicle design optimization should be performed, for various staging Mach numbers, with an objective function of reducing the recurring cost.

The Automation Process

The automation of the branching trajectory optimization encountered some disadvantages when the optimization process did not proceed well. At the subsystem level, this was caused by a lack of robustness in the *Stargazer* POST decks. At this level, an expert system, like that of [83] would help keep the POST decks from resulting in physically invalid trajectories. At the system-level when the optimization progress was stopped, as was the subsequent outcome from the oscillations of the *Stargazer* POBD method, a different type of expert system could be employed. These changes would improve the automation and optimization process.

Comparisons with POST II

Lastly, it is recommended that solution comparisons be made with the non-distributed simulation of POST II when it is available to the public, if a way is found to exactly model the feedback dependencies. Simulation with POST II would allow the same trajectory modeling assumptions to be retained for an accurate comparison of solution values, function calls, and CPU times.

APPENDIX A

Weight Breakdown for the Kistler *K-1*

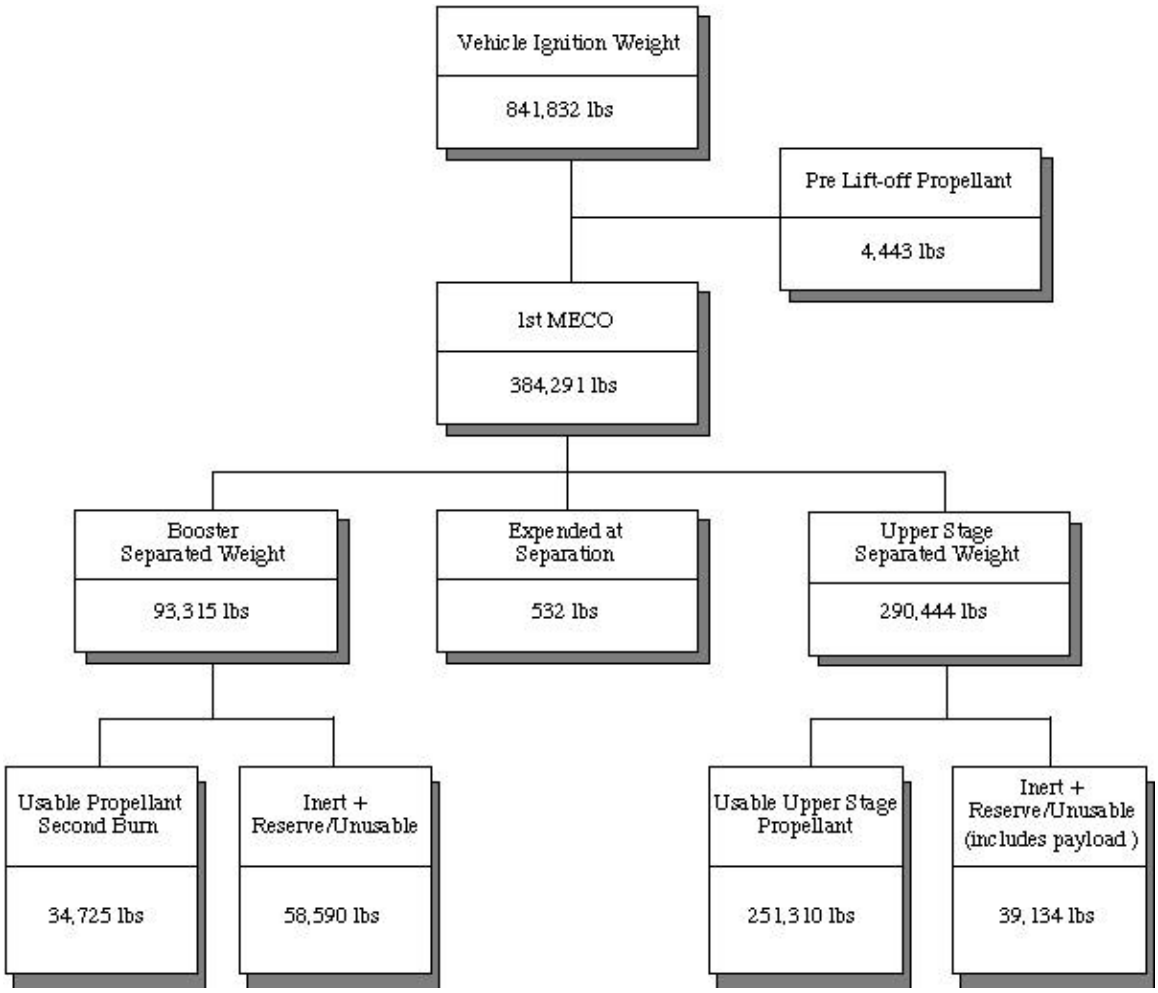

APPENDIX B

Engine and Aerodynamics Information for the *K-1*

Propulsion Information

First Stage (Booster) Engines:

AJ26-59	(NK-33)
Number of engines:	3
Vacuum Thrust:	378,900 lbs/engine
Sea-Level Thrust:	339,800 lbs/engine
Vacuum Isp:	331.3 seconds

Upper Stage Engine:

AJ26-60	(NK-43)
Number of engines:	1
Vacuum Thrust:	398,300 lbs/engine
Vacuum Isp:	348.3 seconds

Reference Aerodynamics Information:

	Diameter (ft)	*Length (ft)*
First (Booster) Stage:	22	60.2
Upper Stage:	13.2	61

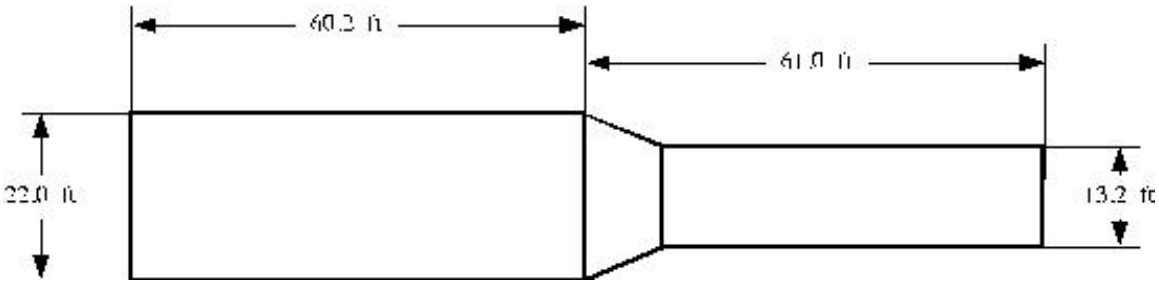

APPENDIX C

Final Design Variables for *K-1* Methods

Normalized* Design Variables	Manual Iteration	FPI	POBD 1	POBD 2	FOBD	CO**
x[1]	1.00000	0.93887	0.92471	0.92518	0.95770	0.98153
x[2]	1.00000	1.03480	1.00458	1.00415	0.98194	1.00622
x[3]	1.00000	0.98765	0.99642	0.99606	1.01467	0.98931
x[4]	1.00000	0.98912	0.99324	0.99443	0.99879	0.96318
x[5]	1.00000	1.00587	1.00568	1.00484	1.01804	1.04452
x[6]	1.00000	0.95039	0.99606	0.99585	0.99162	0.93678
x[7]	1.00000	1.00017	1.00057	1.00070	0.99328	1.00460
x[8]	1.00000	0.99678	0.99877	0.99843	0.99264	0.99218
x[9]	1.00000	0.99761	0.99493	0.99404	0.99191	0.98777
x[10]	1.00000	1.00901	1.00836	1.00989	1.00376	1.00066
x[11]	1.00000	0.99541	0.99472	0.99401	0.99916	1.00348
x[12]	1.00000	0.99904	0.99721	0.99670	1.00185	0.99612
x[13]***	1.00000	1.00429	1.01078	1.01078	1.01595	1.01122
x[14]	1.00000	1.00128	0.99917	0.99921	0.99721	0.99450
x[15]	1.00000	1.01851	0.98953	0.98940	0.99165	0.99284
x[16]	1.00000	1.04009	0.96236	0.96200	0.96753	0.96734
x[17]	1.00000	1.01842	0.99536	0.99527	0.99652	0.99644
x[18]	1.00000	1.00256	0.99174	0.99175	0.98816	0.98627
x[19]	1.00000	1.00715	0.99139	0.99136	0.99137	0.97831
x[20]	N/A	N/A	0.99139	0.99136	0.99137	N/A

x[21]	N/A	N/A	N/A	N/A	0.99648	N/A
x[22]	N/A	N/A	N/A	N/A	0.99714	N/A
x[23]	N/A	N/A	N/A	N/A	0.98665	N/A
x[24]	N/A	N/A	N/A	N/A	1.00018	N/A
x[25]	N/A	N/A	N/A	N/A	1.00023	N/A
x[26]	N/A	N/A	N/A	N/A	0.99993	N/A

* - The design variables are normalized with respect to the Manual Iteration Method results.

** - x[1] – x[19] are the local POST design variables and are listed here for comparison. The system-level target design variables are listed in Chapter 7.

*** - x[13] is the objective function, payload weight.

APPENDIX D

RBCC Engine Inputs to SCCREAM for *Stargazer*

Engine Type: Ejector ScramJet
External Compression: Wedge with 1 Ramp
Rocket Primary Propellants: LOX/LH2
Number of Engines: 4
    Force Accounting Method: Cowl-to-Tail
    SLS Thrust (Ejector Mode Only): 20207.0 lbs per engine
Forebody and Inlet Characteristics
    Inlet Area: 14.4 ft^2 per engine
    Aref for Ct Calculation: 14.4 ft^2 per engine
    Angle of Attack: 0.0 degrees
    Cowl Height: 3.6 ft
    Forebody Width: 16 ft
        Centerline Distance from Nose to Cowl: 70.0 ft
        Wedge Angle: 5.0 degrees
    Rocket Primary Characteristics
        Area Ratio: 18.0
        Chamber Pressure: 1600.0 psi
        Mixture Ratio: 8.0

Engine Station Efficiencies
    Rocket Primary Combustor: 97.5 %
    Rocket Primary Nozzle: 98.0 %
    Combustor: 95.0 %

Nozzle: 98.0 %

Fuel Temperature: 500.0 R

Combustor Length

From Station 3 to 3': 2.0 ft

From Station 3' to 4: 3.0 ft

Subsonic Combustion

Geometry:

A* / A1 = 0.4

A1 / A3 = 1.8

A3' / A3 = 1.3

A4 / A3' = 1.2

Ae / A1 = 2.0

Ae' / A1 = 3.5

Fuel Injector Location & Start of Heat Release: 2.0 ft

End heat release: 5.0 ft

Fuel Injection Velocity: 3000.0 ft/s

Fuel Injection Angle: 0.0 degrees

Friction Coefficient: 0.001

Supersonic Combustion

Geometry:

A* / A1 = 0.4

A1 / A3 = 1.8

A3' / A3 = 1.2

A4 / A3' = 1.1

Ae / A1 = 3.5

Ae' / A1 = 3.5

Fuel Injector Location & Start of Heat Release: 1.0 ft

End heat release: 3.0 ft

Fuel Injection Velocity: 4000.0 ft/s
Fuel Injection Angle: 0.0 degrees
Friction Coefficient: 0.001

All-Rocket Mode

All-Rocket Mode Expansion Ratio: 180
All-Rocket Mode Mixture Ratio: 7.0

APPENDIX E

Stargazer Engine Multipliers & Scaling Equations

The inputs for the *Stargazer* engine deck are listed below with the equations used to calculate each. Wg is the booster gross weight. All engine data is scaled by the original *Stargazer* engine which was analyzed in SCCREAM and appears in Appendix D.

Ejector LOX flow rate = (((Wg*.7/4)/20207.4*83628.4)/420.429)*8/9;
Ejector linear thrust multiplier = 4*(.7*Wg/4)/20207.4;
Ramjet capture area = (57.6*.7*Wg/(20207.2*4));
Scramjet capture area = (57.6*.7*Wg/(20207.2*4));
All-Rocket LOX flow rate = (((Wg*.7/4)/20207.4*83628.4)/420.429)*7/8;
All-Rocket vacuum thrust = (Wg*.7/4)/20207.4*83628.4;
All-Rocket exit area = (Wg*.7/4)/20207.4*39.37464;

The inputs for the upper stage engine and the corresponding equations are as follows, where USWg is the upper stage gross weight:

Upper stage vacuum thrust = USWg;	(T/W of 1.0)
Upper stage exit area = 1.72/3350*USWg;	(scaled by original engine)

The I_{sp}'s for all engines are the same for iteration. For the booster's ejector, ramjet, and scramjet modes, the I_{sp}'s are variable, depending on the Mach number, altitude, and

throttle. The I_{sp} for all-rocket mode is 420.429 seconds. The upper stage engine I_{sp} is 328 seconds.

APPENDIX F

Stargazer Weights Response Surfaces

The response surface equations for the *Stargazer* required weights inputs and output are listed below. These equations were generated by JMP software [84]. Twenty-seven responses were evaluated. The r-squared values are also listed for each equation.

In the equations below the following applies:

Mix = Booster Mixture Ratio,
MRus = Upper Stage Mass Ratio,
MRb = Booster Mass Ratio,
MRfb = Flyback Mass Ratio.

INPUTS:

Sref = 28669.806+3801.6667*Mix-33.83333*MRus-12037.25*MRb-30761.25*MRfb
+294.44445*Mix*Mix-10*MRus*Mix-3.5*MRus*MRus-1163.333*MRb*Mix
+33*MRb*MRus+1197.5*MRb*MRb1933.333*MRfb*Mix+30*MRfb*MRus
+7400*MRfb*MRb+7562.5*MRfb*MRfb;
RSquare = 0.996948

Wg = 5619835.2+580926.67*Mix-20480.33*MRus-2372700*MRb-5555900*MRfb
+34944.445*Mix*Mix-1066.667*MRus*Mix-747*MRus*MRus
-174960*MRb*Mix+8567*MRb*MRus+235119.5*MRb*MRb
-253500*MRfb*Mix+10335*MRfb*MRus+1319190*MRfb*MRb
+1226412.5*MRfb*MRfb;

RSquare = 0.993144

USWg = 1244.6944+246.11111*Mix+812.16667*MRus-586.4167*
MRb-1620.417*MRfb-16.66667*Mix*Mix+30*MRus*Mix
+64.5*MRus*MRus-23.33333*MRb*Mix-106*MRb*MRus
+81*MRb*MRb-133.3333*MRfb*Mix-255*MRfb*MRus
+320*MRfb*MRb+575*MRfb*MRfb;
RSquare = 0.999916

USSref = 44.572361+6.7583333*Mix+4.9258333*MRus-16.45875*MRb
-43.26875*MRfb-.361111*Mix*Mix+.2666667*MRus*Mix
+.0525*MRus*MRus-.633333*MRb*Mix-.9*MRb*MRus+1.705*MRb*MRb
-2.833333*MRfb*Mix-2.05*MRfb*MRus+6.825*MRfb*MRb
+11.5*MRfb*MRfb;
RSquare = 0.999389

OUTPUT:

Dry = 1186063.2+139966.47*Mix-3566.02*MRus-495759.8*MRb-1.2121e6*MRfb
+9580.2595 *Mix*Mix-343.4093*MRus*Mix-191.8127*MRus*MRus
-42297.67*MRb*Mix+1714.0259*MRb*MRus+49110.143*MRb*MRb
-65399.28*MRfb*Mix+2152.255*MRfb*MRus+286660.08*MRfb*MRb
+280425.16*MRfb*MRfb;
RSquare = 0.994115

APPENDIX G

Final Design Variables for *Stargazer* Methods

Normalized* Design Variables	Manual Iteration	POBD	CO**
x[1]	1.00000	1.01343	1.00950
x[2]	1.00000	0.72691	0.74060
x[3]	1.00000	1.34879	1.31626
x[4]	1.00000	0.65429	0.67414
x[5]	1.00000	0.95849	0.96799
x[6]	1.00000	1.00937	1.00937
x[7]	1.00000	0.97143	0.97211
x[8]	1.00000	0.92545	0.89952
x[9]	1.00000	1.00028	0.99722
x[10]	1.00000	1.03181	1.04580
x[11]	1.00000	1.00184	0.98929
x[12]	1.00000	1.04123	1.05636
x[13]	1.00000	1.42828	1.35862
x[14]	1.00000	1.41161	1.33825
x[15]	1.00000	1.59868	1.49127
x[16]	1.00000	1.75435	1.62455
x[17]	1.00000	1.31894	1.27074
x[18]	1.00000	1.00479	1.00612
x[19]	1.00000	1.06526	1.05827
x[20]	1.00000	0.76448	0.82243

x[21]	1.00000	0.66889	0.62573
x[22]	1.00000	0.91506	0.90209
x[23]	1.00000	1.00000	1.00001
x[24]	1.00000	1.00000	1.00000
x[25]	1.00000	1.00000	1.00000
x[26]	1.00000	1.25885	1.37569
x[27]	1.00000	0.75222	0.66925
x[28]	1.00000	0.97972	0.95254
x[29]	1.00000	1.00000	1.00000
x[30]	1.00000	1.00000	1.00000
x[31]	1.00000	1.00000	1.00000
x[32]	1.00000	1.05757	1.06434
x[33]	1.00000	1.02809	0.99030
x[34]	1.00000	0.81443	0.78530
x[35]	1.00000	0.74221	0.82734
x[36]	N/A	1.00812	N/A
x[37]	N/A	1.00210	N/A
x[38]	N/A	0.99357	N/A
x[39]	N/A	0.99177	N/A

*- The design variables are normalized with respect to the manual iteration method results.
** - x[1] – x[35] are the local POST design variables and are listed here for comparison. The system-level target design variables are listed in Chapter 9.

REFERENCES

1. Miele, A. Flight *Mechanics: Theory of Flight Paths*. Reading, PA: Addison-Wesley, 1962.

2. Lawden, D. F. *Optimal Trajectories for Space Navigation*. London: Butterworths, 1963.

3. Vinh, Nguyen X. *Optimal Trajectories in Atmospheric Flight*. New York: Elsevier Scientific Publishing Company, 1981.

4. Etkin, Bernard. *Dynamics of Flight--Stability and Control*. 2nd Edition. New York: John Wiley & Sons, Inc., 1982.

5. Tartabini, P. V., R. D. Braun, and R. S. Chowdry. "A Comparison of Direct Trajectory Optimization Techniques: Collocation vs. Numerical Integration." AIAA Paper 95-3481. August, 1995.

6. Betts, John T. "Survey of Numerical Methods for Trajectory Optimization." *Journal of Guidance, Control, and Dynamics*. Vol. 21, No. 2, pp. 193-207. March-April, 1998.

7. Troutman, John L. *Variational Calculus and Optimal Control: Optimization with Elementary Complexity*. 2nd Ed. New York: Springer-Verlag New York, Inc., 1996.

8. Keller, Herbert B. *Numerical Methods for Two-Point Boundary-Value Problems*. Massachussetts: Blaisdell, 1968.

9. Bailey, P. B., L. F. Shampine, and P. E. Waltman. *Nonlinear Two Point Boundary Value Problems.* New York: Academic Press, 1968.

10. Martos, Bela. *Nonlinear Programming Theory and Methods*. New York: American Elsevier Pub. Co., 1975.

11. Bazaraa, M. S., H. D. Sherali, and C. M. Shetty. *Nonlinear Programming: Theory and Algorithms.* 2nd Ed. New York: Wiley, 1993.

12. Bryson, A. E. and Y. C. Ho. *Applied Optimal Control: Optimization, Estimation, and Control.* Rev. USA: Hemisphere Publishing Corporation, 1975.

13. Leung, M. S. and A. J. Calise. "An Approach to Optimal Guidance of an Advanced Launch Vehicle Concept." Proceedings of the American Control Conference. pp. 1824-1828. 1990.

14. Speyer, Jason L. 'Approximate Optimal Guidance for Aerospace Systems.' AAS Paper 94-070. February, 1994.

15. Park, S.-Y. "Launch Vehicle Trajectories with a Dynamic Pressure Constraint." *Journal of Spacecraft and Rockets.* Vol. 35, No. 6, pp. 765-773. November - December, 1998.

16. Calise, A.J., N. Melamed, and S. Lee. "Design and Evaluation of a 3-D Optimal Ascent Guidance Algorithm." *Journal of Guidance, Control, and Dynamics*. Vol 21, No. 6, pp 867-875. November-December, 1998.

17. Vlases, W. G., S. W. Paris, R. M. Lajoie, P. J. Martens, and C. R. Hargraves. "Optimal Trajectories by Implicit Simulation, Version 3.0, User's Manual." WRDC-TR-90-3506. Wright Patterson Air Force Base, OH. 1990.

18. Brauer, G. L., D. E. Cornick, and R. Stevenson. "Capabilities and Applications of the Program to Optimize Simulated Trajectories." NASA CR-2770. Feb. 1977.

19. Meder, D. S. and J. L. Searcy. "Generalized Trajectory Simulation (GTS), Volumes I-V." The Aerospace Corporation. SAMSO-TR-75-255. January, 1975.

20. Paris, S. "Overview of OTIS 3.0." NASA Conference Publication No. 10187. August, 1996.

21. Hallman, W. P. "Mission Timeline for a Shuttle-IUS Flight Using a Nonstandard Shuttle Park Orbit." TOR-0083 (3493-14)-1. The Aerospace Corporation. October, 1982.

22. Naftel, J. C. and R. W. Powell. "Flight Analysis for a Two-Stage Launch Vehicle with a Glideback Booster." *Journal of Guidance, Control, and Dynamics*. Vol. 8, No. 3, pp. 340-343. May – June, 1985.

23. Lepsch, R. A. and J. C. Naftel. "Winged Booster Performance with Combined Rocket and Airbreathing Propulsion." *Journal of Spacecraft and Rockets*. Vol. 30, No. 6, pp. 641-646. November – December, 1993.

24. Anderson, R. L., J. T. Aguirre, S. A. Striepe, G. L. Brauer, and M. C. Engel. *Program to Optimize Simulated Trajectories (POST II): Guide for New Users*. Preliminary, Beta Release, Volume I. April, 1999.

25. Vanderplaats, Garret N. *Numerical Optimization Techniques for Engineering Design: with Applications*. New York: McGraw-Hill Publishing Co. 1984.

26. Steward, D. V. Systems Analysis and Management: Structure, Strategy and Design. New York: Petrocelli Books, Inc. 1981.

27. Sobieszczanski-Sobieski, J. "Multidisciplinary Design Optimization: An Emerging New Engineering Discipline." Presented at The World Congress on Optimal Design of Structural Systems in Rio de Janeiro, Brazil. August, 1993.

28. Sobieszczanski-Sobieski, J. and R. T. Haftka. "Multidisciplinary Aerospace Design Optimization: Survey of Recent Developments." AIAA Paper 96-0711. January, 1995.

29. Rowell, L. F., R. D. Braun, J. R. Olds, and R. Unal. "Multidisciplinary Conceptual Design Optimization of Space Transportation Systems." *Journal of Aircraft*. Vol. 36, No. 1, pp. 218-226. January-February, 1999.

30. Sobieszczanski-Sobieski, J. "Sensitivity Analysis and Multidisciplinary Optimization for Aircraft Design: Recent Advances and Results." *Journal of Aircraft*. December, 1990.

31. Celi, R. "Recent Applications of Design Optimization to Rotorcraft—A Survey." *Journal of Aircraft*. Vol. 36, No. 1, pp. 176-189. January-February, 1999.

32. Roy, Ranjit. *A Primer on the Taguchi Method*. New York: Van Nostrand Reinhold, 1990.

33. Phadke, Madhav. *Quality Engineering Using Robust Design*. New Jersey: Prentice-Hall. 1989.

34. Olds, J. and G. Walberg. "Multidisciplinary Design of a Rocket-Based Combined-Cycle SSTO Launch Vehicle Using Taguchi Methods." AIAA Paper 93-1096. February, 1993.

35. Olds, J. R. "Multidisciplinary Design Techniques Applied to Conceptual Aerospace Vehicle Design." Ph.D. Thesis. North Carolina State University. 1993.

36. DeLaurentis, D., P. S. Zink, D. Mavris, C. E. S. Cesnik, and D. P. Schrage. "New Approaches to Multidisciplinary Synthesis: An Aero-Structures-Control Application Using Statistical Techniques." AIAA Paper 96-5501. October, 1996.

37. Zink, P. S., D. N. Mavris, D. M. Flick, and M. H. Love. "Impact of Active Aeroelastic Wing Technology on Wing Geometry Using Response Surface Methodology."

Presented at CEAS/AIAA/ICASE/NASA Langley International Forum on Aeroelasticity and Structural Dynamics. June, 1999.

38. Mavris, D. N., D. A. DeLaurentis, O. Bandte, and M. A. Hale. "A Stochastic Approach to Multidisciplinary Aircraft Analysis and Design." AIAA Paper 98-0912. January, 1998.

39. Mavris, D. N., O. Bandte, and D. A. DeLaurentis. "Robust Design Simulation: A Probabilistic Approach to Multidisciplinary Design." *Journal of Aircraft* . Vol. 36, No. 1, pp. 298-307. January-February, 1999.

40. Gage, P. J., R. D. Braun, and I. M. Kroo. " Interplanetary Trajectory Optimization Using a Genetic Algorithm." *Journal of Astronautical Sciences.* Vol. 43, No. 1, pp. 59-76. January, 1995.

41. Way, D. and J. Olds. "Sirius: A New Launch Vehicle Option for Mega-Leo Constellation Deployment." AIAA Paper 97-3122. July, 1997.

42. Balling, R. J. and J. Sobieszczanski-Sobieski. "Optimization of Coupled Systems: A Critical Overview of Approaches." AIAA Paper 94-4330. September, 1994.

43. Sobieszczanski-Sobieski, J. "Optimization by Decomposition: A Step from Hierarchic to Non-Hierarchic Systems." NASA CP-3031. September, 1989.

44. Altus, S., and I. M. Kroo. "Concurrent Wing Design and Flight-Path Optimization Using Optimizer-Based Decomposition." AIAA Paper 98-4920. September, 1998.

45. Altus, S. S. "Multidisciplinary Aircraft Design Optimization Using Single-Level Decomposition." Ph.D. Thesis. Stanford University. August, 1997.

46. Braun, R. D., R. W. Powell, R. A. Lepsch, D. O. Stanley, and I. M. Kroo. "Comparison of Two Multidisciplinary Optimization Strategies for Launch-Vehicle Design." *Journal of Spacecraft and Rockets*. Vol. 32, No.3, pp. 404-410. May-June, 1995.

47. Kroo, I., S. Altus, R. Braun, P. Gage, and I. Sobieski. "Multidisciplinary Optimization Methods for Aircraft Preliminary Design." AIAA Paper 94-4325. September, 1994.

48. Jacobsmeyer, H. A. and R. J. Balling. "When Can Multi-Level Optimization Reduce Computational Effort?" AIAA Paper 98-4921. September, 1998.

49. Balling, R. J. and C. A. Wilkinson. "Execution of Multidisciplinary Design Optimization Approaches on Common Test Problems." *AIAA Journal*. Vol. 35, No. 1, pp. 178-186. January, 1997.

50. Braun, R. D. "Collaborative Optimization: An Architecture for Large-Scale Distributed Design." Ph.D. Thesis. Stanford University. May, 1996.

51. Braun, R. D., R. W. Powell, R. A. Lepsch, D. O. Stanley, and I. M. Kroo. "Multidisciplinary Optimization Strategies for Launch Vehicle Design." AIAA Paper 94-4341. September, 1994.

52. Braun, R. D., A. A. Moore, and I. M. Kroo. "Collaborative Approach to Launch Vehicle Design." *Journal of Spacecraft and Rockets*. Vol. 34, No. 4, pp. 478-486. July-August, 1997.

53. Sobieski, I. and I. Kroo. "Collaborative Optimization Applied to an Aircraft Design Problem." AIAA Paper 96-0715. January, 1996.

54. Braun, R. D. and I. Kroo. "Development and Application of the Collaborative Optimization Architecture in a Multidisciplinary Design Environment." *Multidisciplinary Design Optimization: State of the Art*.. Philadelphia, PA: SIAM Publications. 1997.

55. Rawlings, M. R. and R. J. Balling. "Collaborative Optimization with Disciplinary Conceptual Design." AIAA Paper 98-4919. September, 1998.

56. Budianto, I. A. and J. R. Olds. "A Collaborative Optimization Approach to Design and Deployment of a Space Based Infrared System Constellation." 2000 IEEE Aerospace Conference Proceedings. Paper 13.0203. Big Sky, Montana. March, 2000.

57. Sobieski, I. P. "Multidisciplinary Design Using Collaborative Optimization." Ph.D. Thesis. Stanford University. August, 1998.

58. Manning, V. Large-Scale Design of Supersonic Aircraft Via Collaborative Optimization." Ph.D. Thesis. Stanford University. June, 1999.

59. Balling, R. J. and J. Sobieszczanski-Sobieski. "An Algorithm for Solving the System-Level Problem in Multilevel Optimization." AIAA Paper 94-4333. September, 1994.

60. Sobieszczanski-Sobieski, J., B. James, and M. Riley. "Structural Design by Generalized, Multilevel Decomposition." *AIAA Journal*. Vol. 25, No. 1, pp. 139-145. January, 1987.

61. Walsh, J. L., K. C. Young, J. I. Pritchard, H. M. Adelman, and W. R. Mantay. "Integrated Aerodynamic/Dynamic/Structural Optimization of Helicopter Rotor Blades Using Multilevel Decomposition." NASA TP-3465, January, 1995.

62. Beltracchi, T. J. "Decomposition Approach to Solving the All-Up Trajectory Optimization Problem." *Journal of Guidance, Control, and Navigation*. Vol. 15, No. 3, pp. 707-716. May-June, 1992.

63. Cramer, E. J., J. E. Dennis, Jr., P. D. Frank, R. M. Lewis, and G. R. Shubin. "Problem Formulation for Multidisciplinary Optimization." *SIAM Journal of Optimization*. Vol. 4, No. 4, pp. 754-776. November, 1994.

64. Sobieszczanski-Sobiesk, J., J.-F. Barthelemy, and K. M. Riley. "Sensitivity of Optimum Solutions to Problem Parameters." *AIAA Journal*. Vol. 20, pp. 1291-1299. September, 1982.

65. Braun, R. D., I. M. Kroo, and P. J. Gage. "Post-Optimality Analysis in Aerospace Vehicle Design." AIAA Paper 93-3932. August, 1993.

66. Kodiyalam, S. "Evaluation of Methods for Multidisciplinary Design Optimization (MDO), Phase 1." NASA CR-1998-208716. September, 1998.

67. Alexandrov, N. M. and S. Kodiyalam. " Initial Results of an MDO Method Evaluation Study." AIAA Paper 98-4884. September, 1998.

68. Zang, T. A. and L. L. Green " Multidisciplinary Design Optimization Techniques: Implications and Opportunities for Fluid Dynamics Research." AIAA Paper 99-3798. June-July, 1999.

69. Korte, J. J., R. P. Weston, and T. A. Zang. "Multidisciplinary Optimization Methods for Preliminary Design." AGARD Interpanel Symposium "Future Aerospace Technology in the Service of the Alliance." Paris, France. April, 1997.

70. Kohrs, R. and R. Petersen. "Development of the K-1 Two-Stage, Fully-Reusable Launch Vehicle." AIAA Paper 98-1540. April, 1998.

71. J. Andrews. "Status of the Kistler Reusable Launch Vehicle." AIAA Paper 98-3955. July, 1998.

72. Kistler Aerospace web site: http://www.kistleraerospace.com.

73. Anisimov, V. S., T. C. Lacefield, and J. Andrews. "Evolution of the NK-33 and NK-43 LOX/Kerosene Engines." AIAA Paper 97-2680. July, 1997.

74. Mecham, M. "Aerojet Acquires Major K-1 Engine Shipment." *Aviation Week and Space Technology*. Vol. 147, No. 10, pp. 61-62. September, 1997.

75. Kohrs, R. Personal Communications. June, 1999 and November, 1999.

76. Sova, G. and P. Divan. "Aerodynamic Preliminary Analysis System II, Part II – User's Manual." NASA CR-182077. April, 1991.

77. *DOT™ User's Manual*, Version 4.20. Vanderplaats Research & Development, Inc. Colorado: 1995.

78. Olds, J.R., L. Ledsinger, J. Bradford, A. Charania, D. McCormick, and D. R. Komar. " *Stargazer*: A TSTO Bantam-X Vehicle Concept Utilizing Rocket-Based Combined Cycle Propulsion." AIAA Paper 99-4888. November, 1999.

79. Bradford, J. E. and J. R. Olds. "SCCREAM v. 5: A Web-Based Airbreathing Propulsion Analysis Tool." AIAA Paper 99-2104. June, 1999.

80. Ryan, Richard M., W. J. Rothschild, and D. L Christensen. "Booster Main Engine Selection Criteria for the Liquid Fly-Back Booster." JANNAF JPM. July, 1998.

81. Rothschild, W. and E. Schuster. "Airbreathing Propulsion System Design Concepts for a Reusable First Stage Rocket Booster." AIAA Paper 99-2380. July, 1999.

82. Anonymous. Lockheed Martin literature.

83. Budianto, I. A., J. R. Olds, and N. C. Baker. "Demonstration of CLIPS as an Intelligent Front-End for POST." AIAA Paper 99-0110. January, 1999.

84. Anonymous. JMP Version 3.1. SAS Institute, Inc.: Cary, NC, 1995.

VITA

Laura Anne Ledsinger was born on May 26, 1972 in Baltimore, Maryland. After many years of preparatory education, she graduated as valedictorian from Patapsco High School in 1990. In September of that year, she joined the Georgia Institute of Technology for her undergraduate studies in Aerospace Engineering. She received her Bachelor of Science degree, with Highest Honor, in June of 1994. Laura was a recipient of the Donald Dutton Outstanding Aerospace Senior Award in 1994.

That September, she continued her studies at Georgia Tech, this time, as a graduate student. Laura received her Master of Science degree in Aerospace Engineering in March of 1996 while working for Dr. C.-H. Chuang. For that degree, her research was in the area of the second variation in optimal guidance and control.

In January of 1997, Laura joined Dr. John R. Olds who supervised her doctoral research. The culmination of her doctoral research is the thesis entitled, "Solutions to Decomposed Branching Trajectories with Powered Flyback Using Multidisciplinary Design Optimization." In addition to her thesis work, she was the performance/trajectory analyst on many team design projects including *Hyperion*, Space Solar Power (ETO), *Stargazer*, and *Starsaber*. Laura was the project lead and trajectory analyst for the *Stargazer/Starsaber* designs from June, 1998 through December, 1999. Beginning in January, 2000, Laura took a less involved role in the *Starsaber* designs, as operations and economics analyst, in order to concentrate on this thesis. In the summer of 1998, she carried out work on the *Stargazer* design, among others, at NASA Marshall Space Flight Center in Huntsville, AL. Another interesting note is that Laura was a member of the design team that won the X-Prize® University Design Competition in May of 1998. Laura is a member of the American Institute of Aeronautics and Astronautics.